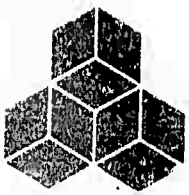

SYSTEMS, SCIENCE AND SOFTWARE

3SR-1034

THE EFFECTS OF MESO-SCALE AND SMALL-SCALE INTERACTIONS ON GLOBAL CLIMATE

Semiannual Technical Report
for Period
1 September 1971 to 1 March 1972

Sponsored by:

Advanced Research Projects Agency
ARPA Order No. 1752
Program Code No. G1101D

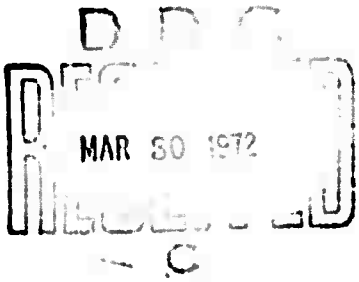

Contract No.: DAHC 04-71-C-0018
Effective Date of Contract: 15 February 1971
Contract Expiration Date: 14 August 1972
Amount of Contract: $299,059.00

31 March 1972

P.O. BOX 1620, LA JOLLA, CALIFORNIA 92037, TELEPHONE (714) 453-0060

DISCLAIMER NOTICE

THIS DOCUMENT IS THE BEST QUALITY AVAILABLE.

COPY FURNISHED CONTAINED A SIGNIFICANT NUMBER OF PAGES WHICH DO NOT REPRODUCE LEGIBLY.

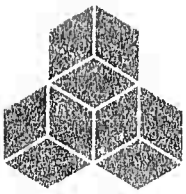

SYSTEMS, SCIENCE AND SOFTWARE

3SR-1034

THE EFFECTS OF MESO-SCALE AND SMALL-SCALE INTERACTIONS ON GLOBAL CLIMATE

Semiannual Technical Report
for Period
1 September 1971 to 1 March 1972

Sponsored by:

Advanced Research Projects Agency
ARPA Order No. 1752
Program Code No. G11D1D

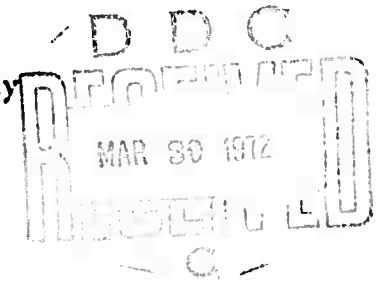

Contract No.: DAHC 04-71-C-0018
Effective Date of Contract: 15 February 1971
Contract Expiration Date: 14 August 1972
Amount of Contract: $299,059.00

31 March 1972

P.O. BOX 1620, LA JOLLA, CALIFORNIA 92037. TELEPHONE (714) 453-0060

ABSTRACT

The results reported are part of a continuing study to improve numerical models for meso-scale and small-scale effects which influence global weather and its modification. The two major areas being studied are the effects of mountain ranges on energy and momentum transfer and the transient interaction of solar radiation with the Earth's atmosphere.

In the study of orographic effects on global climate two new codes to investigate the effects of compressibility and moisture are described and calculations are reported. Several modifications made to the general Boussinesq code described in the last semiannual are outlined and results of test problems reported. Additional computations completed with the meso-scale codes are shown including a comparison of calculational results and experimental data for flow over the Sierra Nevada Range.

A new theoretical and numerical scheme for solving the radiative transfer equation in the Earth's atmosphere has been developed. It involves the approximation of the transmission function by a sum of exponentials, some plausible assumptions about frequency-averaging, based on the idea of Lebesgue quadrature, and the use of the Grant and Hunt algorithm to solve a formally equivalent set of monochromatic problems within each frequency group. In addition to being able to handle simultaneous band absorption and scattering,

this method allows the use of zones of arbitrary size and is non-iterative. Difficulties with numerical ill-conditioning and non-uniqueness in exponential-sum approximation are described and a resolution of these difficulties proposed. Some improvements in the treatment of Mie scattering are presented, and the overall status of the radiation code is reviewed.

TABLE OF CONTENTS

TABLE OF CONTENTS, contd.

TABLE OF CONTENTS, contd.

NOMENCLATURE

C = phase speed

C_p = specific heat at constant pressure

C_s = sound speed

D = drag force on the obstacle

$\frac{d}{dt}$ = $\frac{\partial}{\partial t} + \vec{U}\cdot\nabla$

η = fluid vorticity = $\frac{\partial u}{\partial z} - \frac{\partial v}{\partial x}$

e_s = saturation vapor pressure

F = advective flux across a boundary

f = Coriolis parameter

g = acceleration of gravity

Γ = dry adiabatic lapse rate = g/C_p

i,j = numerical grid indices

k = horizontal wave number

κ = R/C_p

L = latent heat of vaporization for water, or a characteristic distance

ℓ_c = cloud water content

ℓ_r = rain water content

m = ratio of molecular weight of water and dry air

p_r = water production terms

P = pressure

π = Helmholtz pressure function

NOMENCLATURE, contd.

q = total water content excluding rainwater

ϕ = compressibility stream function defined in Eq. (3.6), or angle between mountain range and northern direction (Section 4)

ψ = stream function

Ω = rotational velocity of Earth

μ = defined by Eq. (5.7a)

R = gas constant for air

R_v = gas constant for water vapor

r = relative humidity

r_s = saturated water vapor mixing ration

ρ = density

S = static stability

s = density stratification

T = temperature

t = time

θ = potential temperature latitude (Section 4)

V_t = terminal velocity of water droplet in atmosphere

$\vec{U}$ = $\hat{i}u + \hat{k}w$ = total two-dimensional velocity

u = horizontal velocity component (x-direction)

v = horizontal velocity component (y-direction)

w = vertical velocity

x = horizontal Cartesian coordinate

NOMENCLATURE, contd.

y = horizontal Cartesian coordinate

z = vertical Cartesian coordinate

ζ = compressibility vorticity function

$= \frac{\partial}{\partial z}(\rho u) - \frac{\partial}{\partial x}(\rho w)$

SUBSCRIPTS, SUPERSCRIPTS

o = value associated with the static atmosphere

$'$ = perturbation quantity

i,j = numerical grid indices

g = geostrophic state

NOMENCLATURE for Section 6

p = pressure

T = temperature

z = vertical coordinate (measured from top of atmosphere)

τ, τ_i = total optical depth

τ_n = optical depth of zone boundary n

N = number of zones

$\tau^{(s)}$ = scattering optical depth

$\tau_a, \tau_i^{(a)}$ = absorption optical depth

ν = frequency

$\vec{\Omega}$ = unit vector

θ, ϕ = spherical angular coordinates of $\vec{\Omega}$

μ = cos θ

μ_i = one of the set of Gaussian or Radau quadrature angles

m = number of angles μ_i

μ_s = cosine of scattering angle θ_s

μ_{sun} = cosine of solar zenith angle

κ_ν = volume extinction coefficient = $\alpha'_\nu + \beta_\nu$

α_ν = volume absorption coefficient = $\alpha_\nu^{(line)} + \alpha_\nu^{(cont)}$

NOMENCLATURE, contd.

$\alpha_\nu^{(line)}$ = line absorption coefficient

$\alpha_\nu^{(cont)}$ = continuum absorption coefficient

α_ν' = $(1 - e^{-h\nu/kT})\alpha_\nu$

h = Planck's constant

β_ν = volume scattering coefficient = $\beta_{\nu,M} + \beta_{\nu,R}$

$\beta_{\nu,M}$ = Mie scattering coefficient

$\beta_{\nu,R}$ = Rayleigh scattering coefficient

$\alpha_{\nu,M}$ = Mie absorption coefficient

$k_\nu^{(c)}$ = smooth part of extinction coefficient
= $\alpha_\nu'^{(cont)} + \beta_\nu$

S_ν = solar flux

P_ν = scattering phase function

$\bar{P}_\nu$ = azimuthal average of P_ν

$P_{\nu,M}$ = Mie phase function

$\bar{I}_\nu$ = azimuthal average of specific intensity of radiation I_ν

$\bar{I}_\nu^{solar}$ = solar-beam part of $\bar{I}_\nu$

i_ν, i_i = diffuse intensity ($\bar{I}_\nu$ with solar beam subtracted out)

Q_ν = solar-beam scattering source for diffuse intensity

NOMENCLATURE, contd.

$\bar{\rho}_\nu$ = azimuthal average of the surface bidirectional reflectivity ρ_ν

ε_ν = surface directional emissivity

T_g = surface temperature

$T_{\Delta\nu}$ = transmission function

α_1, α_2 = factors in scaling approximation ($\alpha_\nu^{(line)} = \alpha_1(\nu)\alpha_2(p,T)$)

$u_{\bar{\nu}}$ = equivalent absorber amount for scaling approximation

k_ν = $\alpha_\nu^{(line)}(p_o, T_o)$, where p_o and T_o are STP

a_i = coefficients in exponential-sum fit to $T_{\Delta\nu}$

k_i = exponents in exponential-sum fit of $T_{\Delta\nu}$

M = number of terms in exponential-sum fit to $T_{\Delta\nu}$

α_i = absorption coefficient corresponding to k_i

u_j = one of a discrete set of $u_{\bar{\nu}}$'s at which $T_{\Delta\nu}$ is to be fitted by an exponential sum

N_u = number of u_j's

$u^\pm$ = positively- and negatively-directed intensity vectors

$u_n^\pm$ = $u^\pm(\tau_n)$

$r, r_{ij}, r_n, r_{n,n\pm1}$ = reflection matrices

$t, t_{ij}, t_n, t_{n,n\pm1}$ = transmission matrices

NOMENCLATURE, contd.

$\Sigma^{\pm}, \Sigma^{\pm}_{ij}, \Sigma^{\pm}_{n}, \Sigma^{\pm}_{n,n+1}, \Sigma^{\pm}_{(i,n)}$ = source vectors

I = identity matrix

ω = albedo for single scattering = β_ν/κ_ν

c_i = one of Gaussian or Radau weights

$\Delta\tau_{max}$ = maximum allowable primary-layer thickness

h_n = $e^{-2^n\Delta\tau/\mu_{sun}}$, where $\Delta\tau$ is the primary-layer thickness in a zone

B_o, B'_o, B' = quantities involved in the linear-in-τ interpolation of B_ν

Y_n = intermediate quantities involved in source doubling for the Planck source

E_n, G_n, H_n = m×m matrices computed in the forward pass of the Grant and Hunt algorithm and used on the backward pass to calculate intensities

$V_n^{(1)}, V_n^{(2)} mV_n^{(3)}$ = m-vectors computed in the forward pass of the Grant and Hunt algorithm and used on the backward pass to calculate intensities

r_G = reflection matrix

w = vector connected with the surface boundary condition

F_ν = radiation flux

a = radius of spherical aerosol particle

λ = wavelength

α = $2\pi a/\lambda$

$n(a)$ = distribution of aerosol radii

NOMENCLATURE, contd.

$(\Delta\theta)_o$ = fundamental angular interval in tabulation of Mie phase function

θ^t = angle below which Mie phase function is truncated

p_ν^t = truncated Mie phase function

β', p' = adjusted Mie scattering coefficient and phase function after truncation

$c_{jk}, c_j, c_j^{(1)}, c_k^{(2)}$ = various quantities used in re-normalizing the phase function

1. INTRODUCTION

The results reported herein are the continuation of the development of numerical codes which are being utilized in the study of meso-scale phenomena related to flow over mountain ranges and the interaction of solar radiation with the Earth's atmosphere.

1.1 OROGRAPHIC EFFECTS ON GLOBAL CLIMATE

The scope of work during the past six months study has emphasized a continuing effort to develop and expand numerical codes which may be used to understand the physical processes which influence momentum transfer. The last semi-annual report[1] gave results of flow over an obstacle arrived at by using a numerical code based on the Boussinesq approximation. Some indications of codes which we hoped to develop to study compressible effects and moisture effects were outlined. This report will further describe the development of those codes and present some test problems run with two new codes. In addition, a problem based on experimental data measured in the Owens Valley area of California has been completed using our Boussinesq code for flow over the Sierra Nevada Range. Comparisons made between the experimental and calculated results show good agreement.

Further developments which have been completed during the past six months include a scheme to take into account

variable grid sizes in the vertical direction, triangular zones which allow a better description of the obstacles representing mountain ranges, a linear analysis of the equations used in the codes developed to date with comparisons with the complete compressible and incompressible equations, and an outline of a code to be developed which takes into account Coriolis forces.

1.2 RADIATIVE TRANSFER

The atmospheric radiation effort has been concentrated on a revamping of the method of solution proposed in the semi-annual report in order to take advantage of a sophisticated new method of Grant and Hunt[50] for monochromatic radiative transfer problems. Grant and Hunt's method is the most advanced available for plane-parallel problems, and has two large advantages over other techniques: (1) it imposes no restrictions on zone size, except that there will be an inevitable loss of accuracy if atmospheric structure (p, T, etc.) is specified too coarsely; (2) it is non-iterative, whether or not there is scattering. Since the technique is only applicable to monochromatic problems, however, it is not directly useful unless one is willing to do a line-by-line calculation in band absorption regions. Barring this, some approximation is necessary. The one chosen involves fitting the transmission function for a frequency group $\Delta\nu$ (containing many lines) with a sum of M exponentials,

$$T_{\Delta\nu}(u) = \sum_{i=1}^{M} a_i \, e^{-k_i u} \qquad (1.1)$$

Then by invoking certain plausible assumptions based on the idea of Lebesgue quadrature, the frequency-averaged form of the radiative transfer equation may be broken down into N monochromatic problems, each of which may be solved by Grant and Hunt's method. The technique just described, if it proves accurate when compared with line-by-line calculations, will be very powerful indeed, and will solve some long-standing difficulties which have clouded all atmospheric heating-rate calculations up to now. For example, it will improve calculations in all infrared absorption bands in which scattering cannot be neglected.

Code development has proceeded apace with the development of the theory. Further improvements have been made in the treatment of Mie scattering, and excessively large forward peaks in the phase function are now truncated and replaced by pure forward scattering. Great difficulties were encountered in numerically implementing the exponential fit of Eq. (1.1), due to numerical ill-conditioning and non-uniqueness but the resolution of that problem is now in sight. Most of the straightforward subroutines have been coded, including those for calculating (1) zone structure, angle structure, and frequency group structure; (2) astronomical parameters such as the solar flux S_ν, solar zenith angle, and Earth-Sun distance; (3) Rayleigh scattering parameters; (4) the frequency average of the Planck function; (5) transmission functions from tabular data; (6) the index of refraction of water at any frequency, from extensive tables, for use in Mie scattering and water surface reflection computations; and (7) the size distribution of Mie scatterers, from card input or from one of a number of analytic forms proposed in the literature. The Grant and Hunt algorithm and associated subroutines are partially complete, and the exponential

fitting subroutine should be ready soon. Appropriate editing routines will complete the code, and comparisons with standard (Rayleigh-scattering) solutions and with the Mintz-Arakawa radiation package may then begin.

2. OROGRAPHIC EFFECTS: TEST CALCULATIONS USING HAIFA

Several test problems were completed during the initial six-month study under this contract and the results reported in the previous semiannual report.[1] HAIFA (Hydrodynamics in an Almost Incompressible Flow Approximation), the numerical code incorporating a numerical solution of the fluid dynamic equations in the Boussinesq approximation, was used to study two additional test problems which are reported herein. The first problem describes flow over an obstacle with an atmospheric stability and horizontal wind profile for which linear analysis indicates the formation of two separate waves similar to one of the test problems previously reported. The second problem is an attempt to calculate flow over a portion of the Sierra Nevada mountain range for which there are published experimental data. Comparisons between the calculated and measured results are made.

2.1 TWO WAVE PROBLEM

The results of the two wave problem presented previously may have been affected by interference with the top boundary located at 10.9 km where the vertical velocity is zero. The problem was re-run using a vertical grid size of 811 meters and an obstacle height of 111 meters. This placed the upper boundary at 13.1 km. The other initial conditions were identical to those noted in the previous semiannual.

They are reiterated in Table 2.1. The initial horizontal velocity profile is shown in Figure 2.1.

TABLE 2.1

PROBLEM TITLE	LAPSE RATE*	GRID CHARACTERISTICS	HORIZONTAL VELOCITY PROFILE
Two Wave	$\gamma = \frac{1}{2}\Gamma$	Δx = 1500 meters Δz = 441 meters Obstacle: Height = 441 meters Length = 4500 meters	Exponential profile as shown in Figure 2.1

*Initial surface temperature = 300°K
Γ = adiabatic lapse rate = 10°K/km

The linear analysis of Pain and Foldvik[2] indicates that under these conditions two waves should be present in the lee of the mountain - one wave of approximately 9.2 km wavelength and a second wave of approximately 25 km wavelength. The HARTA calculation was run to a time of 4950 seconds. Computer plots of the streamlines and the vertical velocity profiles from the calculation at a time of 4691 seconds are shown in Figure 2.2. The shorter wave appears just above and behind the obstacle displaying a wavelength of approximately 10 km. A second wave appears behind the obstacle at a height of 7 to 8 km with a wavelength of approximately 25-35 km. Pain and Foldvik's analysis indicated the maximum amplitude of the wave would appear at 7.4 km. Consequently, the main features of the linear theory are obtained in the numerical calculation. These waves are

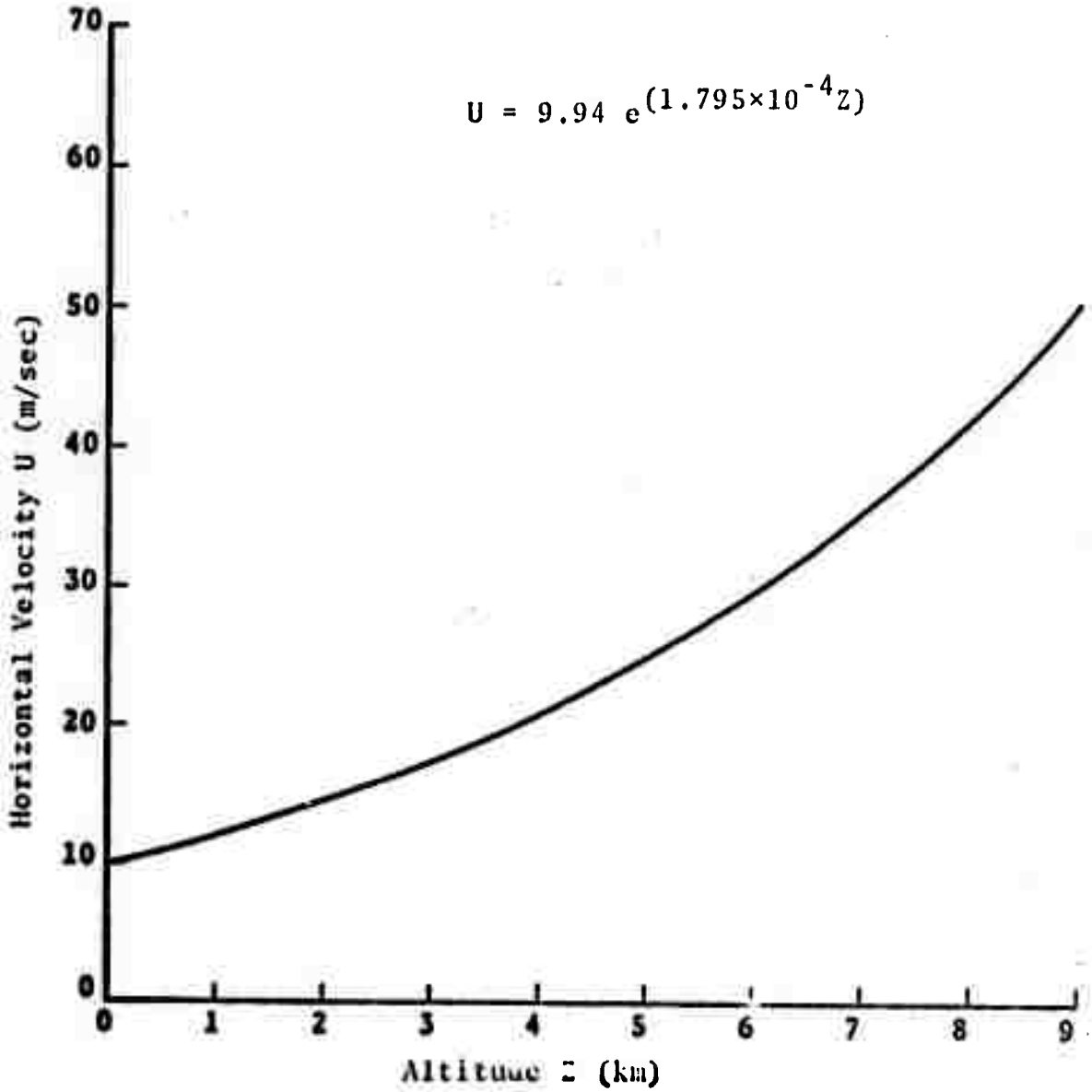

Figure 2.1. Initial velocity profile – two wave problem.

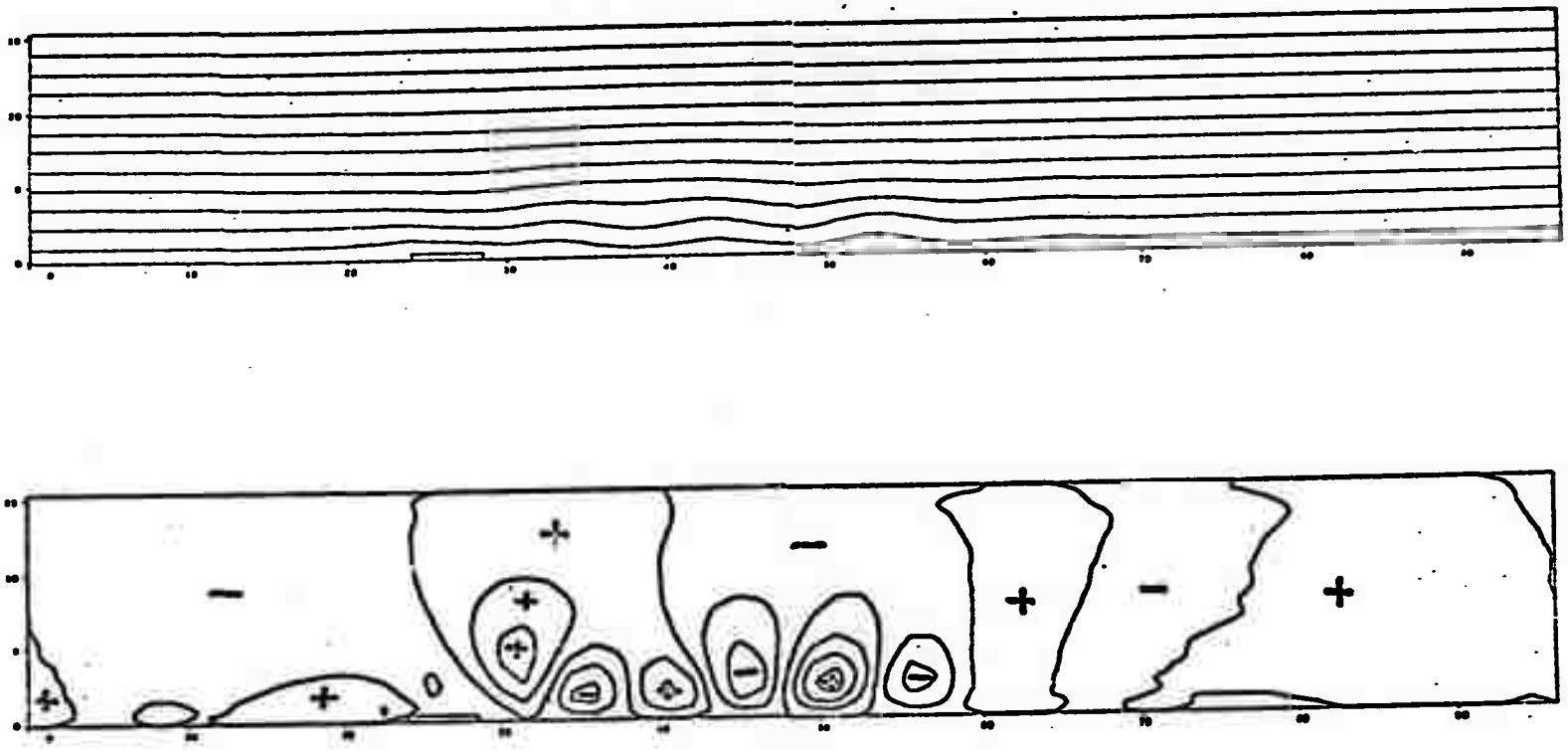

Figure 2.2. Streamlines and vertical velocity profiles for the two-wave problem. (time = 4691 seconds)

distinctly indicated in the vertical velocity contour plots also shown in the figure.

2.1.1 Wave Drag Results

In stratified flow over an obstacle the pressure is systematically higher on the upstream side, resulting in a drag force on the obstacle, and a corresponding drag of opposite sign on the air stream.

This drag force of the air on the mountain is obtained by integrating the momentum transport along the x-axis. For a symmetrical mountain of height H,

$$\text{Drag} = - \int_{-\infty}^{\infty} (\rho u'w')|_{Z=H} \, dx \quad ,$$

where u', w' = velocity perturbation quantities.

An edit routine was written to integrate the results obtained in these calculations. The results are presented as

$$\overline{\rho u'w'} = \frac{1}{2L} \int_{-L}^{L} \rho u'w' \, dx$$

where L is one-half the computational x-interval. The drag units $\overline{\rho u'w'}$, as presented here, are in dynes/cm^2. The quantity L is 48 km. The values presented may be related to other studies where drag force is presented in dynes/cm by multiplying the values shown here by 2L.

The momentum edits $\overline{\rho u'w'}$, located one cell above the mountain top, are shown as a function of time in Figure 2.3. The largest value of the drag which was reached at

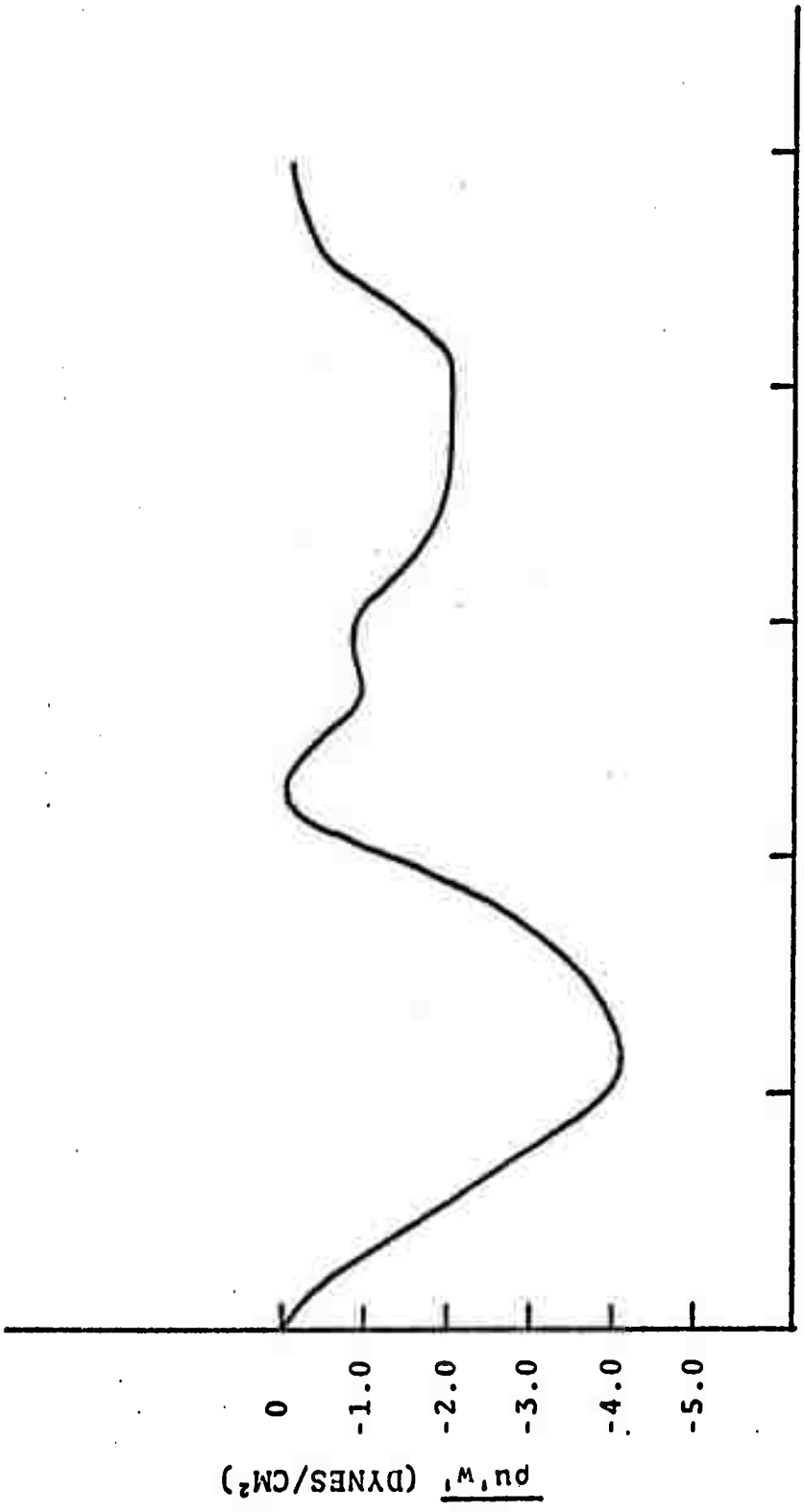

Figure 2.3. Two-wave problem – vertical transport of horizontal momentum above the obstacle.

1000 seconds, was approximately equal to 4 dynes/cm^2. This value agrees qualitatively with measured values of the momentum flux reported by D.K. Lilly[3] for measurements at Boulder, Colorado (7 dynes/cm^2). Palm and Foldvik, and Vergeiner[4] present calculated values of 7×10^6 to 2×10^7 dynes/cm for similar problems. The value of 4 dynes/cm^2 corresponds to 3.8×10^7 dynes/cm and thus we also see qualitative agreement here.

The other important feature of the momentum flux edit is the oscillatory character of the values with time. It is thought to be related to the formation of the individual vertical velocity cells, i.e., as new positive or negative cells are formed, there is an increase or decrease in the horizontal average of the vertical flux of horizontal momentum.

Figure 2.4 presents the two-wave momentum flux as a function of height at several times. The momentum edits indicate a cyclic character at late times at a height of 3 to 5 km. The interaction of the long and short waves takes place in this altitude range and is thought to be responsible for this phenomenon.

2.2 SIERRA NEVADA WAVE PROBLEM

A test problem using the HAIFA code was formulated based on experimental data (see Figure 2.5) gathered from flights over the Owens Valley on February 16, 1952.[5] These data included measurements taken on two sailplane flights which extended over a time period of 3-1/2 hours. An altitude of 33,000 feet was attained. The data are especially interesting because of its completeness and the presence of a strong lee wave.

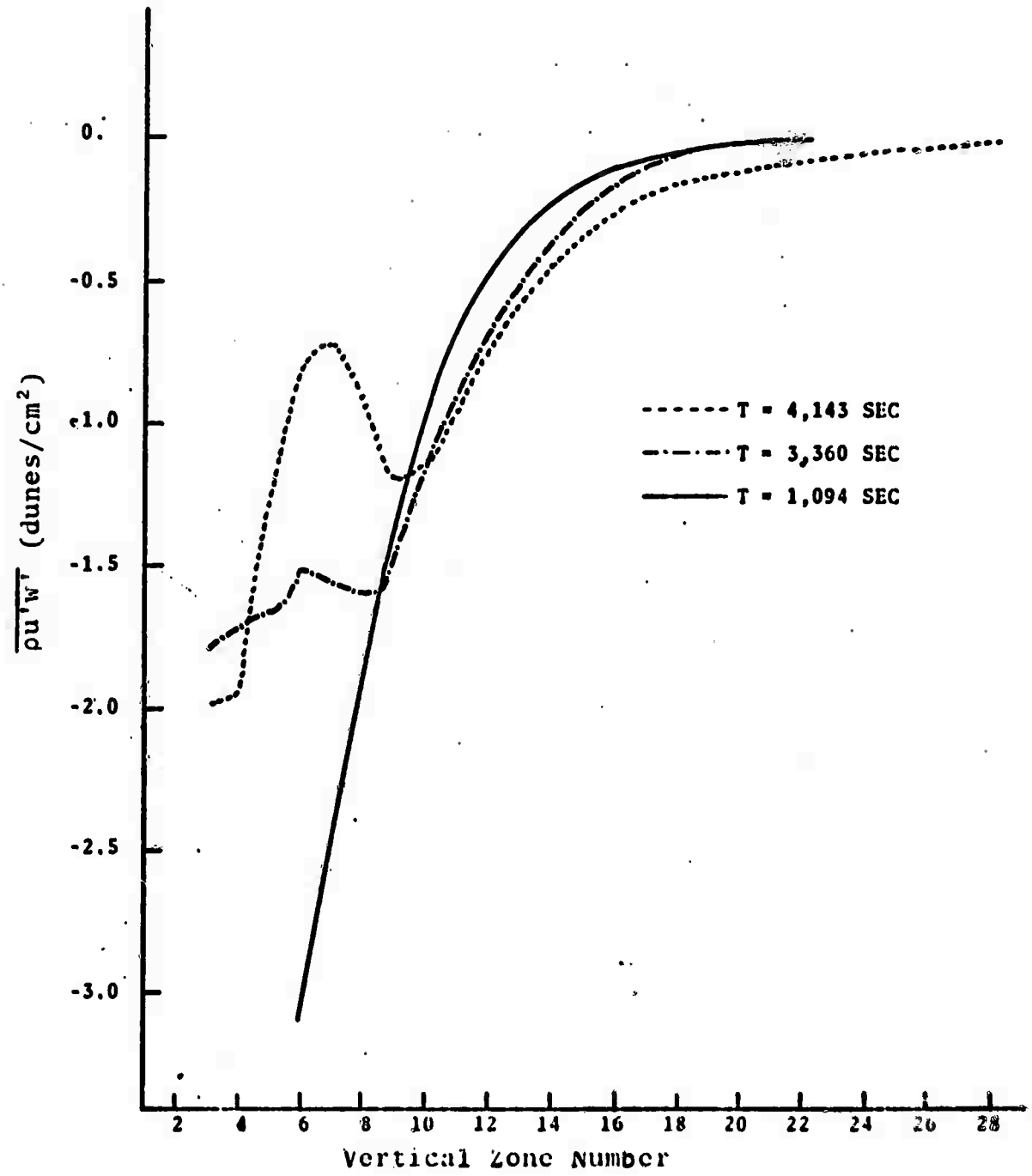

Figure 2.4. Momentum flux as a function of height for two-wave problem.

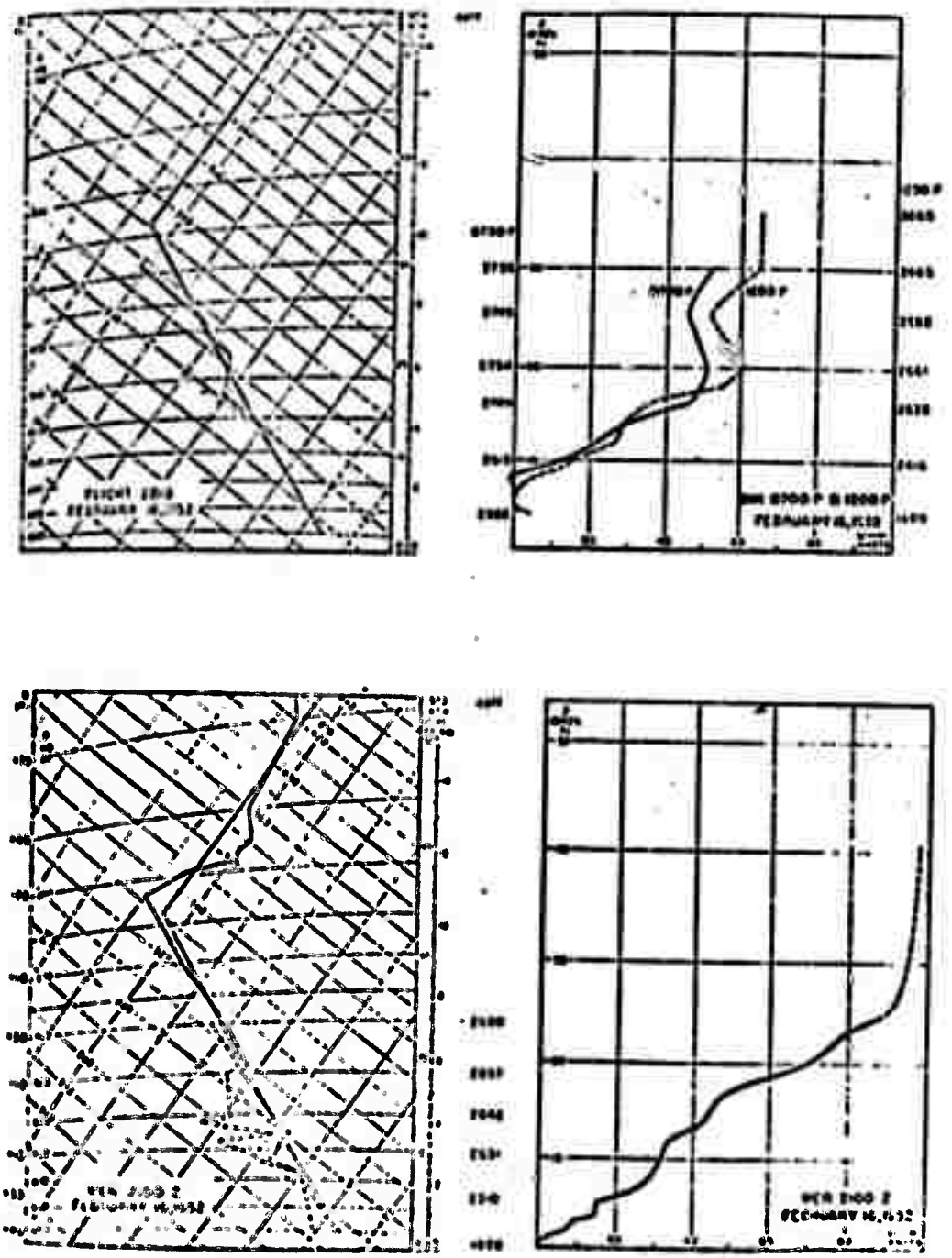

Vertical temperature distribution

Horizontal wind velocity

Figure 2.5. Experimental data for the Sierra Nevada lee wave problem.

The numerical calculation was made using constant zone sizes with $\Delta x = 2.0$ km and $\Delta z = 0.5$ km. The total height of the grid was 17.5 km while the horizontal length was 128 km. The horizontal velocity was treated as a constant above 9.5 km and the temperature was assumed constant above 14 km. The Sierra Nevada range was treated as a triangular barrier with a front face assumed perpendicular to the Earth's surface, with a maximum height of 2 km and a horizontal length of 8 km.

Figure 2.6 gives the measured streamline pattern directly in the lee of the mountain. The wavelength of the major lee wave above the mountain is 21 to 22 km. A rotor was also observed in the Owens Valley in the lee of the mountain range.

The results of our calculation, to a time of approximately 2000 seconds, are shown in Figures 2.7 and 2.8. The results indicate a small rotor was formed in the lee of the obstacle and the calculated lee wavelength is 22 km. These comparisons are especially significant as the problem presents a very severe test of the HAIFA code. The temperature profile is not smooth and, in fact, a small inversion layer exists at an altitude of 20 km. A large portion of the horizontal velocity profile is treated as uniform flow and, as noted from our previous results,[11] this type of flow excites a continuous spectrum of waves. Also, numerical stability associated with uniform flows adds to the difficulty of the computer calculation. A direct comparison with the experimental streamline results shown in Figure 2.6 is presented in Figure 2.9 at a time of 2000 seconds. The presence of the two small rotors at that time, in contrast to the larger single rotor observed in the experiment, may be a consequence of the fact that the calculation has not yet reached a steady state.

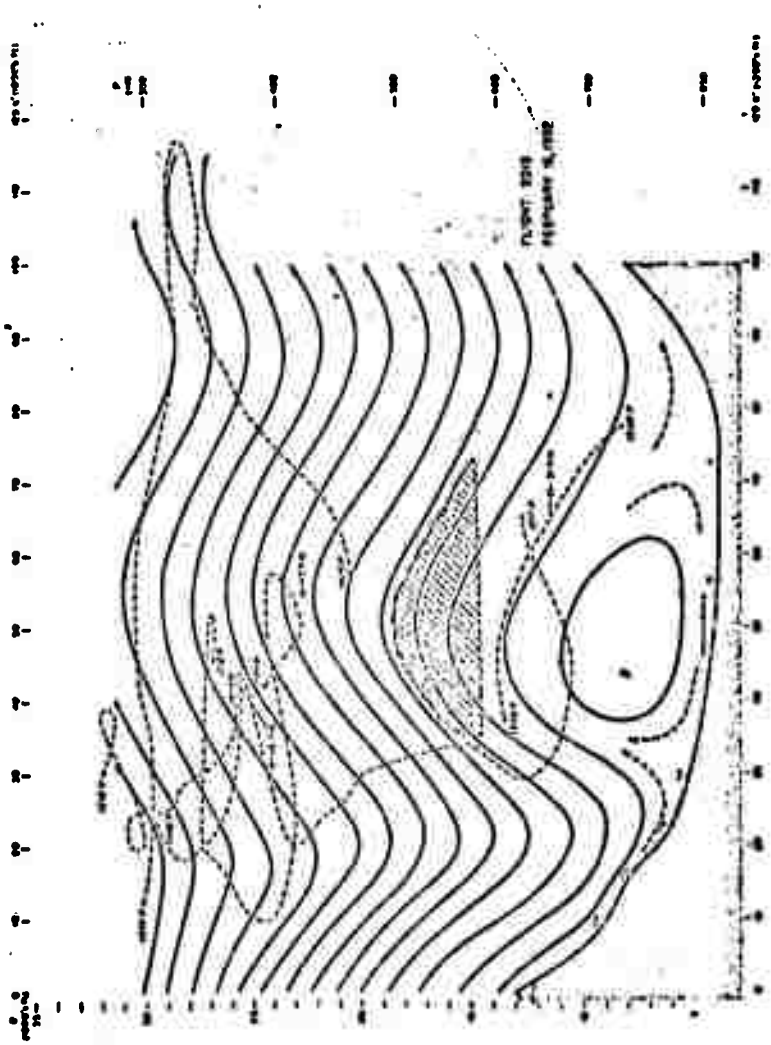

Figure 2.6. Streamline pattern taken from experimental data – Sierra Nevada lee wave problem.

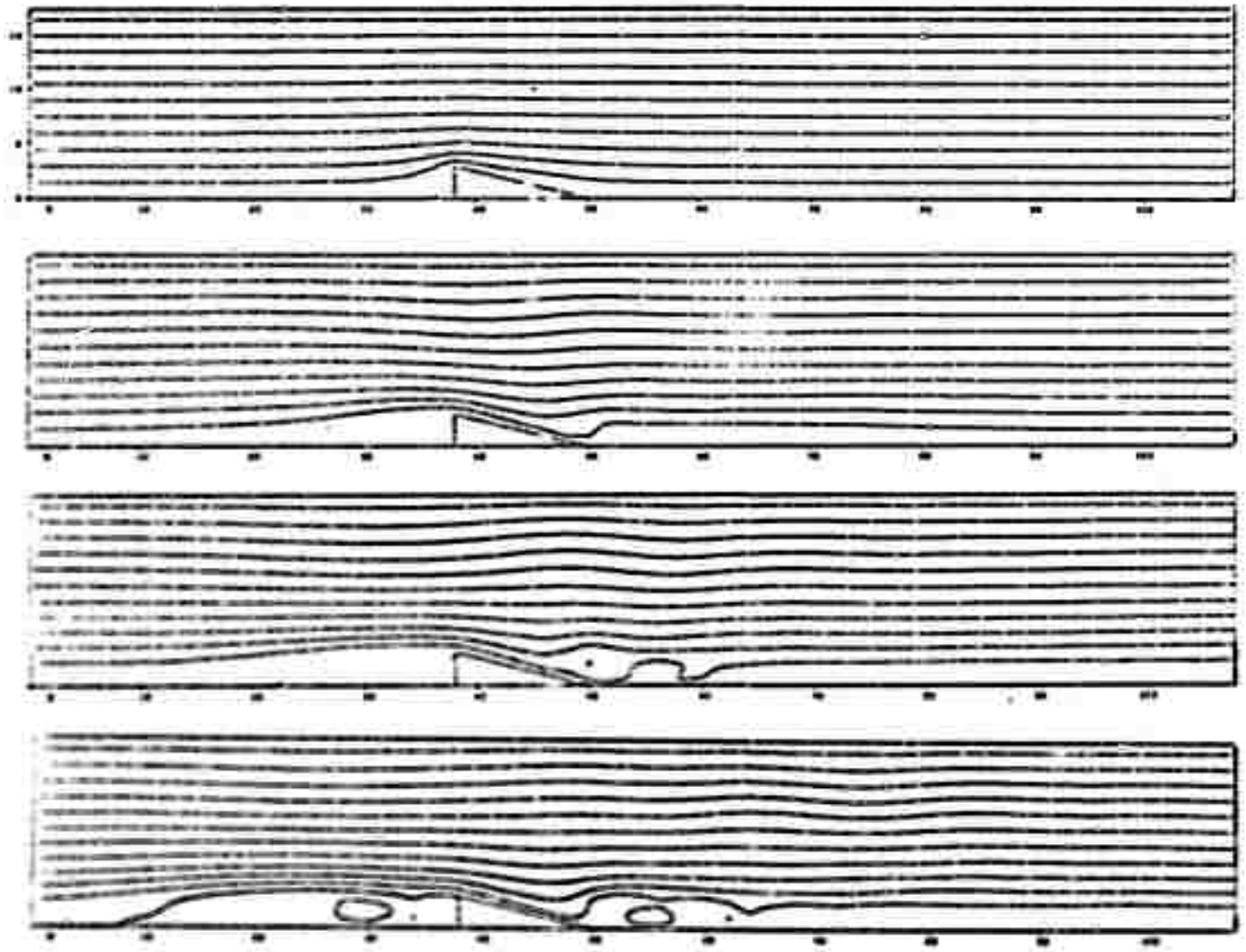

Figure 2.7. Calculated streamlines – Sierra Nevada lee wave problem.

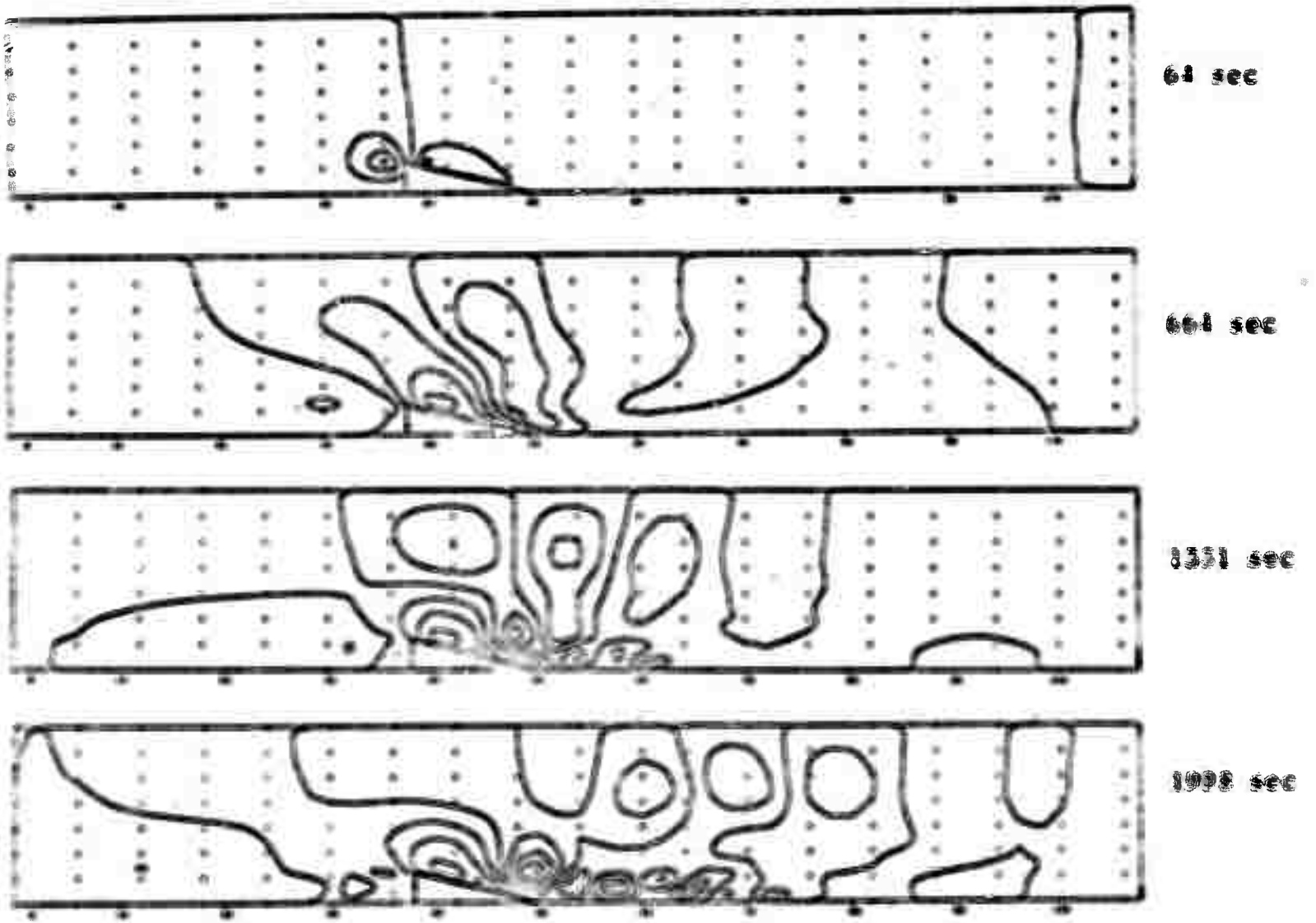

Figure 2.6. Vertical velocity contours — Sierra Nevada lee wave problem.

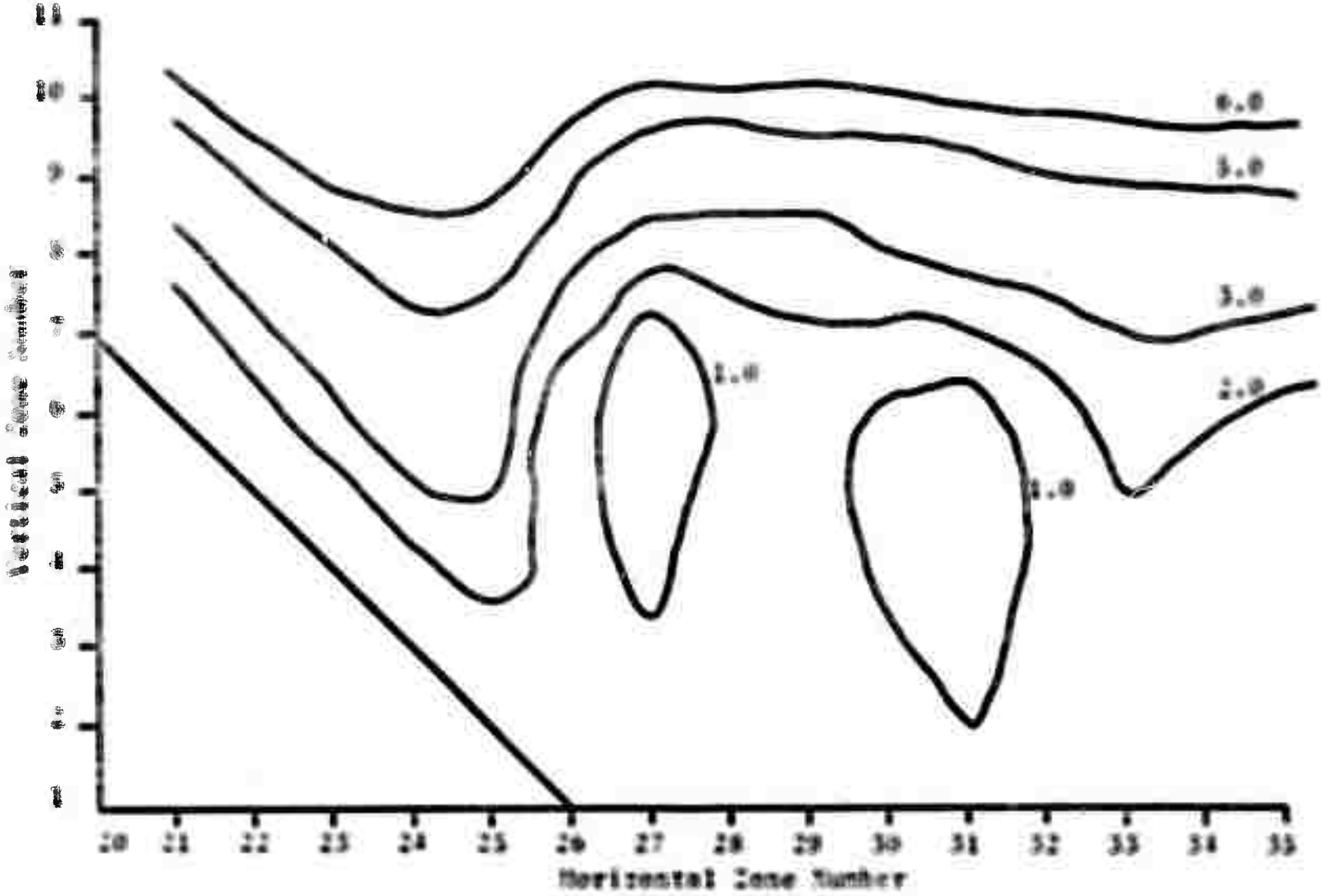

Figure 2.9. Streamline pattern in lee of mountain - Sierra Nevada lee wave problem.

The momentum flux at a point just above the mountain top is shown as a function of time in Figure 2.10. The results are similar in appearance to those previously reported in connection with this research.

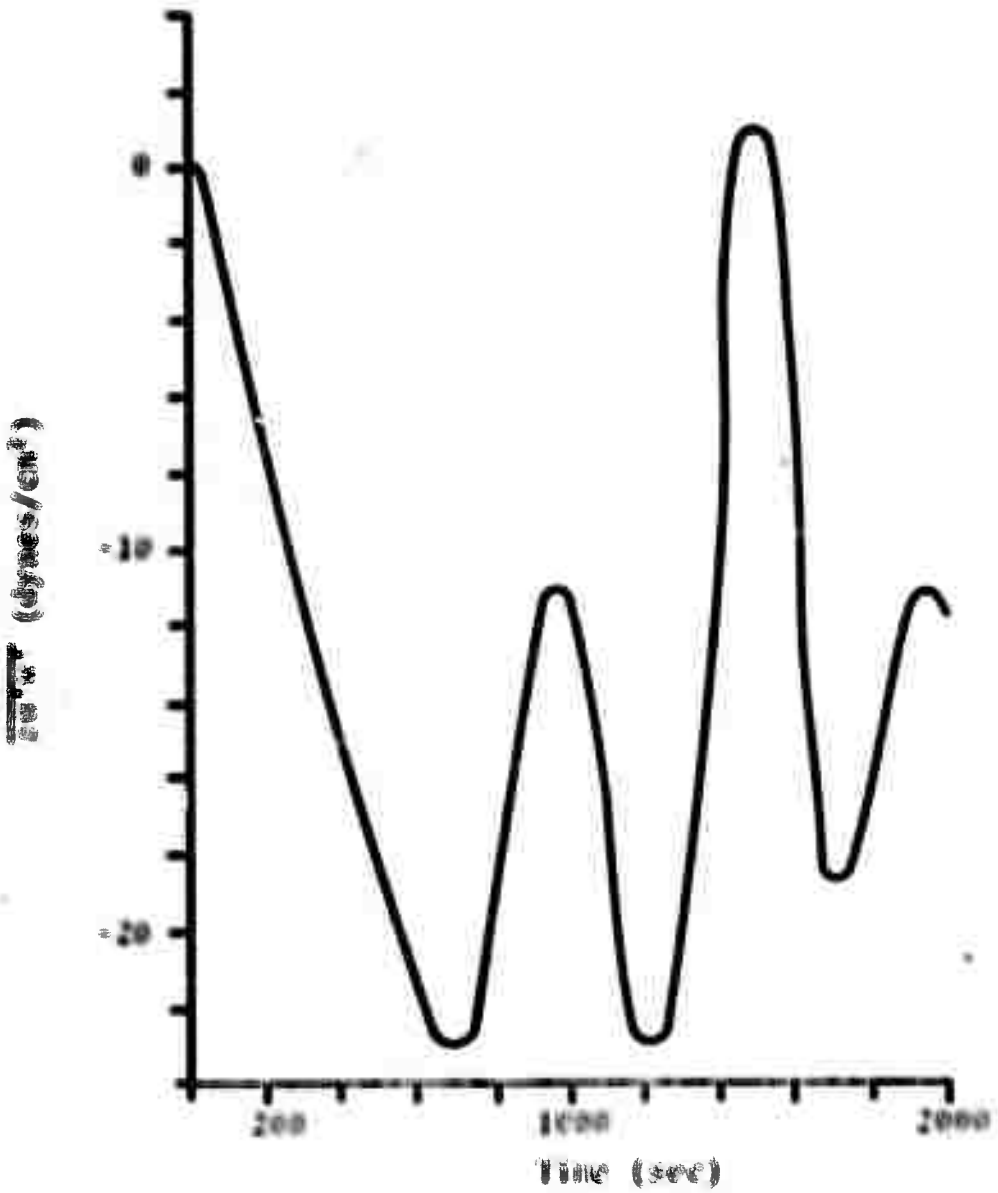

Figure 2.10. Momentum flux above mountain - Sierra Nevada wave problem.

3. CODE MODIFICATIONS

Two major code modifications have been completed in the past six months. A code similar to HAIFA but which includes compressibility of the atmosphere was completed and the two wave test problem was run with it, and compared with the Boussinesq flow calculations. A second code which includes moisture effects was also completed, and a test calculation made. Both of these codes are discussed in detail in this section.

In addition to the two major developments noted, several other general improvements in the codes were completed. These included modifications to allow the use of variable grid sizes in the vertical direction, the use of triangular zones to improve the description of mountain ranges, a test of the Crowley[1,6] advection scheme and a modification to improve its accuracy, and finally an edit routine to calculate pressure throughout the flow field, particularly for the compressible code.

Each of these modifications is also described in this section. In addition, a listing of the compressible code is included as Appendix C of this report.

3.1 COMPRESSIBILITY EFFECTS

Modifications to the basic HAIFA equations to take account of the compressibility of the atmosphere have been previously reported.[1,7] The resulting system of compressibility equations (3.1 through 3.4) have been put in finite difference form, and a computer code has been written which incorporates these in a two-dimensional, time-dependent calculation.

The compressibility equations are:

$$\frac{\partial \rho u}{\partial t} + \frac{\partial \rho u^2}{\partial x} + \frac{\partial \rho uw}{\partial z} + \frac{\partial p}{\partial x} = 0 \qquad (3.1)$$

$$\frac{\partial \rho w}{\partial t} + \frac{\partial \rho uw}{\partial x} + \frac{\partial \rho w^2}{\partial z} + \frac{\partial p}{\partial z} = - g\rho \qquad (3.2)$$

$$\frac{\partial \rho u}{\partial x} + \frac{\partial \rho w}{\partial z} = 0 \qquad (3.3)$$

$$\frac{\partial \rho T'}{\partial t} + \frac{\partial \rho T'u}{\partial x} + \frac{\partial \rho T'w}{\partial z} = -w\left[\rho \frac{\partial T_o}{\partial z} + \rho_o \Gamma\right] . \qquad (3.4)$$

Here we recall the assumption that the density at every position can be determined from the perfect gas equation of state, in which the pressure takes the value associated with the static atmosphere, p_o, through the relation

$$\rho = \frac{p_o}{RT} \qquad (3.5)$$

The system of equations (3.1 through 3.4) have a form similar to the Boussinesq equations of standard HAIFA, and can be solved in a similar manner.

A stream-function-like quantity ϕ can be introduced, such that Eq. (3.3) is satisfied and

$$\rho u = \frac{\partial \phi}{\partial z} \quad , \quad \rho w = - \frac{\partial \phi}{\partial x} \quad . \tag{3.6}$$

If a vorticity-like function ζ is defined,

$$\zeta = \frac{\partial \rho u}{\partial z} - \frac{\partial \rho w}{\partial x} \tag{3.7}$$

then the same Poisson equation as for the Boussinesq approximation results,

$$\zeta = \frac{\partial^2 \phi}{\partial x^2} + \frac{\partial^2 \phi}{\partial z^2} \quad . \tag{3.8}$$

The prognostic equation for ζ is obtained by cross differentiating Eqs. (3.1) and (3.2) and subtracting,

$$\frac{\partial \zeta}{\partial t} + \frac{\partial}{\partial x}(u\zeta) + \frac{\partial}{\partial z}(w\zeta) + \frac{\partial}{\partial x}\left(\frac{\partial \phi}{\partial x}\frac{\partial u}{\partial x} + \frac{\partial \phi}{\partial z}\frac{\partial u}{\partial z}\right)$$

$$+ \frac{\partial}{\partial z}\left(\frac{\partial \phi}{\partial x}\frac{\partial w}{\partial x} + \frac{\partial \phi}{\partial z}\frac{\partial w}{\partial z}\right) = g\frac{\partial \rho}{\partial x} = - \frac{g\rho}{T_o + T'}\frac{\partial T'}{\partial x} \quad . \tag{3.9}$$

Eq. (3.9) replaces the vorticity equation of the Boussinesq system of equations, differing principally in having the additional terms containing the derivatives of ϕ, u, and w. These additional terms, which for convenience we call the chi terms, will be discussed in detail in a following section.

3.1.1 Method of Numerical Solution

3.1.1.1 Calculational Logic – The sequence of calculations for one cycle of the compressible code is:

SUBROUTINE	FUNCTION
UPDATE	(1) Eq. (3.4) is solved for new values of $(\rho T')$
	(2) Eq. (3.9) is solved for ζ
	(3) As adjuncts, ρ is computed from $\rho = \rho_o - \frac{(\rho T')}{T_o}$ and T' follows from $T' = \frac{(\rho T')}{\rho}$
LAPLAC	(4) Eq. (3.8) is solved for new values of ϕ
VELOC	From Eq. (3.6)
	(5) u is derived from $u = \frac{\partial \phi}{\partial z} / \rho$
	(6) v is derived from $v = - \frac{\partial \phi}{\partial x} / \rho$

3.1.1.2 Finite Difference Scheme – The centering of the dependent variables in the compressible code is identical to the centering of the analogous variables in standard HAIFA, viz.,

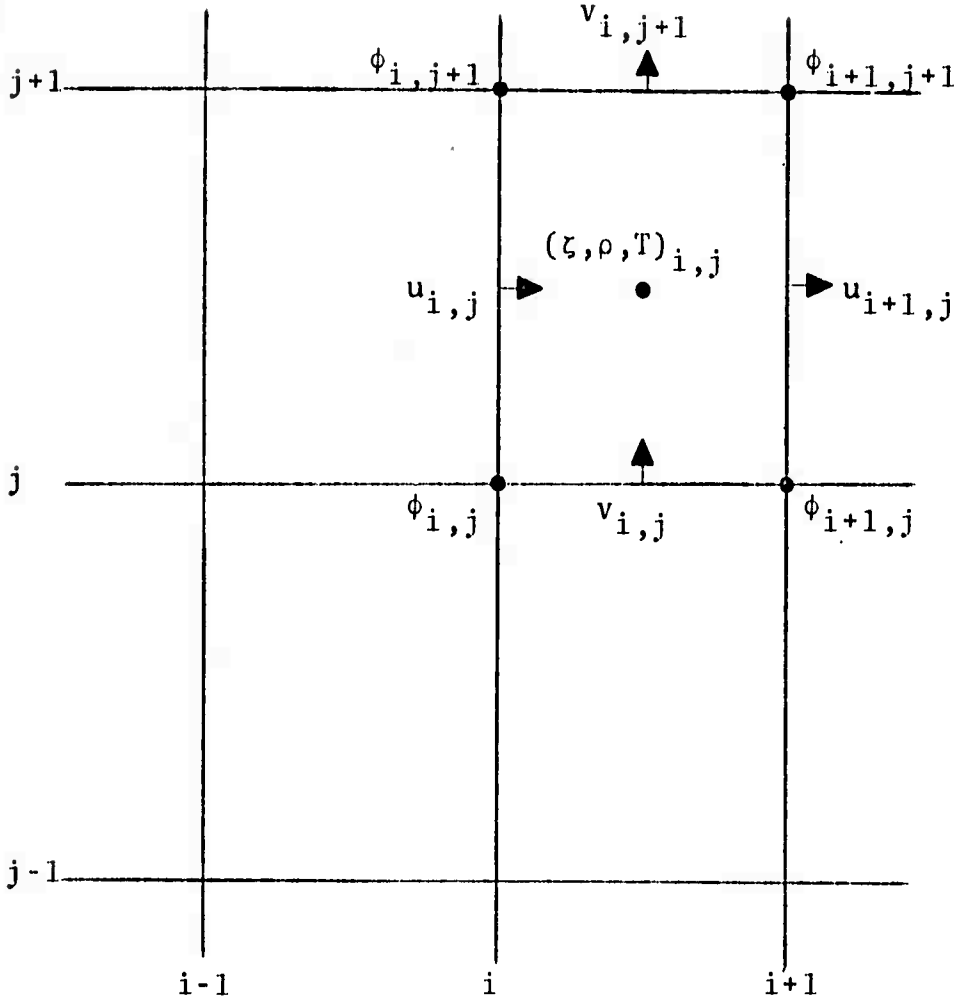

The difference scheme used in the standard HAIFA equations is applied directly to the compressible system of equations, and need not be reviewed here. The differencing of the chi term, which is unique to the compressible code, is discussed below.

To form

$$\chi = \frac{\partial}{\partial x}\left[\frac{\partial \phi}{\partial x}\frac{\partial u}{\partial x} + \frac{\partial \phi}{\partial z}\frac{\partial u}{\partial z}\right] + \frac{\partial}{\partial z}\left[\frac{\partial \phi}{\partial x}\frac{\partial w}{\partial x} + \frac{\partial \phi}{\partial z}\frac{\partial w}{\partial z}\right]$$

we define X_R, X_L, Z_U, and Z_D

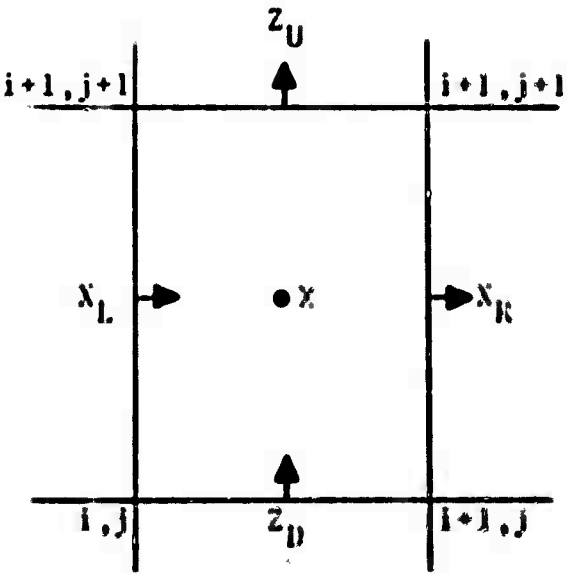

so that

$$X = \frac{X_R - X_L}{\Delta x} + \frac{Z_U - Z_D}{\Delta z}$$

is cell centered. Then, the difference form used is

$$X_R = \frac{\phi_{i+2,j} + \phi_{i+2,j+1} - \phi_{i,j+1} - \phi_{i,j}}{4\Delta x} \cdot \frac{u_{i+2,j} - u_{i,j}}{2\Delta x}$$

$$+ \frac{\phi_{i+1,j+1} - \phi_{i+1,j}}{\Delta z} \cdot \frac{u_{i+1,j+1} - u_{i+1,j-1}}{2\Delta z}$$

$$Z_U = \frac{\phi_{i+1,j+1} - \phi_{i,j+1}}{\Delta x} \cdot \frac{w_{i+1,j+1} - w_{i-1,j+1}}{2\Delta x}$$

$$+ \frac{\phi_{i,j+2} + \phi_{i+1,j+2} - \phi_{i,j} - \phi_{i+1,j}}{4\Delta z} \cdot \frac{w_{i,j+2} - w_{i,j}}{2\Delta z} \quad . \tag{3.10}$$

Note that

$$\chi_L\big]_{i,j} = \chi_R\big]_{i-1,j}$$

and

$$z_D\big]_{i,j} = z_U\big]_{i,j-1}$$

3.1.2 Initial Conditions

As with HAIFA, the values of $u_o(z)$ and $T_o(z)$ are specified by input to the compressible code. In addition, the initial surface pressure $p_o(z=0)$ must be specified. The remaining initial pressures are found using the static atmospheric equation

$$\frac{dp_o}{dz} = -g\rho_o = -\frac{gp_o}{RT_o} \quad . \tag{3.11}$$

so that

$$p_o(z) = p_o(z=0)\ \exp\left[-\frac{g}{R}\int_0^z \frac{dz}{T_o(z)}\right] \quad .$$

The initial density profile then follows from

$$\rho_o(z) = \frac{p_o(z)}{RT_o(z)} \quad .$$

The stream-function-like quantity ϕ is formed by integrating

$$\frac{\partial\phi}{\partial z} = \rho_o(z)\ u_o(z) \quad ,$$

and the vorticity-like quantity ζ is initialized from the application of Eq. (3.7) to yield

$$\zeta = \frac{\partial}{\partial z}\left(\rho_0(z)\, u_0(z)\right) \quad .$$

As in standard HAIFA, initially there is no x-dependence of any quantity.

3.1.3 Modification of Advection Scheme

The quantities to be advected in the system of compressibility equations are ζ, Eq. (3.9), and $(\rho T')$, Eq. (3.4). Since the equation of continuity is the form

$$\frac{\partial \rho u}{\partial x} + \frac{\partial \rho w}{\partial z} = 0 \quad ,$$

it was necessary to modify Crowley's second-order scheme for advection in order to use (ρu) and (ρw) as pseudo-velocities.

3.1.4 Timing Comparison

The major computational difference between the Boussinesq and compressible codes is the calculation of the chi term. Timing studies of the two code versions were performed, based on a grid of 64 x-direction cells and 35 y-direction cells, and incorporating an interior boundary condition (which requires two passes per cycle in the Poisson Equation Solver). The results are summarized in the table below:

	COMPRESSIBLE	STANDARD
UPDATE TOTAL	1.58 sec	0.51 sec
2nd Order Scheme	0.33 sec	0.33 sec
Chi Term	1.02 sec	---
LAPLAC TOTAL	1.14 sec	1.14 sec
VELOC TOTAL	0.14 sec	0.11 sec
TIMSTP TOTAL	0.03 sec	0.03 sec
BASIC TOTAL/CYCLE	2.89 sec	1.79 sec

3.1.3 Test Problem

A two wave problem identical to that discussed in Section 2.1 was used for comparative calculations between the compressible and the Boussinesq versions of the HAIFA codes.

Comparative plots (Figures 3.1 and 3.2) of the results from the compressible code and HAIFA at a time of approximately 1500 seconds indicates a single wave (in each case) with a 10-12 km wavelength. The vertical velocity pattern indicates that only the single wave is forming in the compressible case while a second wave is appearing in the Boussinesq case. However, since the compressible calculation was run to a time of only 2000 seconds, these results are inconclusive. The first wavelength in each case agrees with the shorter of the two waves predicted by Palm and Foldvik.

Figure 5.5. Streamlines and vorticity contours for the flow over a backward facing step at Re = 800 (Grid 2).

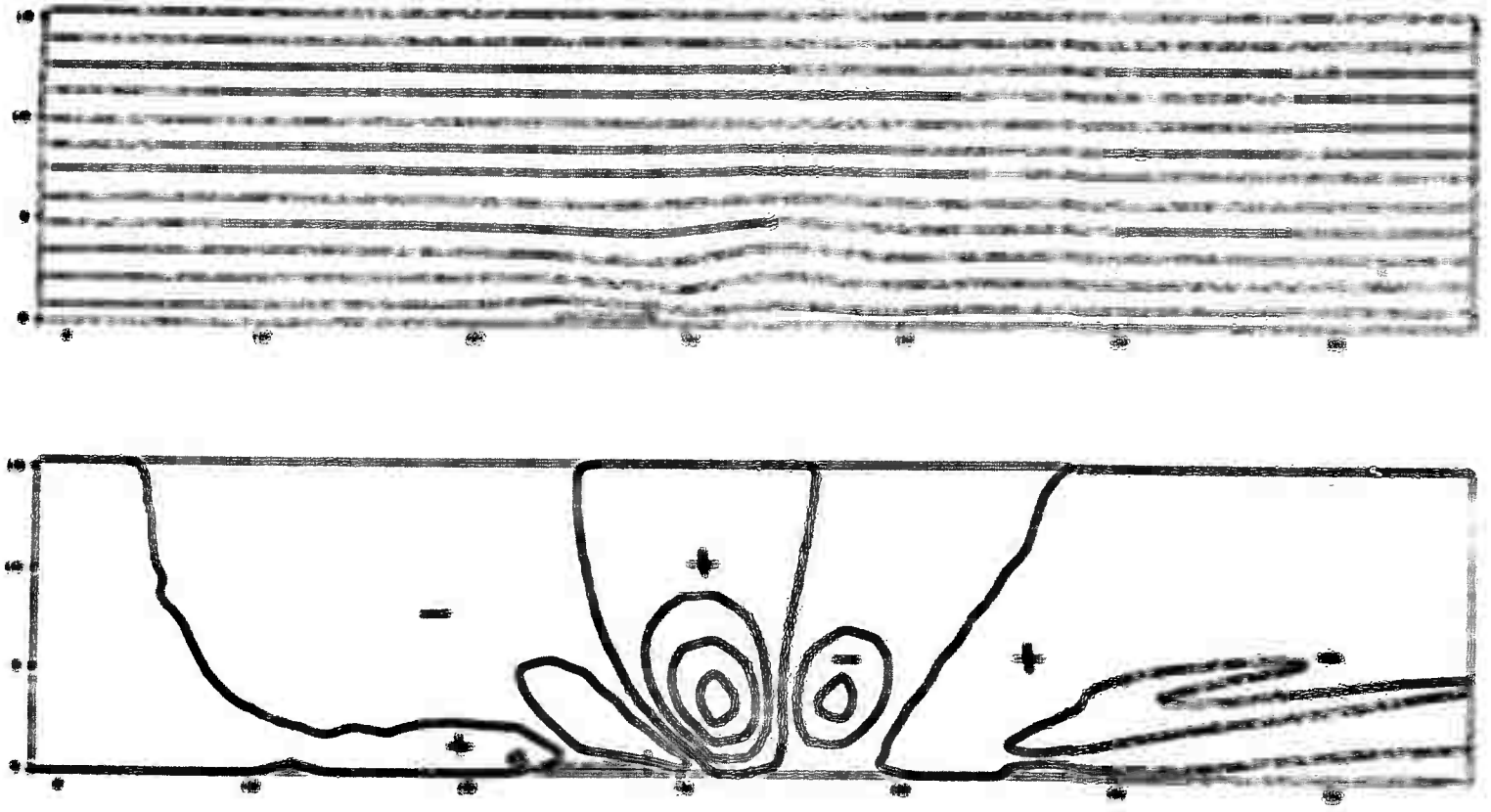

Figure 5.2. Streamlines and vertical velocity profiles for the HIFI problem. (time = 1505 seconds)

3.1.5.1 Wave Drag Results - The momentum eddy $\overline{\rho u''w''}$, located one cell above the mountain top, are shown as a function of time for the Boussinesq and compressible calculations in Figure 3.3. The maximum value of the drag reached during 2000 seconds of integration time was approximately equal to 5 dyne/cm^2 and 3.8 dyne/cm^2, respectively.

Figures 3.4, 3.5 and 3.6 show the momentum eddy as a function of height at a time of approximately 1000, 1500 and 2000 seconds. This sequence indicates that the solution has not yet reached a steady state value, since the drag for a steady problem will be constant with height.

The major characteristics of the momentum flux results are:

(1) a larger value of the vertical flux of horizontal momentum just above the mountain (600 meters) is predicted by the Boussinesq code than by the compressible code; and

(2) above a height of approximately 8.5 km, the compressible results indicate a larger flux of momentum than the Boussinesq calculations.

These results are explainable to a certain degree by the linear analysis of the equations in Section 5. The analysis shows that the vertical velocity resulting from the compressible equations increases with increasing altitude by a factor of $(\rho/\rho_0)^{-0.34}\ (c/c_0)^{-1/2}$ relative to the Boussinesq equations. This velocity is reflected directly in the value of the momentum flux $\overline{\rho u''w''}$ and the cross over of the drag results seen in the figures as a function of height is qualitatively expected.

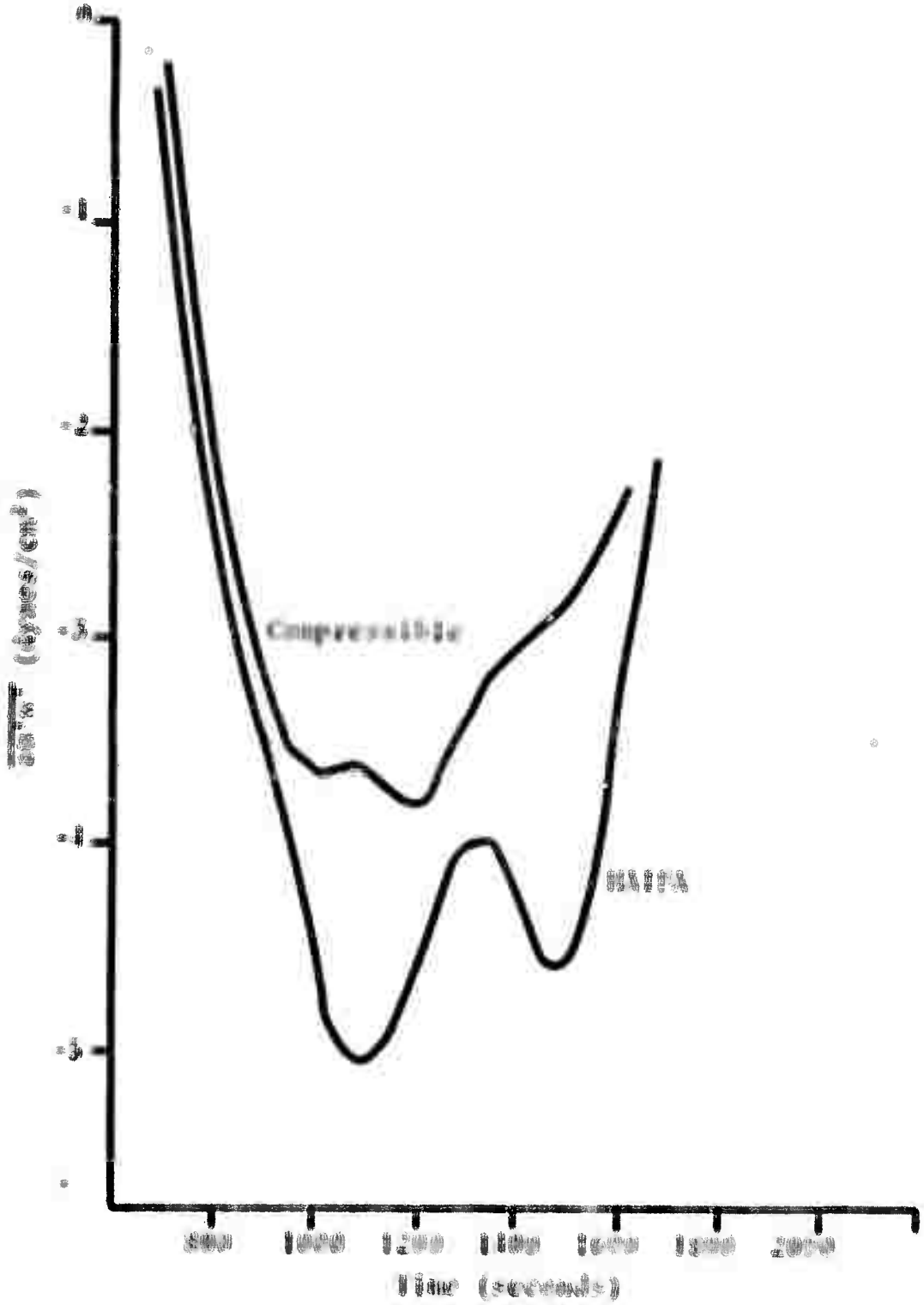

Figure 3.3. Vertical transport of horizontal momentum above the obstacle.

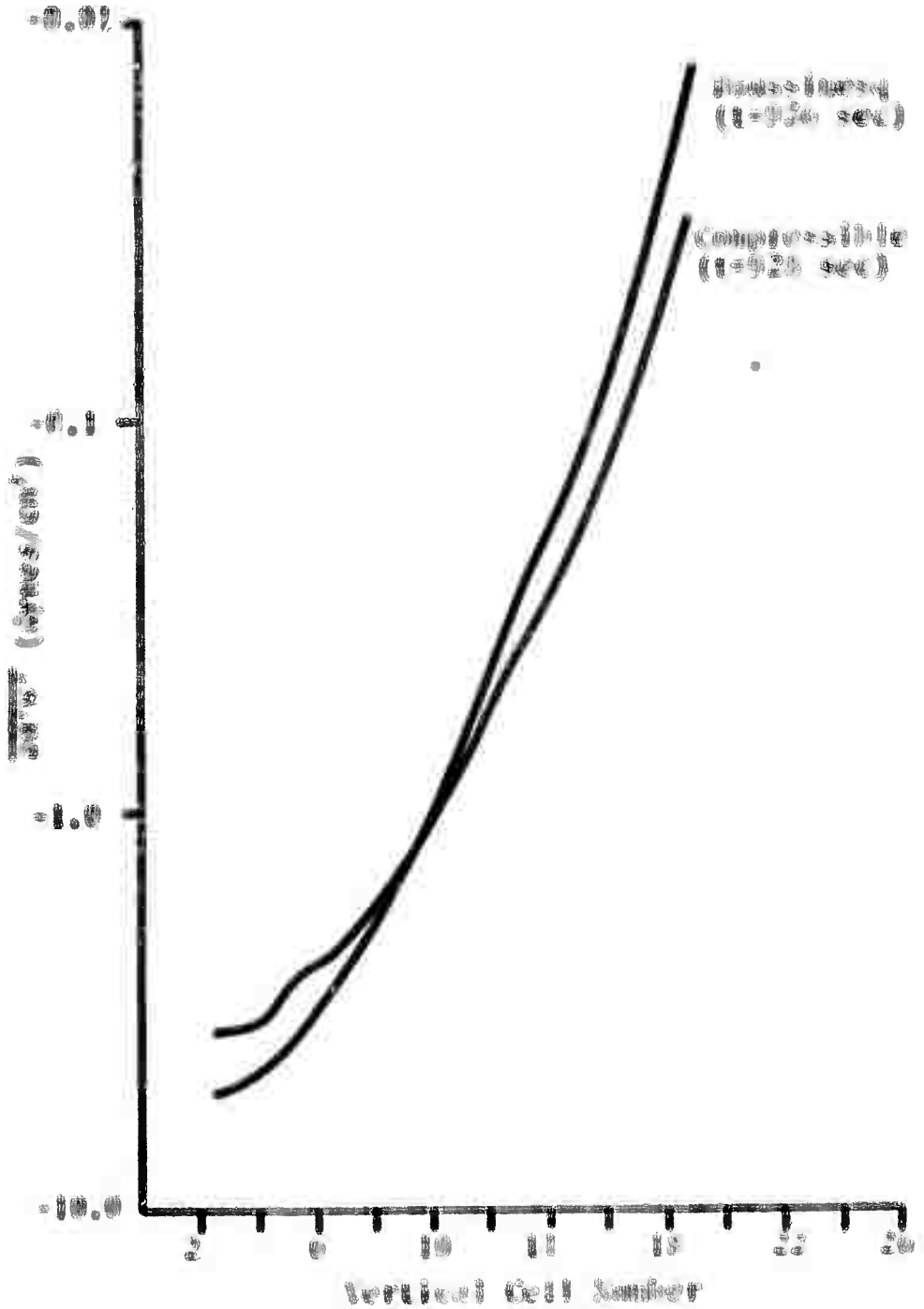

Figure 3.1. Momentum flux as a function of vertical height centered over the obstacle. (time = 1000 sec)

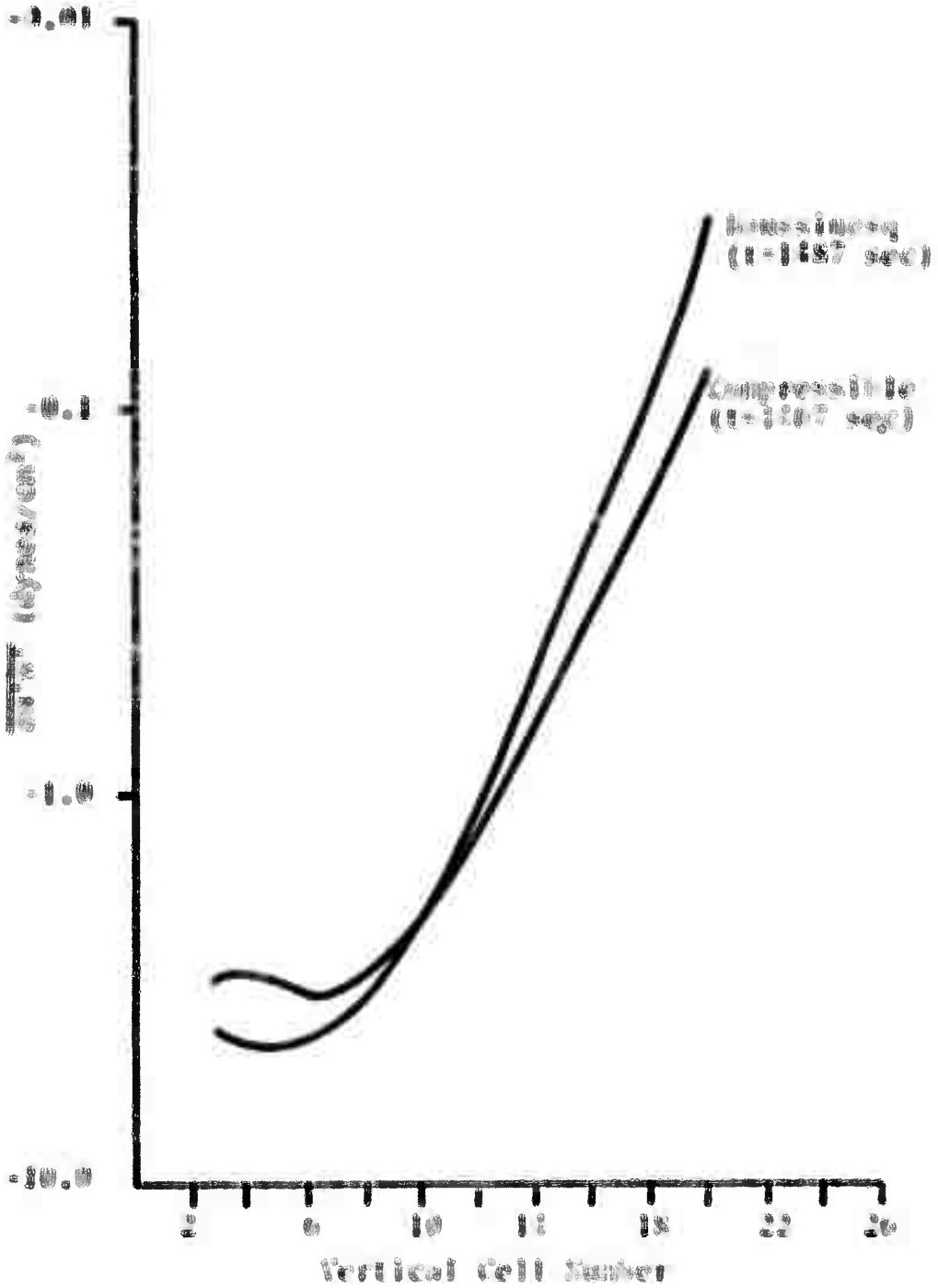

Figure 3.5. Momentum flux as a function of vertical height centered over the obstacle. (time = 1500 sec)

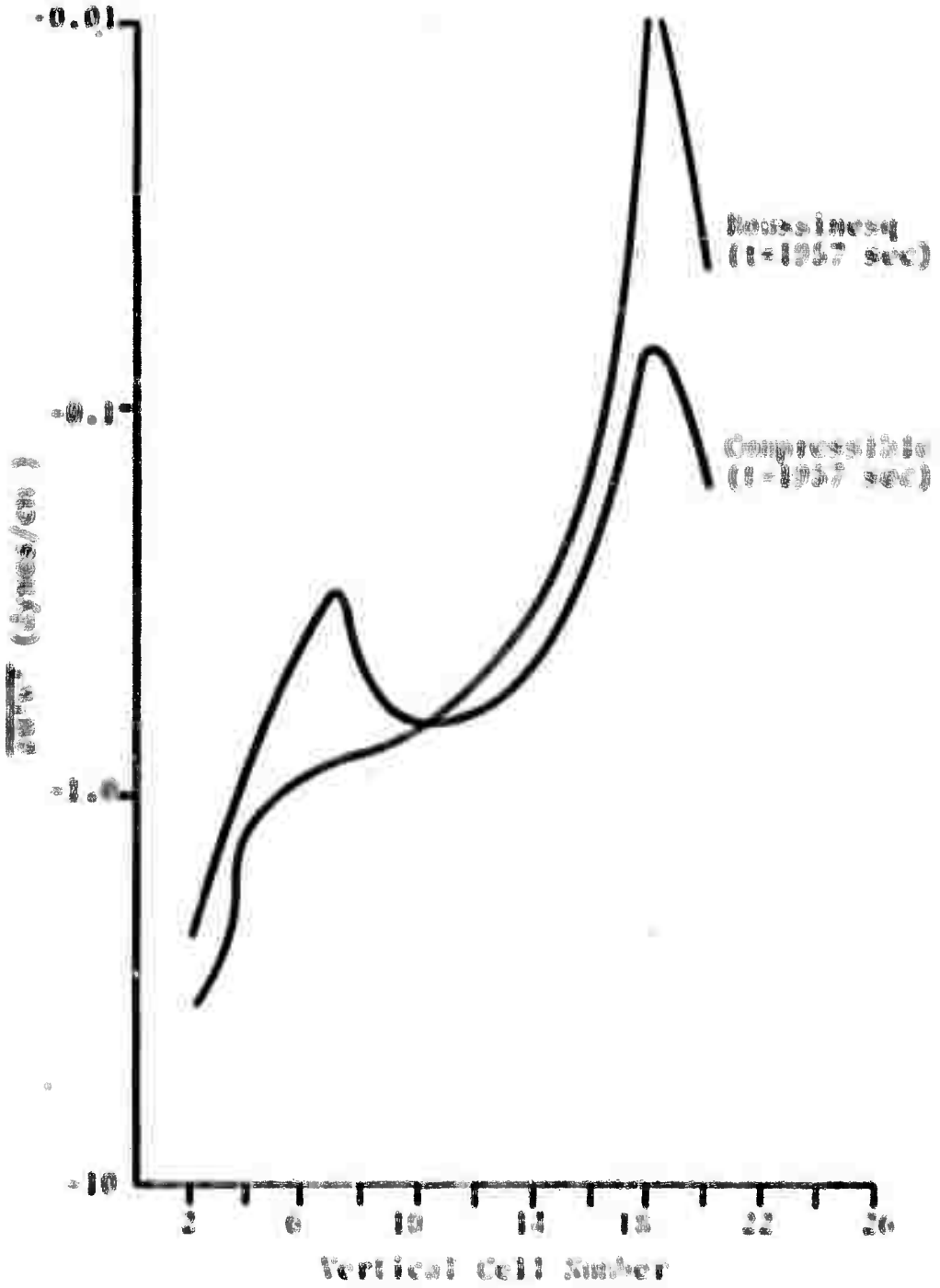

Figure 3.6. Momentum flux as a function of vertical height centered over the obstacle. (time = 2000 sec)

3.1.5.2 Numerical Stability – The stability of the compressible finite difference equations is not well understood at this time. Originally, the time-step criterion of the Boussinesq formulation,

$$\Delta t < \min\left(\frac{\Delta x}{u_{max}} , \frac{\Delta z}{w_{max}}\right)$$

was also used for the compressible equations. In some instances, calculational instabilities developed. Lacking a comprehensive stability analysis upon which to base new time-step criteria, sensitivity experiments were performed in an attempt to bound the stable range for the compressible code. A quantity $\alpha < 1.0$ defined by

$$\Delta t_{compr} = \alpha \Delta t_{boussinesq}$$

was introduced in an attempt to simplify the investigation. This approach did not yield useful results, as α proved to be highly problem dependent. Indeed, values as small as $\alpha = 0.2$ have failed to provide a stable compressible solution in some cases.

Surprisingly, the major stability problems have been observed in the regions of highest speed flow, which typically are the uppermost portions of the calculational grid for many atmospheric test problems. This is true, for example, of the two wave test problem of this section. Further, the effects of most interest in code comparisons for the two wave problem take place near the obstacle, far removed from the upper atmosphere. This suggested another approach; the introduction of strong artificial diffusion in the upper cells of the grid, forcing the solution there to become spatially

smoothed. While the use of diffusion proved successful in this application, not enough is known yet about the stability characteristics of the compressible formulation. Further theoretical and numerical research is warranted in this area, both to improve the accuracy and economics of the compressible formulation, and to advance understanding of atmospheric meso-scale codes.

3.2 MOISTURE EFFECTS

Atmospheric water in the form of water vapor, cloud water, and precipitation may have important effects on the characteristics of gravity waves caused by mountains. Lee waves are frequently accompanied by clouds which can be expected to modify the stability of the air through the presence of the latent heat of condensation which the cloud water adds to the air. Consequently, the terms resulting in changes of stability of the air in which clouds are forming are of primary interest.

The development of a code to determine the effects of moisture on the equations for a Boussinesq fluid is essentially complete. The differential equations describing the physical problem have been reported previously.[11] The HAIFA equations have been modified to incorporate the following changes:

(1) the momentum equation incorporates the effects of moisture in the buoyancy term,

(2) the equation of state for air takes account of a water vapor component,

(3) the energy equation includes energy changes equivalent to the latent heat of water being given to or taken from the air,

(4) an equation is added to account for the conservation of all moisture except rain water, and

(5) a conservation equation is added which governs the rain water content in the atmosphere including sources and sinks at the boundaries.

The differential equations are outlined below. All terms are defined in the nomenclature list.

$$\nabla^2\psi = \eta \quad , \tag{3.12}$$

$$\frac{\partial T''}{\partial t} + u\frac{\partial T''}{\partial x} + w\frac{\partial T''}{\partial z} = -w\Gamma \quad , \tag{3.13}$$

$$\begin{aligned}\frac{\partial \eta}{\partial t} + u\frac{\partial \eta}{\partial x} + w\frac{\partial \eta}{\partial z} = &-\frac{g}{T_o}(1 + \ell_c + \ell_r)\frac{\partial T''}{\partial x} \\ &+ \frac{g}{T_o}\frac{L}{C_p}(1 + \ell_c + \ell_r)\frac{\partial r}{\partial x} + g\left(\frac{\partial \ell_c}{\partial x} + \frac{\partial \ell_r}{\partial x}\right) \quad ,\end{aligned} \tag{3.14}$$

$$\begin{aligned}\frac{\partial \ell_r}{\partial t} - \ell_r\frac{\partial V_t}{\partial x} - \frac{\ell_r V_t}{\rho}\frac{\partial \rho}{\partial x} - \ell_r\frac{\partial V_t}{\partial z} - \frac{\ell_r V_t}{\rho}\frac{\partial \rho}{\partial z} \\ + u\frac{\partial \ell_r}{\partial x} + w\frac{\partial \ell_r}{\partial z} - V_t\left[\frac{\partial \ell_r}{\partial x} + \frac{\partial \ell_r}{\partial z}\right] = P_r \quad ,\end{aligned} \tag{3.15}$$

$$\frac{\partial q}{\partial t} + u\frac{\partial q}{\partial x} + w\frac{\partial q}{\partial z} = -\ell_r \frac{\partial V_t}{\partial x} - p_r \quad , \qquad (3.16)$$

where p_r = source terms for the conversion of water substance to rain water. These source terms are described in detail in a following section of this report.

3.2.1 Integration of the Finite Difference Equations

The Eqs. (3.12) through (3.16) are written in finite difference form and integrated numerically in a similar manner to the HAIFA equations.

The basic scheme used in the integration is shown in Figure 3.7. The locations of the major variables with respect to the grid cells are shown in Figure 3.8.

3.2.1.1 The Advection Scheme – The advection terms for vorticity, water vapor content and rain water are calculated using the second order scheme of Crowley. The scheme is written in conservation form and is based on a forward time difference and centered space differences. Test calculations performed by Crowley indicated that for the same order of accuracy, the conservation form produced more accurate solutions than the advection form.

In the conservation form, the time derivative and advection terms of the vorticity, temperature, or moisture equations may be written as

$$\frac{\partial \alpha}{\partial t} + \frac{\partial (u\alpha)}{\partial x} + \frac{\partial (v\alpha)}{\partial z} = S \quad ,$$

where α represents T, η, q, or ℓ_r and S is the source term.

STEP 1	Initial values of temperature, vorticity, velocities and water content are specified.
STEP 2	Set water vapor content calculated and initial water content values are redistributed as rain water, clouds and vapor.
STEP 3	New values of temperature, rain water, water content other than rain water, and vorticity are obtained accounting for the advection terms only.
STEP 4	Vorticity, water content and rain water are updated to time t^{n+1} by evaluating source terms with the quantities obtained in Step 3.
STEP 5	The Poisson equation is solved for ψ using values of η at t^{n+1}.
STEP 6	Velocities are updated using ψ values from Step 4. Initial data for a new cycle are now available for edit or continuation of the calculation beginning at Step 2.

Figure 3.7. HAIFA*MOISTURE calculation sequence used in numerical integration of Eqs. (3.12) through (3.16).

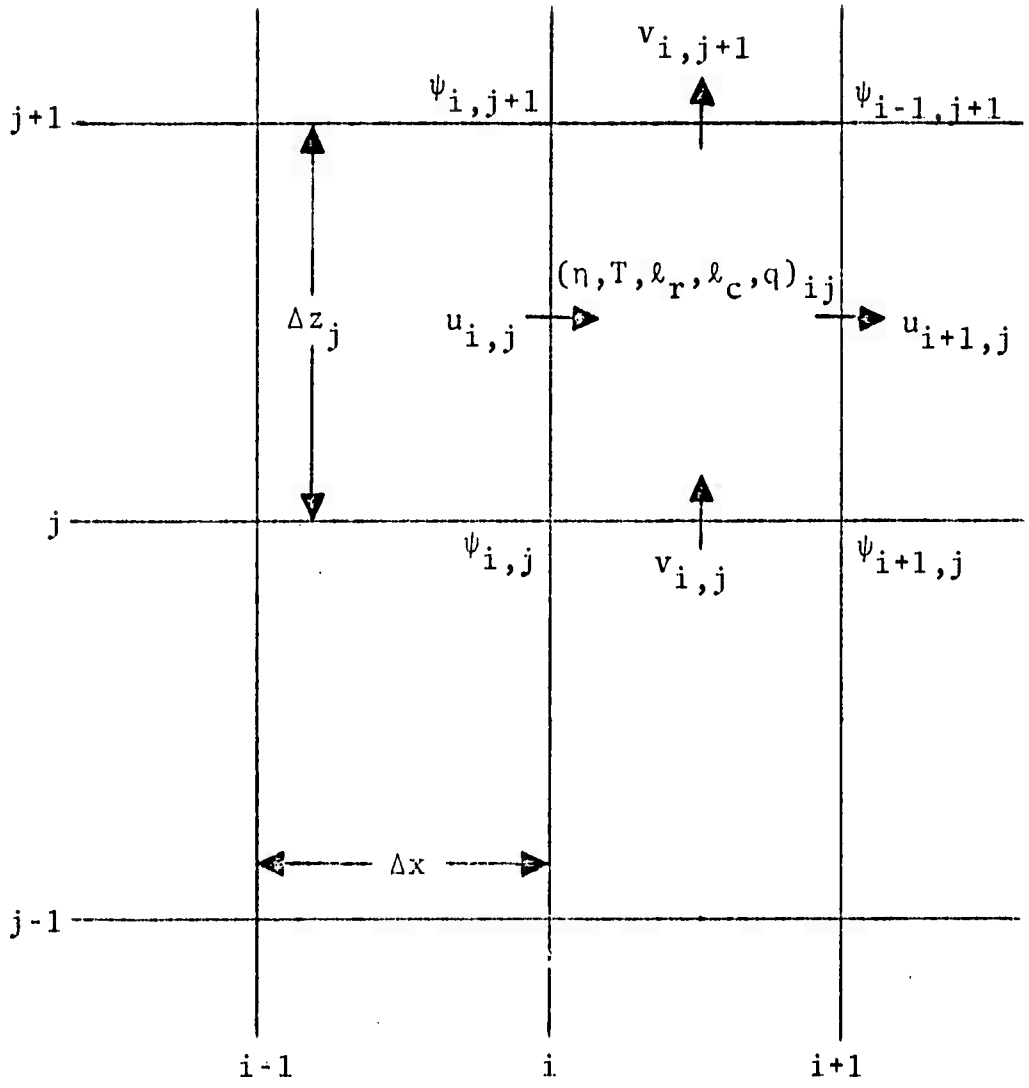

Figure 3.8. Finite difference grid -- HAIFA*MOISTURE.

In two dimensions a splitting technique is used; the calculational scheme calls for solving two one-dimensional equations sequentially. First, the net flux of vorticity or temperature is solved for in the horizontal, the quantity solved for in the zone being updated due to this flux. The procedure is then repeated in the vertical direction using the partially updated values from the horizontal calculation.

The temperature equation is transformed from the form shown in Eq. (3.13) in order to write it in conservation form. A new variable β is defined, at $T'' + \Gamma z$. Since Γ is at most a function of z only, Eq. (3.13) then becomes

$$\frac{\partial \beta}{\partial t} + u\frac{\partial \beta}{\partial x} + w\frac{\partial \beta}{\partial z} = 0 \quad .$$

In this manner, only the advection scheme is required to update the temperature since all source terms have been removed. Solving the temperature equation in conservation form should increase the accuracy of the solution.

3.2.1.2 Changes in Vorticity and Water Content Due to Other Terms in the Conservation Equations – All source terms in Eqs. (3.14) through (3.16) are evaluated as zone centered quantities containing centered space differences. Update takes place after the effects of advection have been calculated.

3.2.2 Moisture Equation Source Terms

The source terms in the conservation equations (3.12) through (3.16) depend on complicated physical processes which have been parameterized from experimental measurement data. These include the terminal velocity of rain drops, the

equilibrium vapor pressure of water, and several constants dealing with the water production term. Parametric representations of these terms are given below; we have attempted to obtain the most comprehensive results available but we have not yet performed critical evaluations of these terms.

3.2.2.1 Terminal Velocity – The terminal velocity of rain drops is given by

$$V_t = 5.32(\ell_r)^{1/5}$$

where V_t is in m/sec and ℓ_r in gm/Kgm .

This expression, derived by Liu and Orville[8] has been compared to data from the Smithsonian Meteorological Tables[9] and an expression developed by Srivastava.[10]

3.2.2.2 Saturation Vapor Pressure – The saturation vapor pressure is defined as

$$e_s = 6.11 \times 10^{7.5(\tilde{T}_o - 2.73)/(\tilde{T}_o - 36)} \text{ millibars}$$

where $\tilde{T}_o = T_o - gz/C_p$ and r_s , the saturated water vapor mixing ratio in gm/Kg, is given by

$$r_s = \frac{R\, e_s(T_o)}{R_v\, p_o(z)} \exp \frac{L(T'' - L_r/C_p)}{R_v\, T_o^2} \quad .$$

Both expressions are obtained from the work of Orville,[8,11] Ogura,[12] and Ogura and Phillips.[13]

3.2.2.3 Water Production Term – The water production consists of three physical phenomena which can add to, subtract from, or change the state of the water in the atmosphere. This includes (1) the evaporation of rain water outside the clouds, (2) the conversion of cloud water to rain water, and (3) the growth of rain through coalescence. These terms were originally expressed in Orville's work as

$$P_r = \beta(r-r_s) + \alpha(r_c-r_{c_r}) + 4.0 \times 10^{-3} r_c(r_r)^{0.95} \quad .$$

During our initial test calculations, it was discovered that treating β, the evaporation parameter, as a constant led to computational difficulties. This term was modified to agree with that used in Kessler's work[14] which expressed β as

$$\beta = 3.807 \times 10^{-8}(\rho r_r)^{0.65} \quad .$$

3.2.2.4 Density of Air Containing Water Vapor – The equation of state utilized is that of a perfect gas consisting of air and water vapor. The expression is

$$p = \rho RT\left[\frac{1 + r/m}{1 + r}\right]$$

where m is the ratio of the molecular weight of water and dry air. The pressure p is treated as $p_0(z)$, the initial atmospheric distribution, while T and r are allowed to vary in both the horizontal and vertical directions.

3.2.3 Test Problem

The test problem selected for the moisture code was chosen such that the initial water vapor content input into the atmosphere was an amount equal to the saturated value calculated by the prescription described in Section 3.2.2. The configuration of the problem was identical to the two wave problem described in Ref. 1, i.e., an obstacle height of 625 meters and a cell height of 312.5 meters. All other variables are identical to those described for the two wave problem of Section 2.

The results of the calculation, run to a time of 1672 seconds, are shown in Figures 3.9 through 3.12. These include streamlines, vertical velocity contours, cloud water contours and rain water contours. The formation of the clouds and their movement downwind of the obstacle as a function of time is realistic physically.

Figures 3.13 and 3.14 show vertical velocity contour plots from the computer printouts at times of 1673 and 1669 seconds for the moisture and dry calculations, respectively. The numbers on the figures indicate the relative velocity in each region, i.e., the larger numbers represent positive velocities while the lower numbers represent the negative velocities.

As the computer results were compared at various times, the buoyancy forces caused by the condensation or evaporation of water as air rises or falls over the obstacle became apparent. As the air rose at the forward position of the mountain, water vapor condensed out creating a positive buoyancy force and an increase in vertical air velocity due to its rise in temperature. As the cloud water falls in the lee of the obstacle, energy is removed from the air, dropping

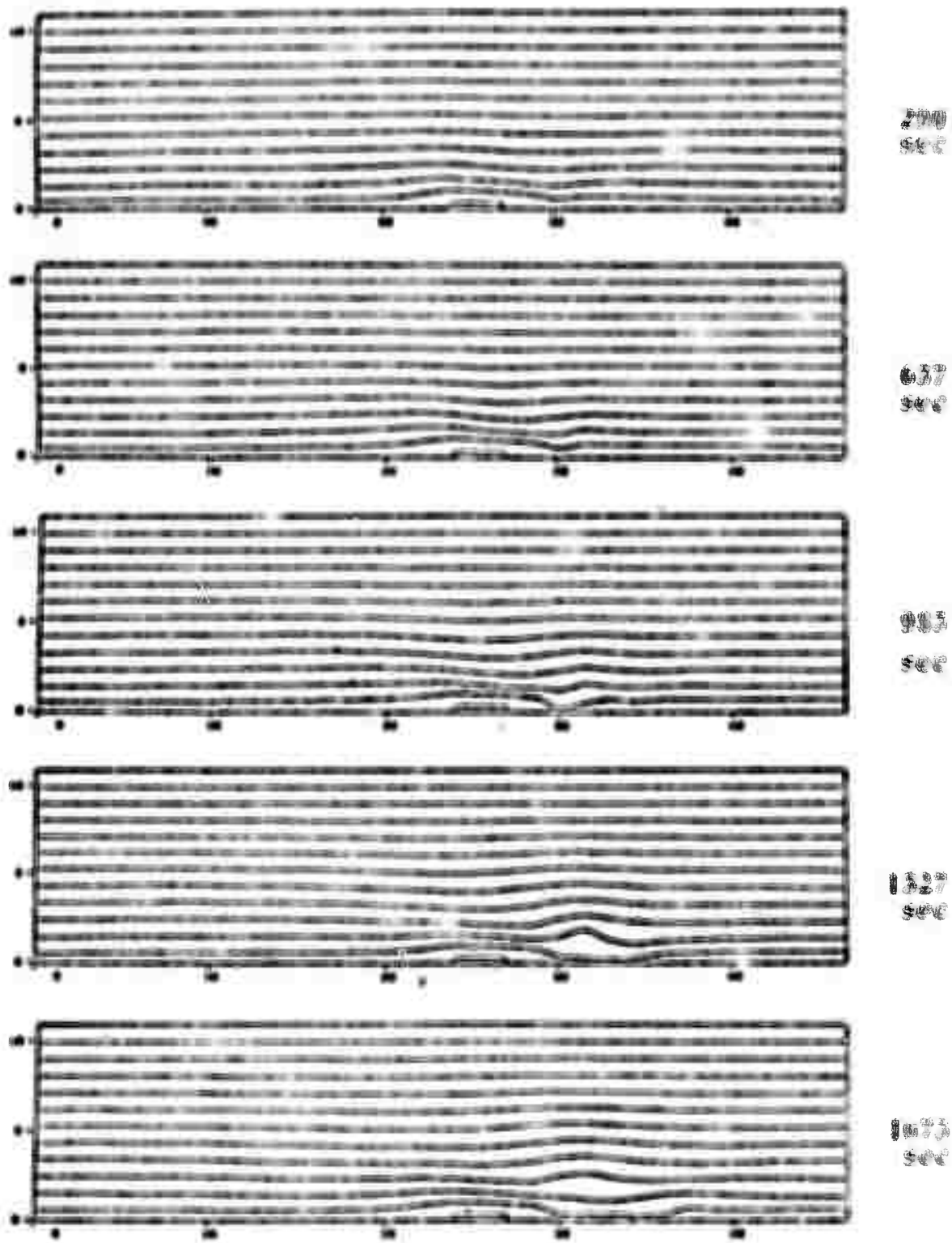

Figure 3.9. Streamline pattern - two wave problem with moisture effects.

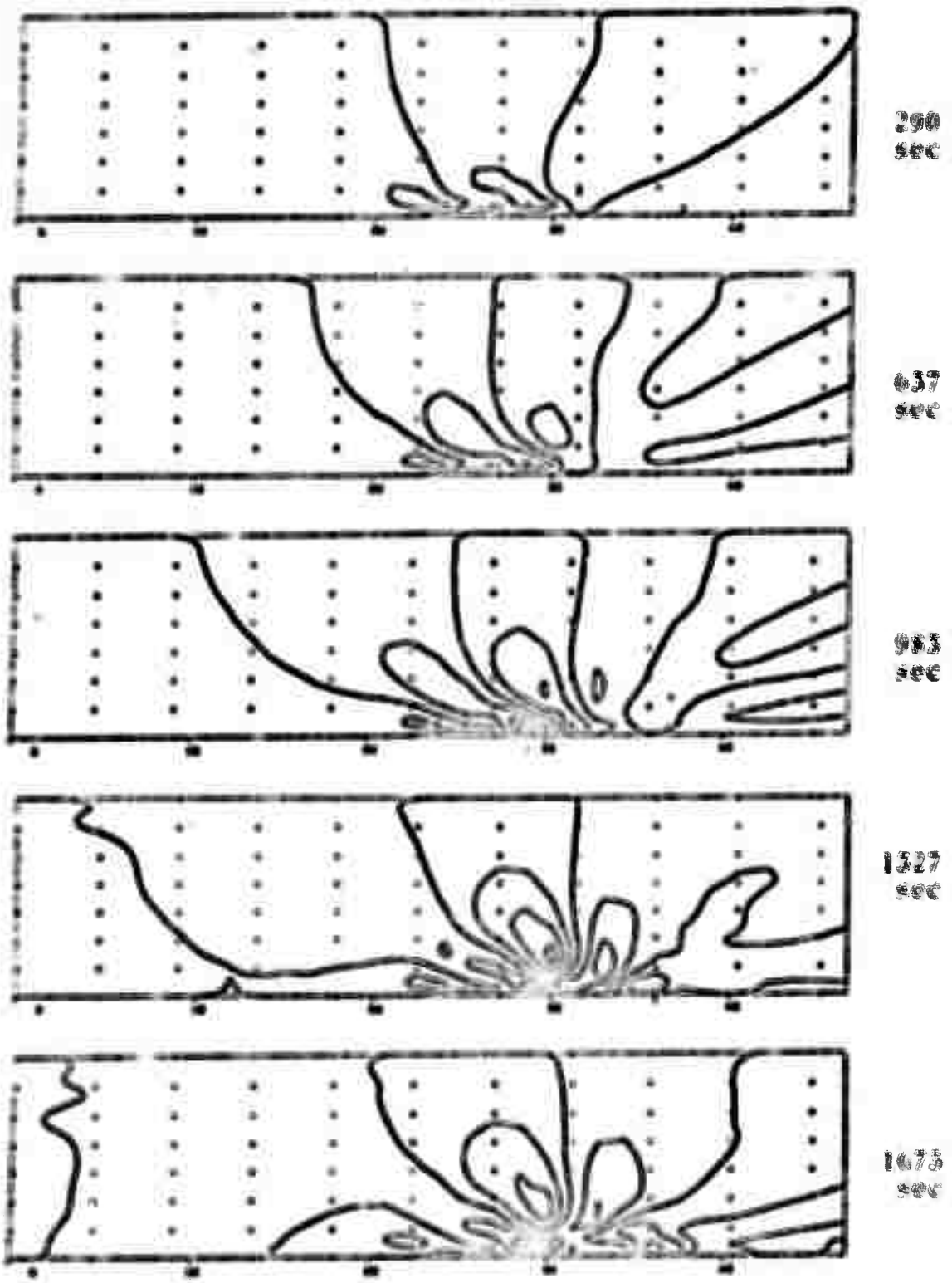

Figure 5.10. Vertical velocity contours – two wave problem with moisture effects.

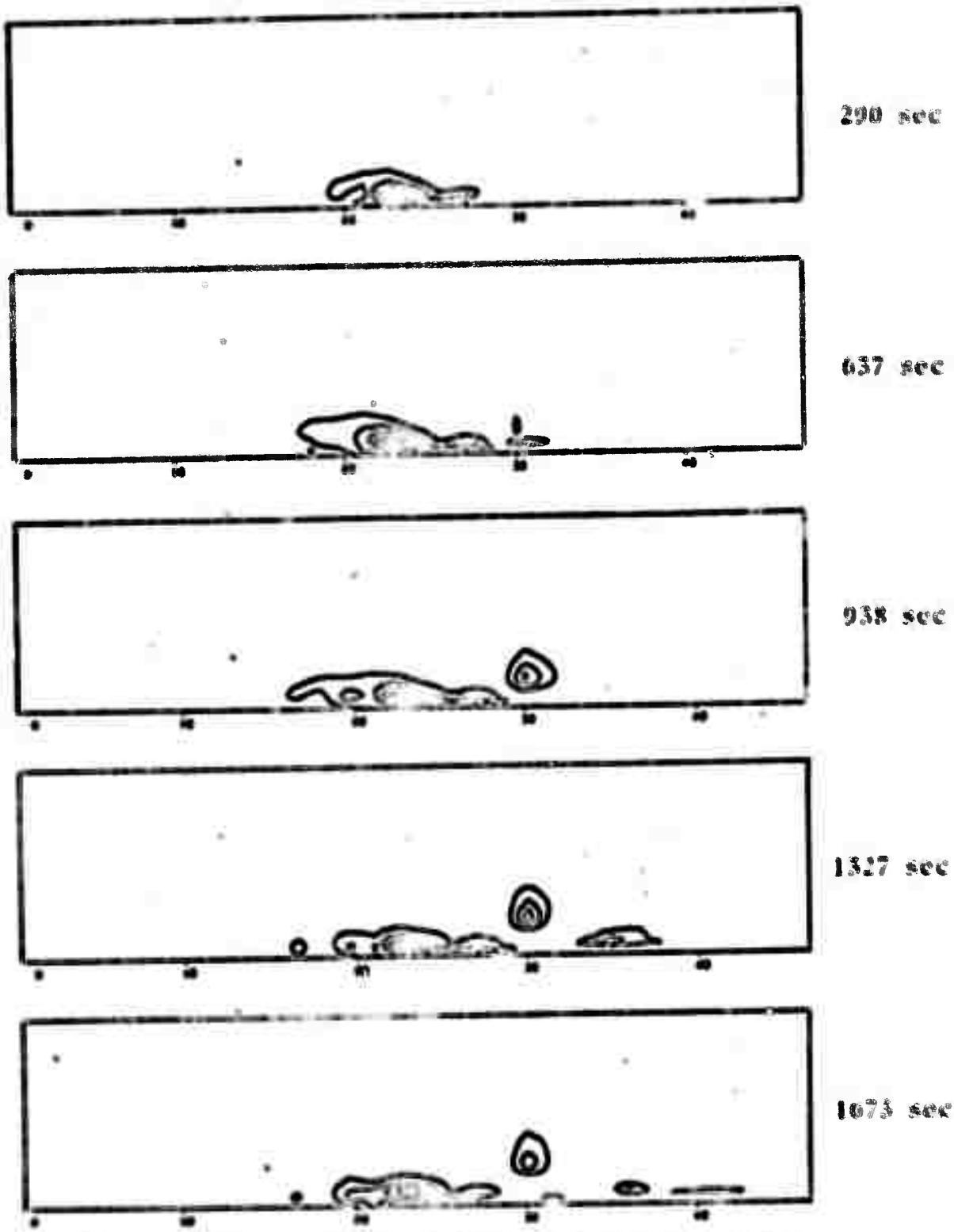

Figure 3.11. Cloud formation – two wave problem with moisture effects.

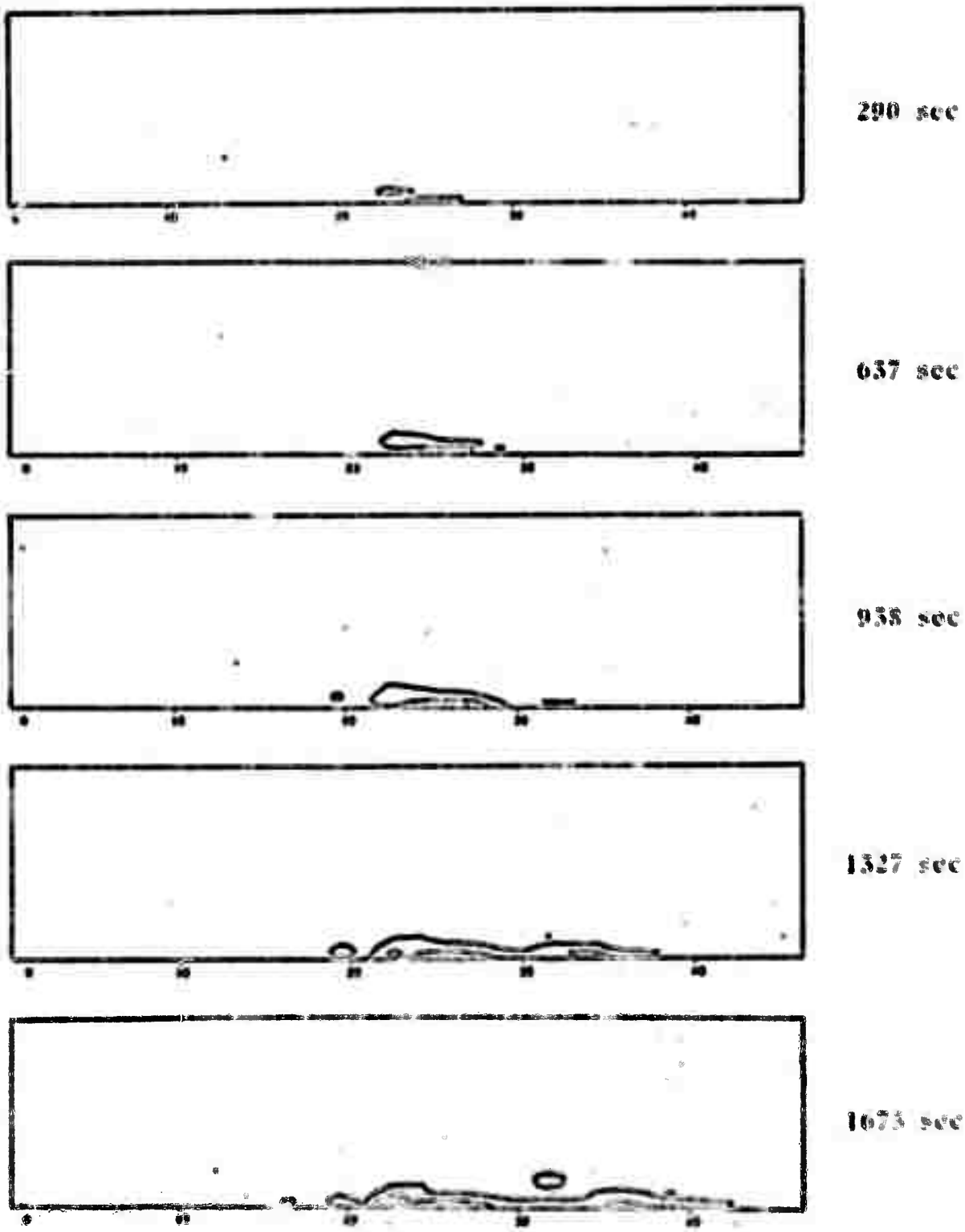

Figure 3.12. Rain water contours – Two wave problem with moisture effects.

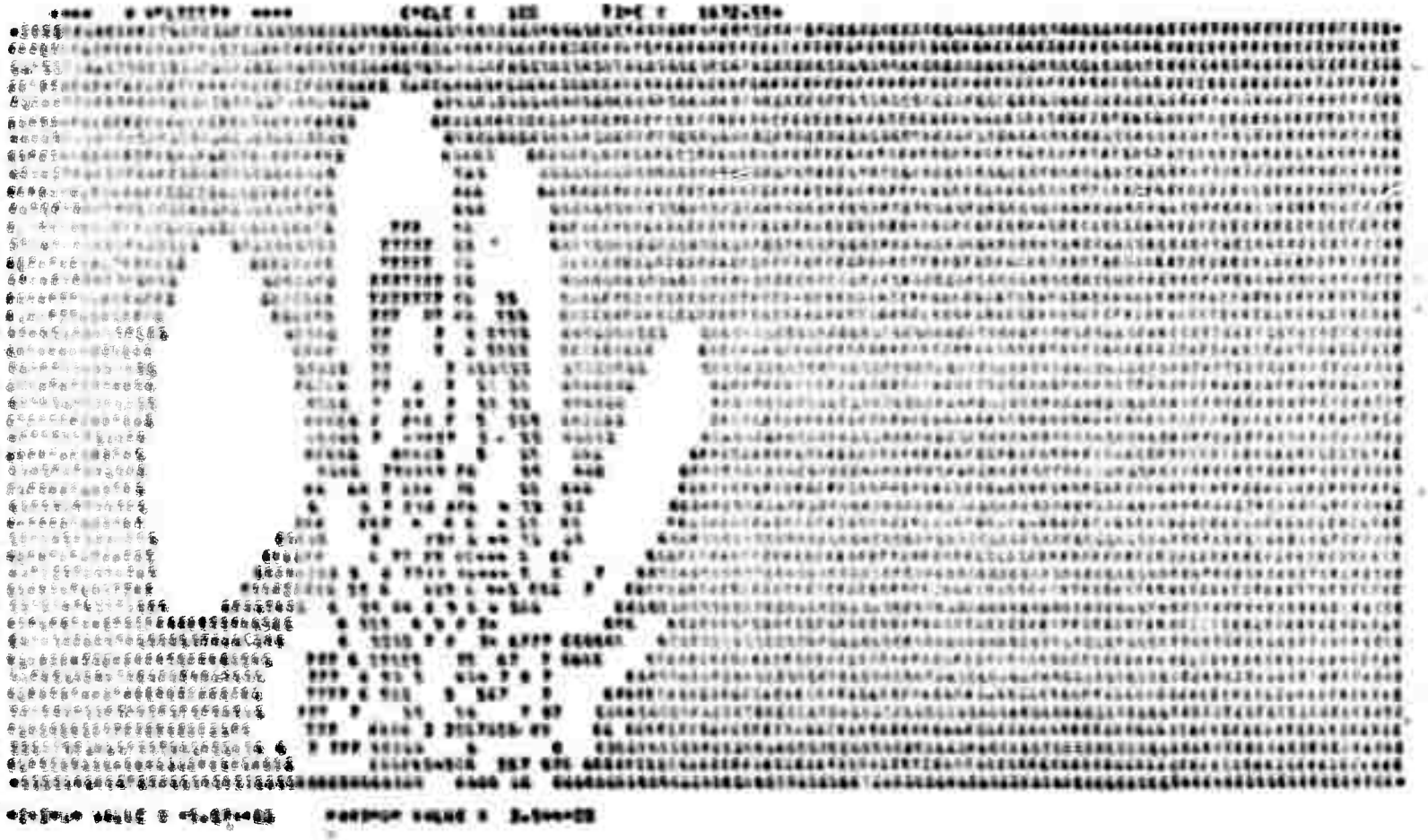

Figure 3.13. Computer plots of vertical velocity contours – Two wave problem with moisture effects.

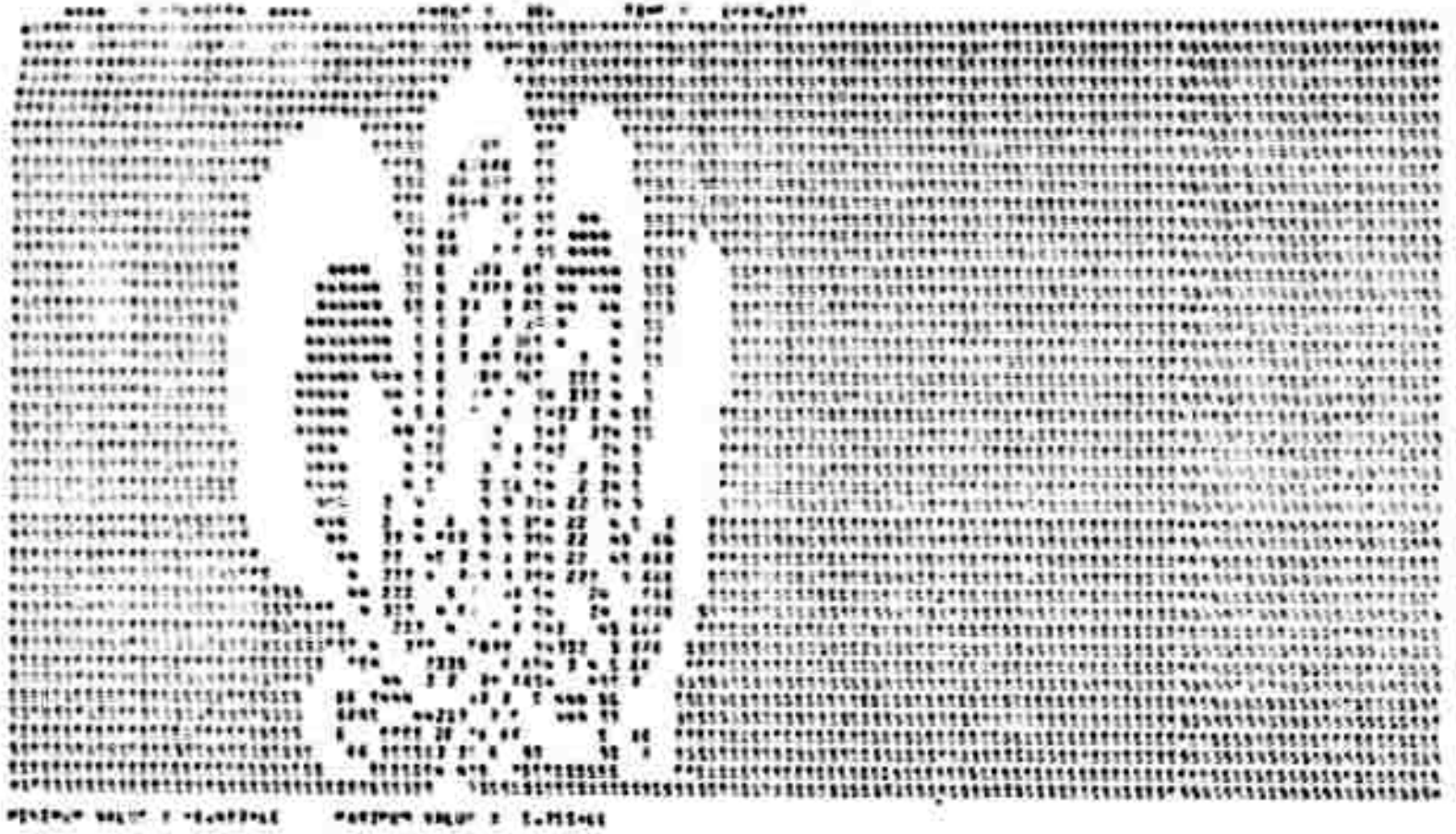

Figure 5.14. Computer plot of vertical velocity contours – Two wave problem.

its temperature and a stronger downdrift is created. These phenomena effect the velocity profiles in different ways at various times.

The momentum flux results shown in Figure 3.15 indicates only minor differences in drag between the moist and dry cases. However, since the problem has only been run a short time, the results do not necessarily reflect those expected near steady state.

3.3 HAIFA WITH VARIABLE VERTICAL ZONING

The modification discussed in the previous semiannual (to the basic HAIFA code) enabling it to operate using a grid mesh of variable spacing in the vertical direction was completed. Three test problems were performed using a 625 meter high mountain similar to the single wave problem described in Ref. 1. The initial inpnt to this problem was (1) a temperature lapse rate equal to one-half the dry adiabatic, (2) an obstacle measuring 625 meters high by 4500 meters long and (3) an exponential horizontal velocity profile described by the equation

$$u = 9.94 \exp (1.795 \times 10^{-4} z) \quad .$$

Two of the test problems used constant vertical grid heights and the standard HAIFA code. The grid heights were 312.5 meters and 208.5 meters. The results were compared with a third problem run using a variable vertical grid size. This grid varied from 125 meters near the lower boundary to 758 meters at the upper boundary. The total number of vertical zones in all three calculations was the same.

Figures 3.16 and 3.17 contain the detailed comparison for the Δz = 312.5 meter problem and the variable Δz problem

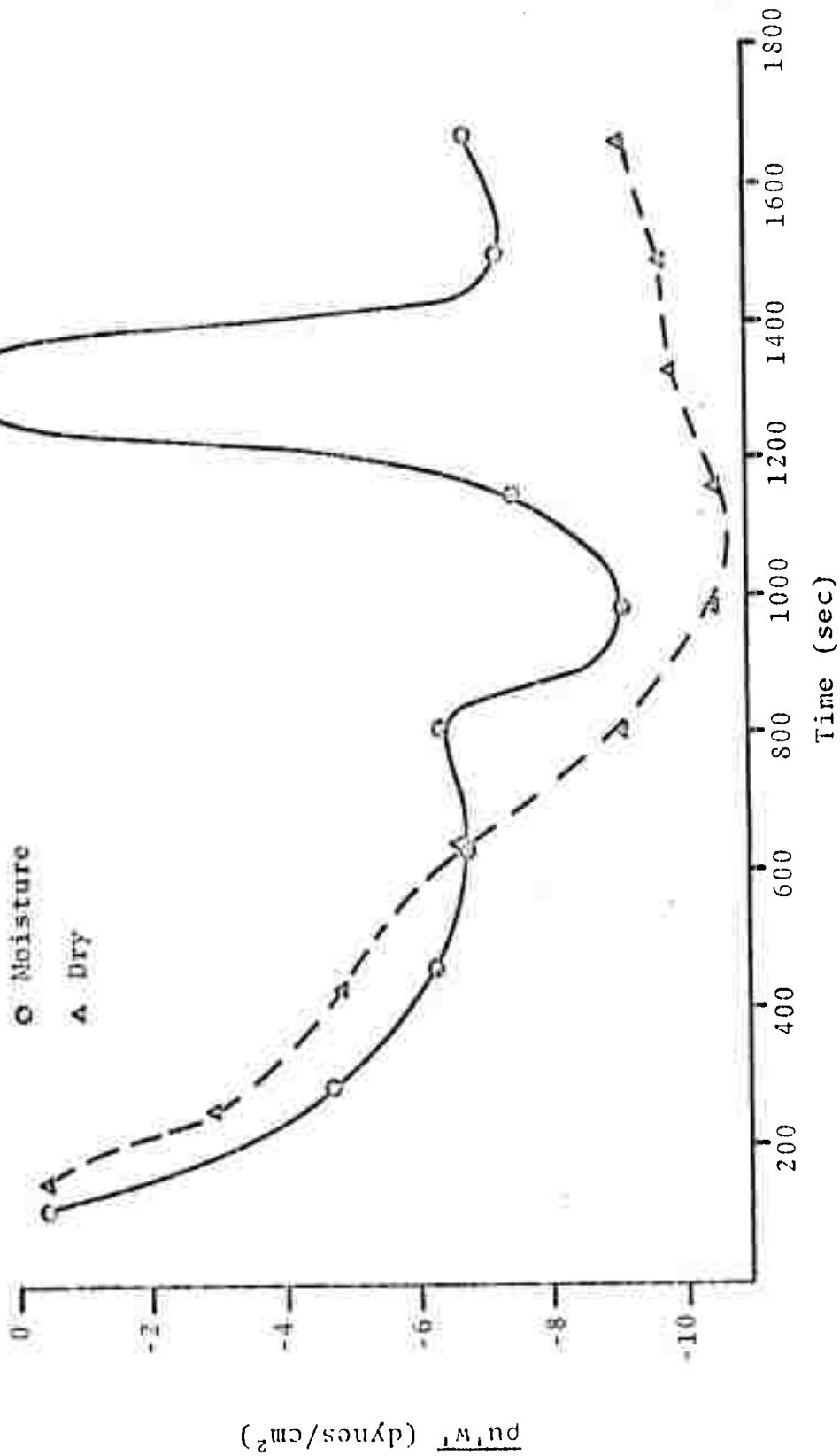

Figure 3.15. Comparison of two wave problem with and without moisture momentum transfer above obstacle.

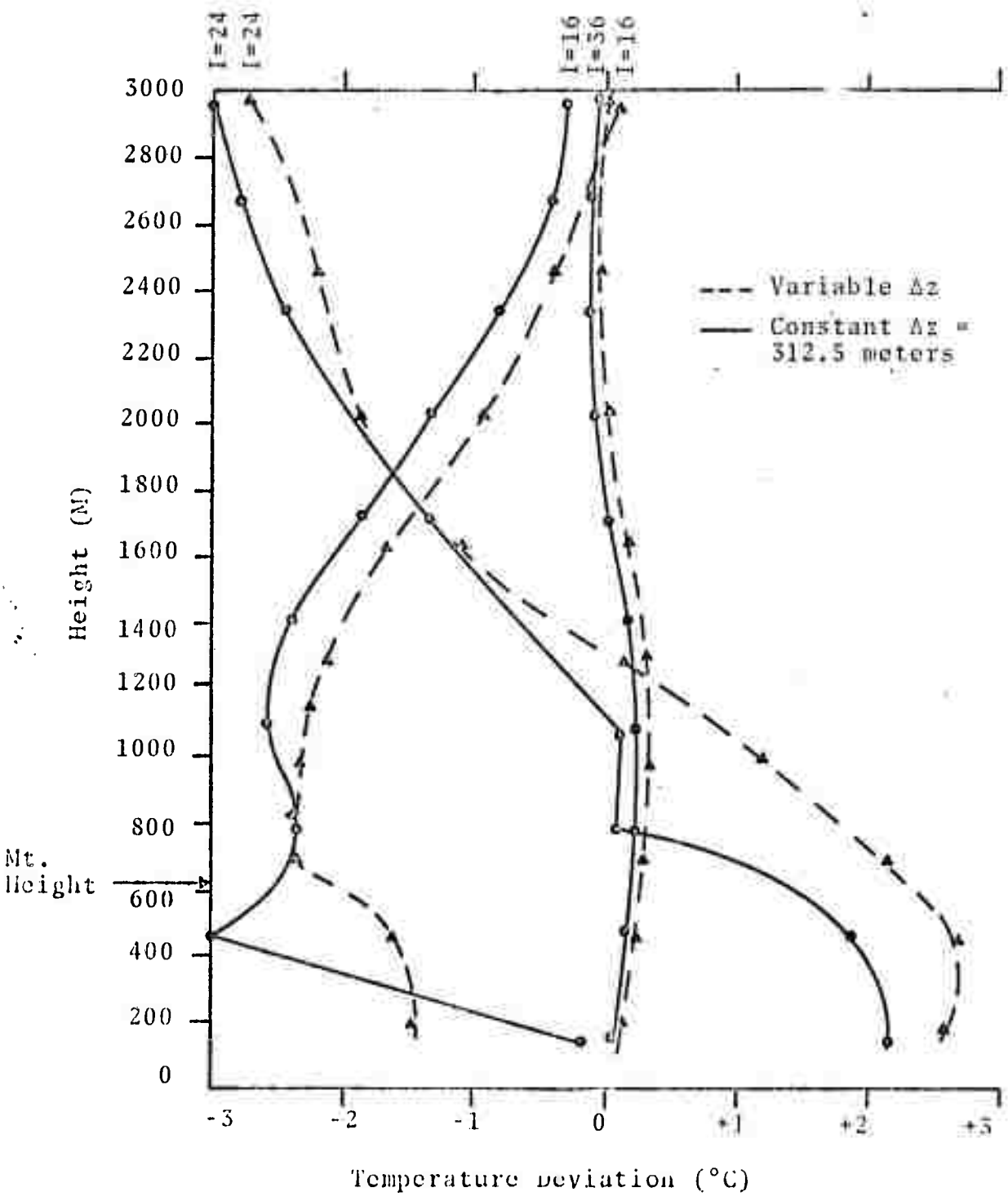

Figure 3.16. Comparison of variable Δz and constant Δz HAIFA — temperature deviations.

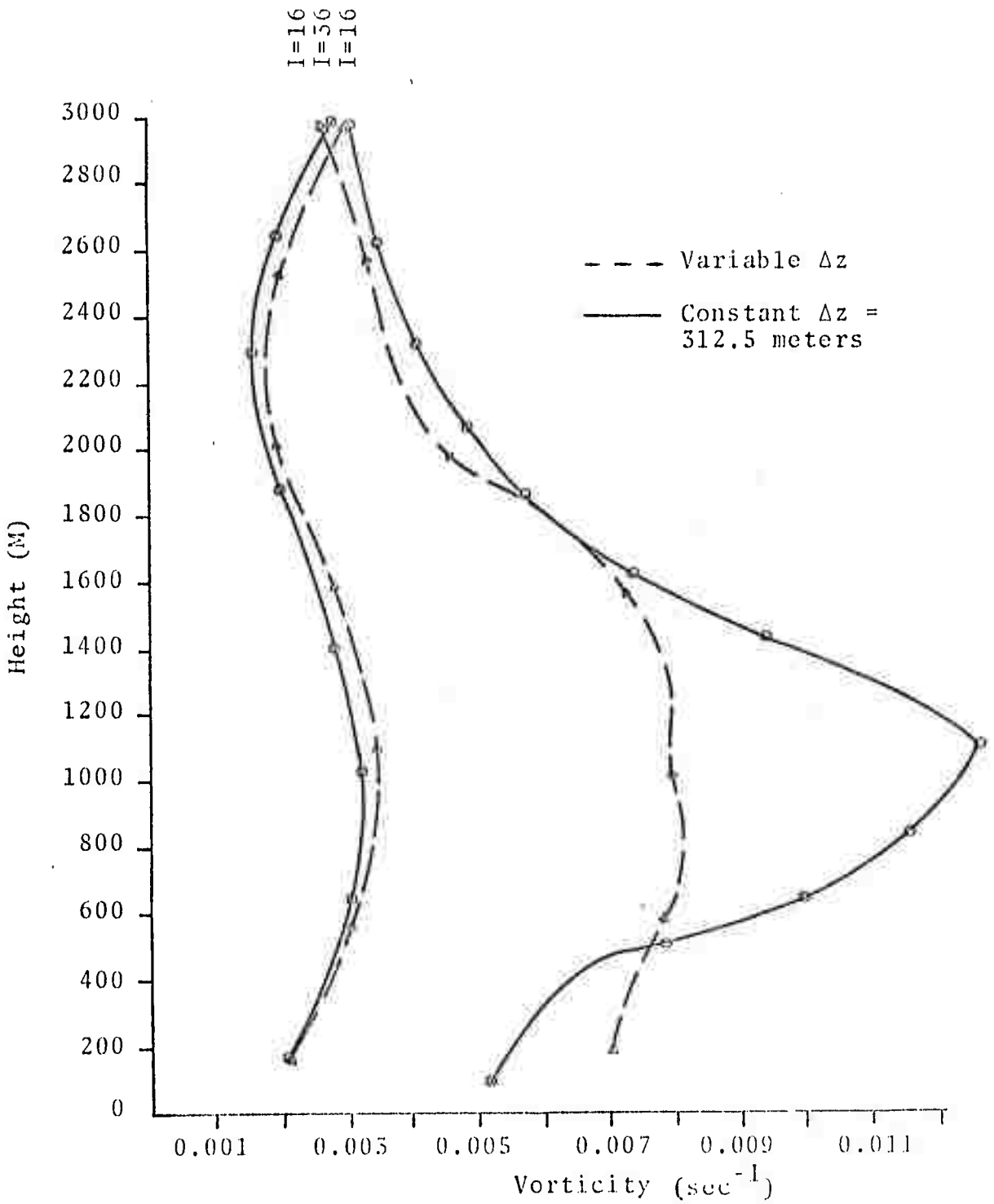

Figure 3.17a. Comparison of variable Δz and constant Δz HAIFA – vorticity.

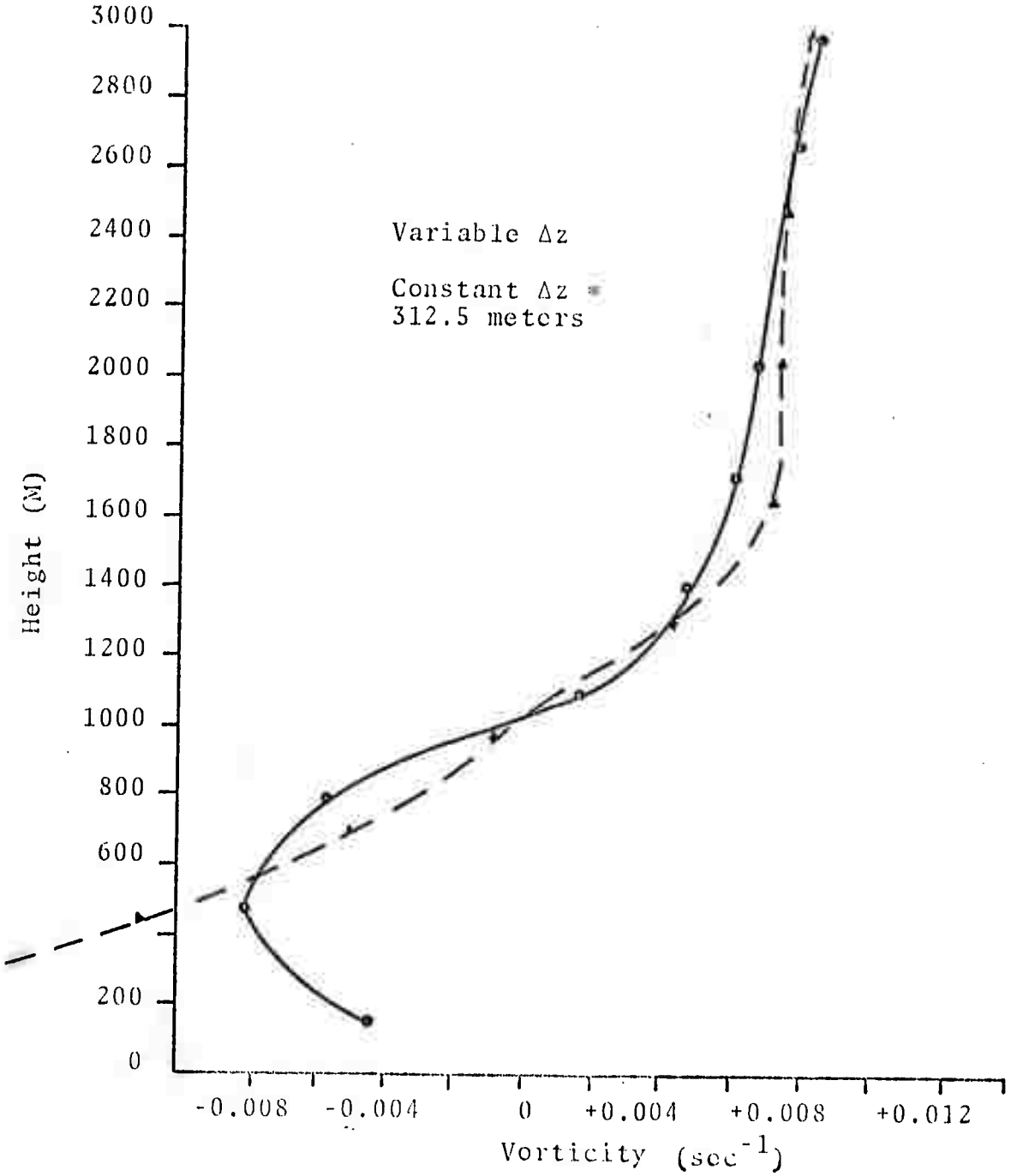

Figure 3.17b. Comparison of variable Δz and constant Δz HAIFA – vorticity.

of the temperature and vorticity at times of approximately 1500 seconds. Quantities are shown as a function of z for three locations; just upstream of the obstacle (I=16), just downstream of the obstacle (I=24), and far downstream of the obstacle(I=36).

It can be noted that the trends in the results are the same for both problems. However, some differences in the computed values, particularly at small heights, are large. Part of this discrepancy was thought to be due to the smaller grid near the lower boundary. As a result, the problem was re-run using constant Δz equal to 208.3 meters. The results were closer to the variable Δz case indicating that the grid size was playing an important role in the detailed results. Figure 3.18 shows the momentum flux at a height of 781 meters for the three problems as a function of time. The good agreement between the small constant Δz case and the variable Δz problem should be noted. In particular, the cyclic behavior of the drag values is not as pronounced as in the larger zoned case.

These phenomena will continue to be investigated as time for more computations becomes available.

3.4 TREATMENT OF TRIANGULAR ZONES IN HAIFA

In order to characterize mountain slopes by zones other than of rectangular shape, two modifications of the HAIFA code were required: First, cell centered variables were assumed to be located at the centroid of the zones and Crowley's advection scheme was derived for flow between triangular and rectangular cells. Second, the solution of the Poisson equation requires the value of the vorticity at a grid point which is normally obtained from an arithmetic average of the vorticity of the four surrounding cells. This

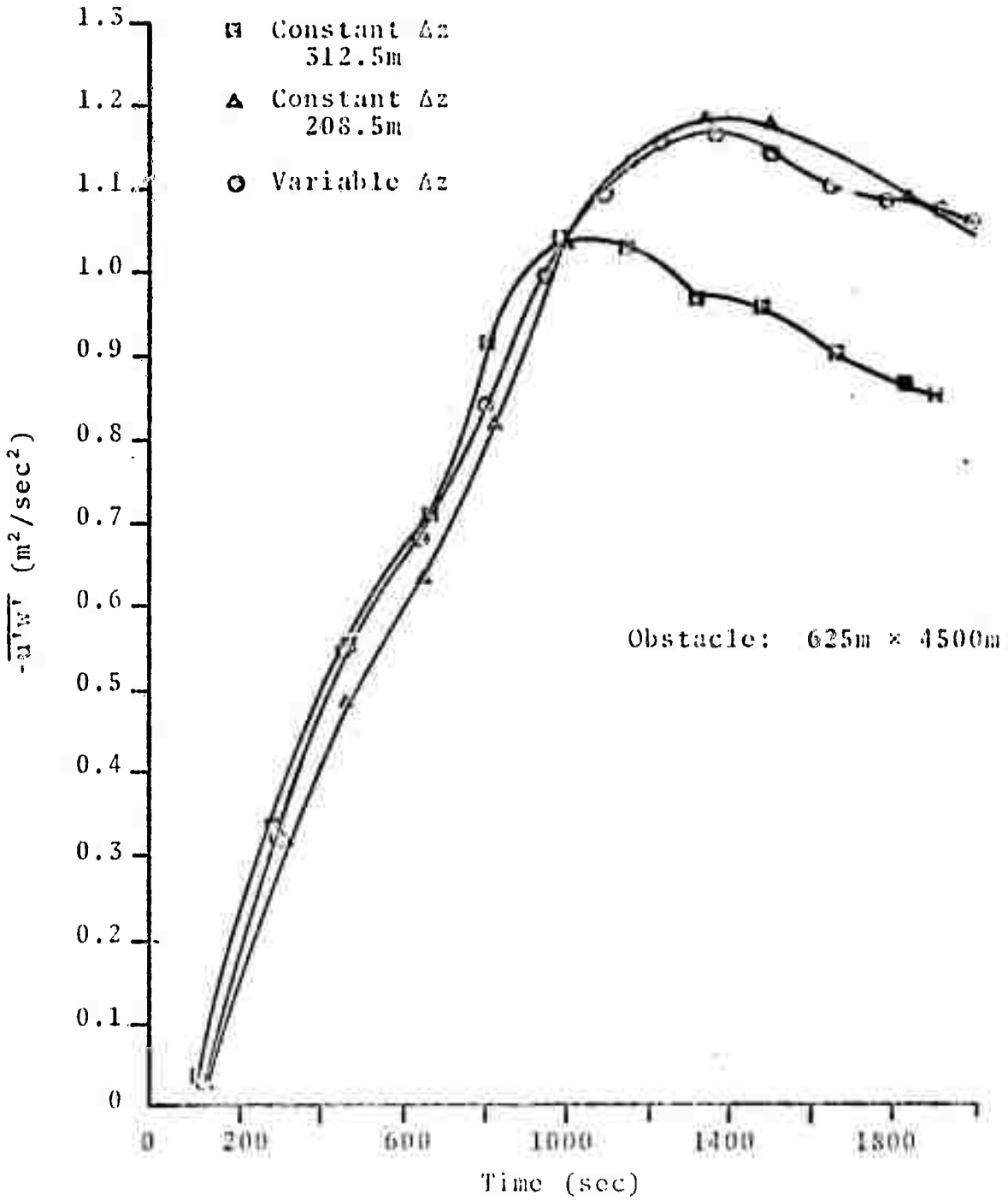

Figure 3.18. Comparison of variable Δz and constant Δz HAIFA codes – momentum flux edits at 781 meters.

average was modified to account for the non-symmetrical positioning of the vorticity. Details of these modifications are described below.

Consider a mountain downslope as shown in the figure below where the diagonal corners a and c are specified as being on the mountain surface and d is internal to the mountain. The fluxes of vorticity and temperature across lines ab and bc are required.

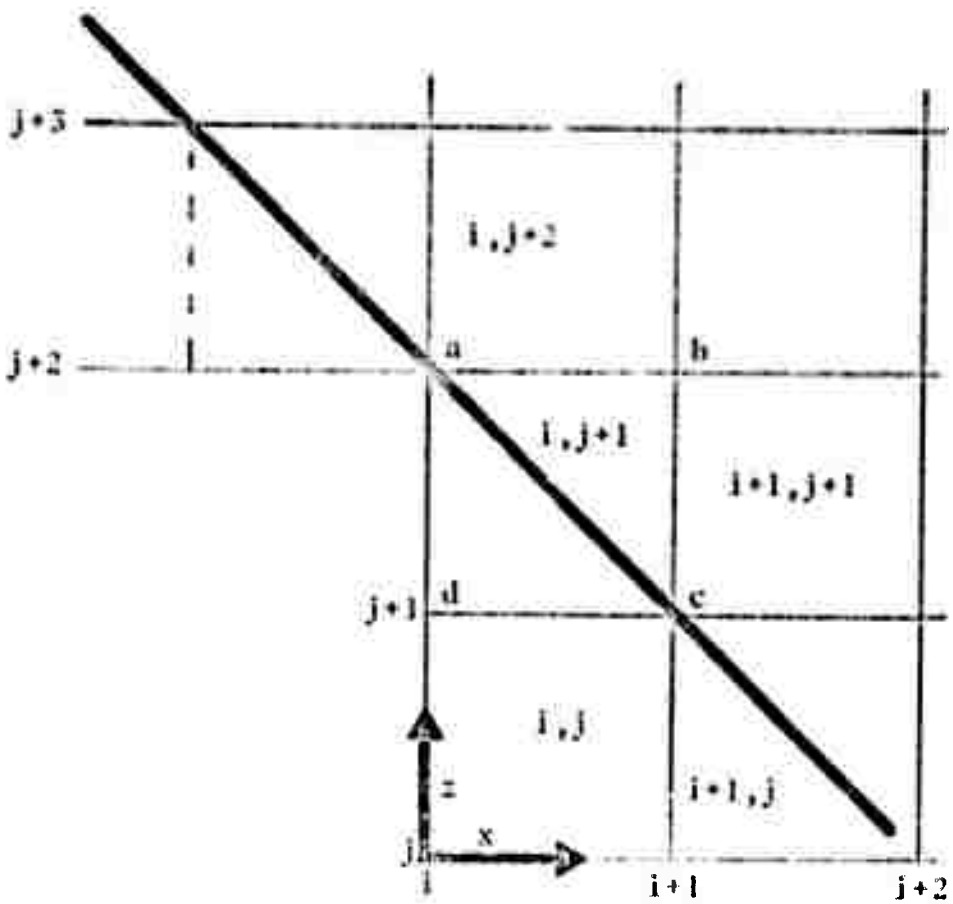

The vorticity and the temperature are specified at the centroid of each grid, and $\psi_a = \psi_c = 0$. For the vertical flux across a,b, the centroids denoted by $\bar{z}, \bar{x}$ for the

adjoining cells are $\bar{z}_{i,j+2} = j + 5/3$, $\bar{z}_{i,j+2} = i + 1/3$, $\bar{z}_{i,j+1} = i + 5/3$ and $\bar{z}_{i,j+1} = i + 2/3$.

A linear relation between the variable, q, to be advected is assumed. In the vertical direction, this may be expressed as:

$$q_{j+2} = \ell + m\, z_{j+5/3}$$

$$q_{j+1} = \ell + m\, z_{j+5/3} \quad .$$

Solving for the values ℓ and m ,

$$m = \frac{q_{j+2} - q_{j+1}}{z_{j+5/3} - z_{j+5/3}}$$

$$\ell = q_{j+1} - m\, z_{j+5/3} \quad .$$

Also,

$$z_{j+5/2} - z_{j+5/3} = \frac{\Delta z_{j+2}}{2} + \frac{\Delta z_{j+1}}{3} \quad .$$

The flux across ab is therefore:

$$F_{ab} = \frac{1}{\Delta t}\int_{z_{j-2}-w_{j-2}}^{z_{j-2}} z\,dz = \frac{1}{\Delta t}\left[\frac{z_{j-2}^2}{2} - \frac{w_{j-2}^2}{2}\right]_{z_{j-2}-w_{j-2}}^{z_{j-2}}$$

$$= \frac{1}{2}w_{j-2} - \frac{1}{2\Delta t}\left(-2z_{j-2}w_{j-2} + w_{j-2}^2\right)$$

$$= w_{j-2}q_{j-1} - w_{j-2}z_{j-2}/\Delta t\,w_{j-2} + w_{j-2}z_{j-2}w_{j-2} - \frac{1}{2}w_{j-2}^2$$

$$= w_{j-2}q_{j-1} - w_{j-2}z_{j-2}w_{j-2} + w_{j-2}\frac{\Delta z_{j-1}}{\Delta t}w_{j-2} + w_{j-2}z_{j-2}w_{j-2}$$

$$- \frac{1}{2}w_{j-2}^2\,\Delta t$$

$$= w_{j-2}q_{j-1} + w_{j-2}\frac{\Delta z_{j-1}}{\Delta t}\left(\frac{q_{j-2}+q_{j-1}}{z_{j-2}+z_{j-1}}\right)$$

$$- w_{j-2}\frac{\Delta t}{2}\left(\frac{q_{j-2}+q_{j-1}}{z_{j-2}+z_{j-1}}\right)$$

$$F_{ab} = w_{j-2}q_{j-1} + \frac{1}{2}w_{j-2}\Delta z_{j-1}\left(\frac{q_{j-2}+q_{j-1}}{z_{j-2}+z_{j-1}}\right)$$

$$- \frac{1}{2}w_{j-2}^2\,\Delta t\left(\frac{q_{j-2}+q_{j-1}}{z_{j-2}+z_{j-1}}\right) .$$

The flux across bc is calculated in a similar manner to yield

$$\zeta_{bc} = u_{i-1}\zeta_i + {}^{2}u_{i-1}\,\Delta x_i\left(\frac{\zeta_{i-1} - \zeta_i}{3\Delta x_{i-1} + 2\Delta x_i}\right)$$

$$+ {}^{3}w_{i-1}\,\Delta x_i\left(\frac{\zeta_{i-1} - \zeta_i}{3\Delta x_{i-1} + 2\Delta x_i}\right) .$$

The remaining change in the coding which is necessary to handle the triangular grids is the averaging of the vorticity to solve for the stream function at b .

$$\zeta_b = \left\{\zeta_{i,j-2}\,\Delta z_{j-1} + \zeta_{i-1,j-2}\left(\Delta z_{j-1} + \frac{\Delta z_{j-2}}{3}\,\frac{\Delta z_{j-1}}{(\Delta z_{j-2} + \Delta z_{j-1})}\right)\right.$$

$$\left. + {}^{2}w_{i-1,j-1}\,\Delta z_{j-2}\left(\frac{\Delta z_{j-2} + \frac{\Delta z_{j-1}}{3}}{\Delta z_{j-2} + \Delta z_{j-1}}\right) + \frac{1}{2}\,\Delta z_{j-2}\,\zeta_{i,j-1}\right\} \Big/$$

$$\left\{2\Delta z_{j-1} + 3\Delta z_{j-2}\right\} .$$

3.5 NUMERICAL CHECKS OF CROWLEY'S ADVECTION SCHEME

The integration of the advection terms in the present NAIFA codes is done using Crowley's second-order finite difference method. This section describes investigations of the accuracy of this scheme, and modifications of the original scheme to improve accuracy.

The standard NAIFA code was used as a test bed to check the accuracy of Crowley's advection scheme. Setting the derivatives of the temperature profile to the adiabatic lapse rate reduces the NAIFA equations to:

$$\nabla^2 \psi = \eta \quad .$$

$$\frac{\partial \eta}{\partial t} + \nabla(\vec{u}\eta) = 0 \quad .$$

$$\frac{\partial \psi}{\partial t} + \nabla(\vec{u}\psi) = 0 \quad .$$

A wind profile with $u = 10 + 0.01$ m/sec was used which gives an initial vorticity field of $\eta = 0.01$ sec^{-1}.

Zoning for a calculation previously reported was used ($\Delta x = 1500$m, $\Delta z = 312.5$) with an obstacle 625 meters high and 1500 meters long. The problem was run for 30 cycles with an edit of the mean kinetic energy, and mean squared vorticity taken every 10 cycles. Since there are no energy terms in the reduced N-S equations, there should be no change in mean square vorticity and the kinetic energy; any change is an indication of the errors induced into the code by the advection scheme. Table 3.1 gives the results of the first test run with the Crowley second-order advection scheme.

A correction procedure for the advection treatment has been suggested.[135] This improvement consists of limiting the value of the updated value to be between the maximum and minimum of the original values of the cell and nearest neighboring cells.

$$\min(C^n_{i-1}, C^n_i, C^n_{i+1}) \leq C^{n+1} \leq \max(C^n_{i-1}, C^n_i, C^n_{i+1})$$

This technique has the advantage of smoothing the solution of the advection equation and thus improving stability and accuracy. However, it also has the disadvantage of not insuring conservation. A test run was made for this modified

TABLE 3.1

Test Advection Scheme:
Crowley Second-Order

Cycle	$\int q\,ds$	$\int q^2\,ds$
0	5.000000·10⁶	2.500000·10⁻¹
1	5.000042	2.250026
10	5.000417	2.210005
20	5.000831	2.210020
30	5.001246	2.210035
% difference per cycle	.2·10⁻⁵	.5·10⁻³

TABLE 3.2

Crowley Second-Order with the Restriction:
$\min(C_{i-1}, C_i, C_{i-1}) < C_{it} < \max(C_{i-1}, C_i, C_{i-1})$

Cycle	$\int q\,ds$	$\int q^2\,ds$
0	5.000000·10⁶	2.500000·10⁻¹
1	"	"
10	"	"
20	"	"
30	"	"
% difference per cycle	0	0

Crowley scheme with the same conditions as the test described previously. The results given in Table 3.2 show that to the limit of accuracy of the computer, the modified Crowley scheme conserved both kinetic energy and mean square vorticity.

4. CORIOLIS TERMS IN 2-D MESO-SCALE EQUATIONS

One of the major tasks to be undertaken in the next contract period will be to consider the effect of Coriolis forces on the flow over mountain ranges.

In the 2-D calculations previously reported, lee waves are formed over the mountain in a time interval of about one hour, during which dynamic effects from the Coriolis force are small. (The geostrophic wind used for the unperturbed flow, of course, is strongly influenced by the Coriolis terms.) If the mountain range were more extensive or if the fate of the waves radiated by the mountain were followed to larger distances it is to be expected that larger effects from the Coriolis terms would be realized.

The characteristic distance scale for the Coriolis force is $L_f = u/f$, where u is a typical wind speed and f is the Coriolis parameter (if $u \sim 10$ m/s, we obtain $L_f \sim 100$ km). When the mountain range is comparable to L_f, an appreciable modification of the gravity waves will result to form a complex system of gravity-inertia waves. An investigation of these waves when they are small in amplitude and the wind speed is uniform has been carried out by Queney.[16] Since the distance L_f is comparable with the extent of mountain ranges which we must consider in climate dynamics, it appears to be important to take account of the Coriolis force in our subsequent investigations.

Since the Coriolis force induces a turning of the wind it is necessary to take into account several new factors in the calculations:

(1) the component of the wind parallel to the mountain must be included;

(2) pressure gradients in directions parallel and perpendicular to the mountain must be included to establish geostrophic balance in the unperturbed flow; and

(3) the vertical atmosphere structure is slightly modified to account for the Coriolis contribution to the hydrostatic balance condition.

In the following formulation we attempt to parallel the numerical treatment of the HAIFA code as closely as feasible in order to be able to compare the effects of the Coriolis terms with those pertaining to a non-rotating Earth.

4.1 FORMULATION

The differential equations of the dry atmosphere are formulated in a system of reference fixed to a rotating Earth. As discussed by Thompson[17] we incorporate the centrifugal terms into the definition of the local gravity to obtain

$$\frac{d\underline{U}}{dt} + 2\underline{\Omega} \times \underline{U} = -\frac{1}{\rho} \nabla P - \underline{k}g \quad , \qquad (4.1)$$

where $\underline{U}$ is the velocity relative to the Earth's surface, $\underline{\Omega}$ is the rotational velocity of the Earth, P is the pressure, ρ is the density of the atmosphere, g is the local acceleration of gravity which is assumed to act in the vertical direction $\underline{k}$. The time derivative is that evaluated following the fluid motion. The equations of mass and energy conservation are not affected by the Coriolis force.

Neglecting the curvature of the Earth's surface (and the resulting centrifugal terms associated with the relative velocity), the Eq. (4.1) can be resolved into components. We choose a Cartesian coordinate system in which the x-axis lies in the surface and forms an angle ϕ with the eastward direction, the y-axis lies in the surface at the same angle ϕ with the northward direction, and the z-axis is perpendicular, positive upward. We shall subsequently assume that the x-axis is perpendicular to the 2-D mountain range which is oriented at the angle ϕ with the northward direction. Denoting x, y, and z components of the velocity by u, v, w, the component equations are

$$\frac{du}{dt} - 2\Omega \sin\theta\, v + 2\Omega \cos\theta \cos\phi\, w = -\frac{1}{\rho}\frac{\partial P}{\partial x} \quad ,$$

$$\frac{dv}{dt} + 2\Omega \sin\theta\, u - 2\Omega \cos\theta \sin\phi\, w = \frac{1}{\rho}\frac{\partial P}{\partial y} \quad , \qquad (4.2)$$

$$\frac{dw}{dt} - 2\Omega \cos\theta\, (u\cos\phi - v\sin\phi) = -\frac{1}{\rho}\frac{\partial P}{\partial z} - g \quad ,$$

where Ω is the magnitude of the rotational velocity, θ is the latitude of the position, and the time derivatives are those formed following the fluid motion.

In the absence of the mountain barrier we consider the atmosphere to be in geostrophic balance; the motion is unaccelerated, the vertical velocity component w is zero, and the pressure gradients are just balanced by the Coriolis and gravity terms. Denoting the geostrophic state by subscripts g we obtain

$$-2\Omega \sin\theta \, v_g = -\frac{1}{\rho_g}\frac{\partial p_g}{\partial x} \quad ,$$

$$2\Omega \sin\theta \, u_g = -\frac{1}{\rho_g}\frac{\partial p_g}{\partial y} \quad , \tag{4.3}$$

$$-2\Omega \cos\theta (u_g \cos\phi - v_g \sin\phi) + g = -\frac{1}{\rho_g}\frac{\partial p_g}{\partial z} \quad .$$

Since the velocity of the unperturbed state is taken to be independent of x and y, Eq. (4.3) shows that the pressure at most need depend linearly on x and y.

When the mountain is present the pressure, density and velocity are perturbed from their geostrophic values. It will be convenient to introduce the deviation p' of the pressure from the geostrophic value:

$$p' = p - p_g \quad . \tag{4.4}$$

We also introduce the Boussinesq approximation, in which the departure of density from the geostrophic value is taken into account only in the gravity term of Eq. (4.3). In all other terms, we use the geostrophic density:

$$\frac{du}{dt} - 2\Omega \sin\theta(v-v_g) + 2\Omega \cos\theta \cos\phi\, w = -\frac{1}{\rho_g}\frac{\partial P'}{\partial x} \quad ,$$

$$\frac{dv}{dt} + 2\Omega \sin\theta(u-u_g) - 2\Omega \cos\theta \sin\phi\, w = -\frac{1}{\rho_g}\frac{\partial P'}{\partial y} \quad , \quad (4.5)$$

$$\frac{dw}{dt} - 2\Omega \cos\theta[(u-u_g)\cos\phi - (v-v_g)\sin\phi] = -\frac{1}{\rho_g}\frac{\partial P'}{\partial z} + \left(1 - \frac{\rho}{\rho_g}\right)g \quad .$$

These equations constitute the Boussinesq approximation for the equations of motion when the geostrophic flow, assumed steady and independent of x and y, is perturbed. Clearly, they are only approximately satisfied in a local region, since u_g and v_g are not constant on the synoptic scale.

We now consider the special case in which the initial and boundary equations are independent of the y-coordinate, corresponding to a uniform but obliquely incident wind encountering a two-dimensional ridge, the topography of which is independent of y. In this case, the initial and boundary conditions and the equations depend only on the coordinates x and z. The resulting 2-D equations derived from Eq. (4.5) are:

$$\frac{\partial u}{\partial t} + u\frac{\partial u}{\partial x} + w\frac{\partial u}{\partial z} - 2\Omega \sin\theta(v-v_g) + 2\Omega \cos\theta \cos\phi\, w = -\frac{1}{\rho_g}\frac{\partial P'}{\partial x} \quad ,$$

$$\frac{\partial v}{\partial t} + u\frac{\partial v}{\partial x} + w\frac{\partial v}{\partial z} + 2\Omega \sin\theta(u-u_g) - 2\Omega \cos\theta \sin\phi\, w = 0 \quad , \quad (4.6)$$

$$\frac{\partial w}{\partial t} + u\frac{\partial w}{\partial x} + w\frac{\partial w}{\partial z} - 2\Omega \cos\theta[(u-u_g)\cos\phi - (v-v_g)\sin\phi] =$$

$$-\frac{1}{\rho_g}\frac{\partial P'}{\partial z} + \left(1 - \frac{\rho}{\rho_g}\right)g \quad .$$

Eqs. (4.6) are to be supplemented with the equations of incompressibility and the temperature equation. The equations are unchanged from those in Ref. 1; they are to be found in that document as Eqs. (2.3) and (2.10).

There are two major modifications of the equations which have resulted from the treatment of the rotation of the Earth:

(1) The component of the wind parallel to the range influences both the x and z momentum equations through the Coriolis terms. The y momentum component equation is only weakly coupled to the others and may be solved in a similar way to the temperature equation.

(2) Additional terms from the Coriolis force enter the momentum equations giving rise to new terms in the vorticity equation.

4.1.1 Difference Equations

The difference equation formulation corresponding to Eq. (4.6) and supplementary equations can be chosen to parallel that of the HAIFA code. The equation for the y-component of vorticity is obtained by cross-differentiation of the x and z components of the momentum, thereby eliminating the pressure from the equations entirely. The resulting equations are:

$$\frac{\partial \eta}{\partial t} + u\frac{\partial \eta}{\partial x} + w\frac{\partial \eta}{\partial z} - 2\Omega \sin\theta\left(\frac{\partial v}{\partial z} - \frac{\partial v_g}{\partial z}\right) - 2\Omega \cos\theta \sin\phi \frac{\partial v}{\partial x} = \frac{g}{\rho_g}\frac{\partial \rho}{\partial x} \quad ,$$

$$\frac{\partial v}{\partial t} + u\frac{\partial v}{\partial x} + w\frac{\partial v}{\partial z} + 2\Omega \sin\theta(u-u_g) - 2\Omega \cos\theta \sin\phi\, w = 0 \quad ,$$

where the y-component of vorticity η is defined by

$$\eta = \frac{\partial u}{\partial z} - \frac{\partial w}{\partial x} \quad .$$

The difference approximation for the above equations also follows that of HAIFA. The time-dependent equations are solved in an explicit two-level formulation. The advection terms are obtained by using a high order conservative scheme in which the two directions are integrated by the splitting technique. Additional terms are centered in space from quantities available at the current time cycle. All of these terms result from the Coriolis force acting on the v-component of velocity. The additional equation for the v-velocity is similar to the temperature equation in structure. Changes in v are principally from advection; the forcing terms are the result of the Coriolis force acting on the u- and v-components of velocity.

5. A LINEAR ANALYSIS OF NUMERICAL APPROXIMATIONS

The application of the equations of fluid dynamics to geophysical phenomena has prompted the development of simplified equations which emphasize the salient features of strongly sub-sonic flow. This investigation of these equations treats only the limiting case of small amplitude disturbances about an initial steady state.

Since sound waves play a very minor role in motions of the atmosphere and oceans, it is convenient to neglect terms which contribute principally to their propagation. The effect of buoyancy, on the other hand, has a profound influence on the flow field; highly stable stratification gives rise to wave motions which are frequently ubiquitous features of atmospheric phenomena. Less stable atmospheric configurations may result in the dissipation of waves through instabilities which arise from the amplification of wave motions, and an unstable atmosphere gives rise to spontaneous motions of a convective nature which provide a mechanism for restoring marginal stability. In much of the motion of the atmosphere and oceans the fluid behaves as though it were substantially incompressible. Consequently, methods of approximation have been designed around the assumption of incompressibility and make greater or lesser use of it.

The fully compressible equations are treated in this report. Comparisons are made with results from Dr. M. G.

Wurtele at the University of California at Los Angeles and the differences are discussed. Following this, the results are modified to the incompressible equations. These two cases are the limiting solutions of our problem.

Three approximations to the fluid dynamic equations are then solved. These include (1) the strict Boussinesq approximation, (2) the "compressible" approximation, and (3) the anelastic equations. The Boussinesq approximation is based on the assumption that the fluid, as far as the dynamical terms are concerned, is incompressible and has a uniform density. The "compressible" approximation[1,7] was developed to take account of the effects of the stratification of the atmosphere on waves which propagate through vertical distances comparable to the atmospheric scale height. The third approximation studied is the anelastic equations introduced by Ogura and Phillips. These equations are based on small departures from a neutrally stratified atmosphere in which the potential temperature has a constant value.

5.1 EULER'S EQUATIONS

Initially, the equations for the motion of a fluid obeying the perfect gas law is considered, as is appropriate for the dry atmosphere. We assume that the gravitational force is constant, that viscous or turbulent transfer can be neglected, that the motion is adiabatic, and that the Coriolis terms have a negligible effect. In addition, the motion is assumed to be confined to a vertical (x,z) plane in which x and z are horizontal and vertical Cartesian coordinates. The resulting simplified equations are:

Mass Conservation --

$$\frac{d\rho}{dt} + \rho\left(\frac{\partial u}{\partial x} + \frac{\partial w}{\partial z}\right) = 0 \quad , \tag{5.1a}$$

Horizontal Momentum --

$$\frac{du}{dt} + \frac{1}{\rho}\frac{\partial P}{\partial x} = 0 \quad , \tag{5.1b}$$

Vertical Momentum --

$$\frac{dw}{dt} + \frac{1}{\rho}\frac{\partial P}{\partial z} = -g \quad , \tag{5.1c}$$

Energy Equation for Adiabatic Motion --

$$\frac{dT}{dt} = \frac{1}{\rho C_p}\frac{dp}{dt} \quad , \tag{5.1d}$$

Perfect Gas Equation of State --

$$p = \rho RT \quad , \tag{5.1e}$$

where the substantive derivative is defined as

$$\frac{d}{dt} = \frac{\partial}{\partial t} + u\frac{\partial}{\partial x} + v\frac{\partial}{\partial z} \quad .$$

In the above equations there are five dependent variables; the horizontal component of velocity u, the vertical component of velocity w, the density ρ, the pressure p, and the temperature T. The specific heat at constant pressure C_p is assumed to be constant.

The unperturbed state of the atmosphere is assumed to be horizontally stratified and in hydrostatic equilibrium. We consider perturbations to this system in which the disturbance amplitude is small enough that only terms linear in the perturbed quantities need be retained. The resulting equations admit solutions which are periodic in the horizontal variable and the time. Due to the linearity of the equations, these wave solutions can be superimposed to describe the behavior of an arbitrary disturbance.

The assumed solution takes the form

$$\rho = \overline{\rho} + \hat{\rho} f \quad , \tag{5.2a}$$

$$u = U + \hat{u} f \quad , \tag{5.2b}$$

$$w = \hat{w} f \quad , \tag{5.2c}$$

$$p = \overline{p} + \hat{p} f \quad , \tag{5.2d}$$

$$T = \overline{T} + \hat{T} f \quad , \tag{5.2e}$$

where $f = e^{ik(x-ct)}$ in which k is the horizontal wave number of the disturbance and c is its phase speed. The remaining quantities depend only on the vertical coordinate z, with the first quantity in each sum representing the unperturbed solution.

The unperturbed quantities must satisfy the equation of state and the hydrostatic condition. This leads to

$$\overline{p} = \overline{\rho} R \overline{T} \quad , \qquad \overline{p}' = -g\overline{\rho} \quad , \tag{5.3}$$

where differentiation with respect to z is denoted with a prime.

In the equations governing the perturbed quantities, we retain only terms linear in the perturbed quantities; the unperturbed terms are removed by subtracting Eq. (5.3). Factoring out the common factor f we obtain

$$ik(U - c)\hat{\rho} + \overline{\rho}'\hat{w} + \overline{\rho}(ik\hat{u} + \hat{w}') = 0 \quad , \tag{5.4a}$$

$$ik(U - c)\hat{u} + U'\hat{w} + \frac{ik}{\overline{\rho}}\hat{p} = 0 \quad , \tag{5.4b}$$

$$ik(U - c)\hat{w} + \frac{\hat{p}'}{\overline{\rho}} + \frac{g\hat{\rho}}{\overline{\rho}} = 0 \quad , \tag{5.4c}$$

$$ik(U - c)(\overline{\rho}R\hat{T} - \kappa\hat{p}) + w(\overline{\rho}R\overline{T}' - \kappa\overline{p}') = 0 \quad , \tag{5.4d}$$

$$\frac{\hat{p}}{\overline{p}} - \frac{\hat{T}}{\overline{T}} - \frac{\hat{\rho}}{\overline{\rho}} = 0 \quad , \tag{5.4e}$$

where

$$\kappa = \frac{R}{C_p} \quad .$$

From Eq. (5.3), the derivative of the unperturbed density and temperature can be related as follows:

$$\frac{\overline{T}'}{\overline{T}} + \frac{\overline{\rho}'}{\overline{\rho}} = -\frac{g\overline{\rho}}{\overline{\theta}} \quad :$$

In terms of the stratifications of density and potential temperature θ

$$s = -\frac{\bar{\rho}'}{\bar{\rho}} \qquad \text{and} \qquad S = \frac{\bar{\theta}'}{\bar{\theta}} \quad ,$$

the above equation becomes

$$s - S = \frac{g}{C_s^2} \quad , \tag{5.5}$$

in which the sound speed C_s is defined as

$$C_s^2 = \frac{1}{1-\kappa} \frac{\bar{p}}{\bar{\rho}}$$

and

$$\theta = T(p/p_o)^{-\kappa} \quad .$$

Eliminating $\hat{T}$ and $\hat{u}$ from Eq. (5.4)

$$ik(U - c)\hat{\rho} - s + \frac{U'}{U - c}\bar{\rho}\hat{w} + \bar{\rho}\hat{w}' - \frac{ik}{U - c}\hat{p} = 0 \quad ,$$

$$g\hat{\rho} + ik(U - c)\bar{\rho}\hat{w} + \hat{p}' = 0 \quad , \tag{5.6}$$

$$-ik(U - c)\hat{\rho} + \bar{\rho}S\hat{w} + \frac{ik(U - c)}{C_s^2}\hat{p} = 0 \quad .$$

Eqs. (5.6) are three equations for the three unknowns $\hat{\rho}$, $\hat{w}$ and $\hat{p}$. Eliminating the density from these equations gives

$$\hat{w}' + S - s - \frac{U'}{U - c}\hat{w} - \frac{ik}{U - c}\mu\beta = 0 \quad ,$$

$$\frac{Sg}{(U - c)^2} - k^2\hat{w} - \frac{ikS\beta}{U - c} + \frac{ik\beta'}{U - c} = 0 \quad , \tag{5.7}$$

where

$$\beta = \hat{p}/\overline{\rho} \qquad \text{and} \qquad \mu = 1 - \left(\frac{U - c}{C_s}\right)^2 . \tag{5.7a}$$

In all but the most violent storms $\mu \approx 1$. Finally, eliminating β from Eq. (5.7) and after some reduction, the equation for $\hat{w}$ is obtained:

$$\hat{w}'' - \left(s + \frac{\mu'}{\mu}\right)\hat{w}' + \left[-\mu k^2 + \frac{g}{(U - c)^2}\left(S + \frac{\mu'}{\mu}\right)\right.$$

$$\left. + \frac{U'}{U - c}\left(s + \frac{\mu'}{\mu}\right) - \frac{U''}{U - c}\right]\hat{w} = 0 \quad . \tag{5.8}$$

Eq. (5.8) is the same as that of Wurtele[18] who derives the equation from the formulation in terms of the potential temperature and the Helmholtz pressure function

$$\pi = C_p\left(\frac{p}{p_o}\right)^{\kappa}$$

It is of interest to consider the limiting form of Eq. (5.8) when the velocity is small compared with the sound

speed. This approximation is basically obtained by replacing μ by 1, but we shall retain certain terms arising from the differentiation of μ. Neglecting terms which contain $\frac{U - c}{C_s}^2$ we obtain

$$\hat{w}'' - \left[s - \frac{2(s - S)(U - c)U'}{g}\right]\hat{w}'$$

$$+ \left[-k^2 + \frac{gS}{(U - c)^2} + \frac{U'}{U - c}(2S - s)\right. \qquad (5.9)$$

$$\left. - \frac{U''}{U - c} - \frac{2(s - S)(U')^2}{g}\right]\hat{w} = 0 \quad .$$

This result differs from that of Wurtele

$$\hat{w}'' - s\hat{w}' + \left[-k^2 + \frac{gS}{(U - c)^2} + \frac{sU'}{U - c} - \frac{U''}{U - c}\right]\hat{w} = 0 \quad , \quad (5.9a)$$

principally in the coefficient of the U' term which contains an additional contribution from $g\mu'/(U - c)^2$ in Eq. (5.8). The remaining additional terms in Eq. (5.9) are small compared with Eq. (5.9a) unless extremely large wind shear is present.

The Euler equations have been considered above in considerable detail in order to provide a basis for comparison with the analogous equations from the several approximations. The subsequent derivations resulting from the approximate equations also give rise to equations for w which have the same form as Eq. (5.9). By comparison of the coefficients of $\hat{w}$ and $\hat{w}'$ it is possible to determine how the vertical wavelength and wave amplitude compare. It was found convenient to transform Eq. (5.9) in these evaluations to remove the first derivative term. The transformation to accomplish this is

$$\eta = \left(\frac{\omega}{c}\right)^{1/2} z \quad , \tag{5.10}$$

and the transformed Eq. (5.9) is

$$\chi''' + \left\{-\mu k^2 + \frac{k^2}{(U-c)^2}\left(s + \frac{\rho'}{\rho}\right) + \frac{U''}{U-c}\left(s + \frac{\rho'}{\rho}\right)\right.$$

$$\left. - \frac{U''}{U-c} + \frac{1}{4}\left(s + \frac{\rho'}{\rho}\right)^2 + \frac{1}{2}\left[s' + \left(\frac{\rho'}{\rho}\right)'\right]\right\}\chi = 0 \quad .$$

In order to make comparisons with the anelastic equations it will be useful to formulate the Euler equations in terms of the dependent variables θ and π. Following Kurtele's derivation the equations become

$$\theta\frac{d\pi}{dt} + c_s^2\left(\frac{\partial u}{\partial x} + \frac{\partial w}{\partial z}\right) = 0 \quad ,$$

$$\frac{du}{dt} + \theta\frac{\partial \pi}{\partial x} = 0 \quad , \tag{5.11}$$

$$\frac{dw}{dt} + \theta\frac{\partial \pi}{\partial z} = -g \quad ,$$

$$\frac{d\theta}{dt} = 0 \quad .$$

The equation of state has been incorporated into the above equations so that the density does not appear. If the density is desired as an auxiliary quantity it can be obtained from the equation of state. Introducing unperturbed and perturbed equations for θ and π analogously to Eq. (5.2), we

obtain the equation corresponding to the hydrostatic balance condition

$$\overline{\theta}\,\overline{\pi}' = -g \quad .$$

The linearized perturbation equations are

$$\begin{aligned}
&\overline{\theta}[ik(U - c)\hat{u} + \overline{\pi}'\hat{w}] + C_s^2(ik\hat{u} + \hat{w}') = 0 \quad , \\
&ik(U - c)\hat{u} + U'\hat{w} + ik\overline{\theta}\hat{\pi} = 0 \quad , \\
&ik(U - c)\hat{w} + \overline{\theta}\hat{\pi}' - \frac{\hat{\theta}g}{\overline{\theta}} = 0 \quad , \\
&ik(U - c)\hat{\theta} + \overline{\theta}'\hat{w} = 0 \quad ,
\end{aligned} \tag{5.12}$$

in which C_s depends on $\overline{T}$, while in Eq. (5.11) it depends on T. Eliminating $\hat{u}$ and $\hat{\theta}$ from Eq. (5.12) we obtain

$$\begin{aligned}
&\left[U' + \frac{g}{C_s^2}(U - c)\right]\hat{w} - (U - c)\hat{w}' = -ik\overline{\theta}\pi\mu \quad , \\
&\left[\frac{gS}{U - c} - k^2(U - c)\right]\hat{w} = -ik\overline{\theta}\pi' \quad .
\end{aligned} \tag{5.13}$$

The elimination of $\hat{\pi}$ from the above equations leads again to Eq. (5.9). This requires differentiation of the first equation giving rise to a term in μ'.

5.2 INCOMPRESSIBLE EQUATIONS

We consider the system composed of an incompressible fluid ($d/dt = 0$) which is initially stratified in density. The equations for the system are

$$\frac{du}{dt} + \frac{1}{\rho}\frac{\partial p}{\partial x} = 0 \quad ,$$

$$\frac{dw}{dt} + \frac{1}{\rho}\frac{\partial p}{\partial x} = -g \quad ,$$

$$\frac{d\rho}{dt} = 0 \quad , \tag{5.14}$$

$$\frac{\partial u}{\partial x} + \frac{\partial w}{\partial z} = 0 \quad .$$

The corresponding perturbation equations are

$$ik(U - c)\hat{u} + U'\hat{w} + \frac{ik}{\bar{\rho}}\hat{p} = 0 \quad ,$$

$$ik(U - c)\hat{w} + \frac{\hat{p}'}{\bar{\rho}} + \frac{g\hat{\rho}}{\bar{\rho}} = 0 \quad ,$$

$$ik(U - c)\hat{\rho} + \bar{\rho}'\hat{w} = 0 \quad , \tag{5.15}$$

$$ik\hat{u} + \hat{w}' = 0 \quad .$$

The equations corresponding to Eq. (5.7) resulting from eliminating $\hat{u}$ and $\hat{\rho}$ are

$$-\frac{U'\hat{w}}{U - c} + \hat{w}' - \frac{ik}{U - c}\beta = 0 \quad ,$$

$$\left[\frac{sg}{(U - c)^2} - k^2\right]\hat{w} - \frac{iks\beta}{U - c} + \frac{ik\beta'}{U - c} = 0 \quad . \tag{5.16}$$

These equations differ from Eq. (5.7) in two respects and can be derived from them by the substitutions $\mu \to 1$ and $S \to s$. The equation for $\hat{w}$ becomes

$$\hat{w}'' - s\hat{w}' + \left[-k^2 + \frac{sg}{(U - c)^2} + \frac{sU'}{U - c} - \frac{U''}{U - c}\right]\hat{w} = 0 \quad . \quad (5.17)$$

As is to be expected, all of the sound wave terms are missing and the term which is frequently the largest is changed. The coefficient of $g/(U - c)^2$, which in the exact equation is the static stability S, is replaced by s.

5.3 BOUSSINESQ APPROXIMATION

In the Boussinesq approximation, the variability of the density in the atmosphere is neglected in all the terms except the buoyancy term. This formulation allows the equations to be transformed to introduce the vorticity and stream functions, a property used in the S^3 numerical solution. The equations are

$$\begin{aligned}
&\frac{du}{dt} + \frac{1}{\rho_o}\frac{\partial P'}{\partial x} = 0 \quad , \\
&\frac{dw}{dt} + \frac{1}{\rho_o}\frac{\partial P'}{\partial z} = \frac{gT'}{T_o} \quad , \\
&\frac{dT'}{dt} + w\left(\frac{dT_o}{dt} + \Gamma\right) = 0 \quad , \\
&\frac{\partial u}{\partial x} + \frac{\partial w}{\partial z} = 0 \quad ,
\end{aligned} \qquad (5.18)$$

where P' , T' are the perturbations of the pressure and temperature from the corresponding static atmosphere quantities denoted by the subscript "zero." The density appearing in the momentum equations is taken to be constant. In the above equations there has been an approximation made in the continuity equation through the neglect of the change of density due to changes in both the static and dynamic pressures. In the momentum equations, in addition to the approximation of a constant density, the density perturbation in the buoyancy term has been replaced by the temperature perturbation; the pressure perturbation has been neglected. In the temperature equation, the effect of the pressure perturbation on the temperature change has also been neglected.

To obtain the equation for small disturbances in a stratified atmosphere, we linearize the Boussinesq equations Eq. (5.18) about the unperturbed state. The substitutions are

$$u = U + \hat{u}f \quad ,$$

$$w = \hat{w}f \quad ,$$

$$T' = \hat{T}f \quad ,$$

$$P' = \hat{p}f \quad .$$

The perturbation equations are

$$ik(U - c)\hat{u} + U'\hat{w} + \frac{ik}{\rho_o}\hat{p} = 0 \quad , \qquad (5.19a)$$

$$ik(U - c)\hat{w} + \frac{\hat{p}'}{\rho_o} - \frac{g\hat{T}}{T_o} = 0 \quad , \tag{5.19b}$$

$$ik(U - c)\hat{T} + (T_o + \Gamma)\hat{w} = 0 \quad , \tag{5.19c}$$

$$ik\hat{u} + \hat{w}' = 0 \quad . \tag{5.19d}$$

Eliminating $\hat{u}$ and $\hat{T}$ we obtain

$$\begin{aligned} -(U - c)\hat{w}' + U'\hat{w} + \frac{ik\hat{p}}{\rho_o} &= 0 \quad , \\ -\left[k^2(U - c) - \frac{gS}{U - c}\right] + \frac{ik\hat{p}'}{\rho_o} &= 0 \quad , \end{aligned} \tag{5.20}$$

where

$$S = \frac{T_o' + \Gamma}{T_o} \quad .$$

The resulting equation for w is

$$\hat{w}'' + \left[-k^2 + \frac{gS}{(U - c)^2} - \frac{U''}{U - c}\right]\hat{w} = 0 \quad . \tag{5.21}$$

Eq. (5.21) can also be derived from the vorticity and stream function form of the equations.

The first two coefficients of $\hat{w}$ in Eq. (5.21), which in most cases are the largest, also are present in the corresponding Euler equation, Eq. (5.19). The third coefficient of Eq. (5.21) also occurs in both equations. Consequently, the

vertical wavelength of the Boussinesq equation should be approximately correct. The $\hat{w}'$ term of Eq. (5.9) is missing, however. As indicated by the transformation of Eq. (5.10), the absence of this term corresponds to a scaling of the velocity amplitude by a factor of $(\bar{\rho})^{1/2}$. Thus, the amplitude of the Boussinesq approximation velocity is expected to fall off more rapidly with altitude by the above factor, which becomes significant when waves are propagated through an atmospheric scale height.

By comparison with Eqs. (5.4) and (5.6) it is clear that the $\hat{w}$ coefficients are obtained correctly from Eq. (5.19) because the temperature perturbation terms in the energy equation and the equation of state are correctly retained. The emitted pressure perturbation terms contribute principally to smaller coefficients of w. The absence of a term in $\hat{w}'$ results from the omission of the density stratification term in the continuity equation and from the approximation of constant density in the momentum equations.

5.4 THE "COMPRESSIBLE" APPROXIMATION

The "compressible" approximation[1,7] was developed to take account of the effects of the stratification of the atmosphere on waves which propagate through vertical distances comparable to the atmospheric scale height. The equations are formulated in such a way that it is possible to reduce them to a Poisson equation for a quantity similar to the stream function and a prognostic equation for a vorticity-like quantity.

The equations are:

$$\frac{\partial \rho u}{\partial x} + \frac{\partial \rho w}{\partial z} = 0 \quad , \qquad (5.22a)$$

$$\frac{\partial \rho u}{\partial t} + \frac{\partial \rho u^2}{\partial x} + \frac{\partial \rho uw}{\partial z} + \frac{\partial P}{\partial x} = 0 \quad , \tag{5.22b}$$

$$\frac{\partial \rho w}{\partial t} + \frac{\partial \rho uw}{\partial x} + \frac{\partial \rho w^2}{\partial z} + \frac{\partial P}{\partial z} = -g\rho \quad , \tag{5.22c}$$

$$\frac{\partial \rho T'}{\partial t} + \frac{\partial \rho uT'}{\partial x} + \frac{\partial \rho wT'}{\partial z} = -(\rho_o \Gamma + \rho \overline{T}')w \quad , \tag{5.22d}$$

$$\rho = \frac{\overline{P}}{R\overline{T}} \quad . \tag{5.22e}$$

The quantity T' is the temperature perturbation from $\overline{T}$, the initial temperature of the stratified atmosphere. As compared with the Euler equations there are three approximations. The continuity equation omits the term containing $\frac{\partial \rho}{\partial t}$. In the energy equation, the pressure perturbation term is omitted from the work term. And in the equation of state, the pressure takes its static value, neglecting the pressure perturbation. The linearized equations corresponding to Eq. (5.22) are

$$ik\overline{\rho}\hat{u} + ikU\hat{\rho} + \overline{\rho}\hat{w}' + \overline{\rho}'\hat{w} = 0 \quad , \tag{5.23a}$$

$$ik(U - c)\hat{u} - \frac{ikUc}{\overline{\rho}}\hat{\rho} + U'\hat{w} + \frac{ik\hat{p}}{\overline{\rho}} = 0 \quad , \tag{5.23b}$$

$$\frac{g\hat{\rho}}{\overline{\rho}} + ik(U - c)\hat{w} + \frac{\hat{p}'}{\overline{\rho}} = 0 \quad , \tag{5.23c}$$

$$ik(U - c)\hat{T} + \overline{T}'\hat{w} + \Gamma\hat{w} = 0 \quad , \tag{5.23d}$$

$$\frac{\hat{\rho}}{\overline{\rho}} + \frac{\hat{T}}{\overline{T}} = 0 \quad . \tag{5.23e}$$

Eliminating $\hat{T}$ and $\hat{u}$, we obtain an equation corresponding to Eq. (5.6):

$$ik\bar{U}^2\hat{\rho} - [s(\bar{U} - c) + \bar{U}']\bar{\rho}\hat{w} + \bar{\rho}(\bar{U} - c)\hat{w}' - ik\hat{p} = 0 \quad ,$$

$$\rho\hat{p} + ik(\bar{U} - c)\bar{\rho}\hat{w} + \hat{p}' = 0 \quad , \qquad (5.24)$$

$$-ik(\bar{U} - c)\hat{\rho} + \bar{\rho}S\hat{w} = 0 \quad .$$

By comparison with Eq. (5.6) we find that Eq. (5.24) lacks several terms: in the first equation the coefficient of $\hat{\rho}$ contains $\bar{U}^2$ rather than $(\bar{U} - c)^2$, and in the third equation the coefficient of $\hat{p}$ is zero. Corresponding to Eq. (5.7) we eliminate $\hat{\rho}$ arriving at

$$\hat{w}' + \left[\left(\frac{\bar{U}}{\bar{U} - c}\right)^2 S - s - \frac{\bar{U}'}{\bar{U} - c}\right]\hat{w} - \frac{ik\beta}{\bar{U} - c} = 0 \quad ,$$

$$\left[\frac{Sg}{(\bar{U} - c)^2} - k^2\right]\hat{w} - \frac{iks\beta}{\bar{U} - c} + \frac{ik\beta'}{\bar{U} - c} = 0 \quad , \qquad (5.25)$$

where

$$\beta = \frac{\hat{p}}{\bar{\rho}} \quad .$$

The most serious difference between Eq. (5.25) is in the second equation where the coefficient of β contains s instead of S. Eliminating β we obtain the equation for the vertical velocity amplitude

$$\hat{w}'' + \left[\left(\frac{U}{U-c}\right)^2 S - 2s\right]\hat{w}' + \left[-k^2 + \frac{Sg}{(U-c)^2} - \frac{U''}{U-c}\right.$$

$$+ \frac{U'}{U-c}\left(\frac{U}{U-c}\right)S\left(2 - \frac{U}{U-c}\right) + s^2 - \left(\frac{U}{U-c}\right)^2 sS \qquad (5.26)$$

$$\left. + \left(\frac{U}{U-c}\right)^2 S' - s'\right]\hat{w} = 0 \quad .$$

The leading terms in the coefficient of $\hat{w}$ in Eq. (5.26) are in agreement with Eq. (5.9), thereby assuring that the vertical wavelength will be substantially correct. A number of additional terms also appear in the coefficient of $\hat{w}$ but in most cases these will be small. The major discrepancy of Eq. (5.26) as compared with Eq. (5.9) is the disagreement in the leading coefficients of $\hat{w}'$, in which (when $c=0$ and the smaller U' term is neglected) the correct coefficient $-s$ is replaced by $-2s + S$. In order to compare the effect of this difference in the $\hat{w}'$ coefficient it is useful to perform the transformation of w in Eq. (5.26) to a quantity x obeying an equation of the form $x'' + \nu^2 x = 0$. The required transformation (when $c=0$) is

$$\hat{w} = \frac{1}{\bar{\rho}\,\bar{U}^{1/2}}x \sim \frac{1}{\bar{\rho}^{1/2}}\frac{1}{\bar{p}^{(1-\kappa)/2}}x \quad . \qquad (5.27)$$

Since the x-equation is substantially the same as that for the transformed Euler equation, as given in the equation following Eq. (5.10), the two formulations may be compared entirely on the basis of the transformations of Eq. (5.27) and Eq. (5.10). The "compressible" approximation velocity amplitude contains an additional factor of $(\bar{p})^{(\kappa-1)/2}$ relative to the Euler equation. Consequently, in the atmosphere the "compressible"

amplitude will increase with increasing altitude by a factor of $(\bar{p}/p_0)^{-0.36}$ relative to the Euler result, which in turn increases with altitude relative to the Boussinesq approximation by a factor of $(\bar{\rho}/\rho_0)^{-1/2}$.

5.5 THE ANELASTIC APPROXIMATION

The "anelastic" approximation to the fluid dynamic equations was introduced by Ogura and Phillips. This approximation is formulated in terms of the potential temperature and Helmholtz function which appear in the form of the Euler equations given in Eq. (5.11). The anelastic approximation is based on small departures from a neutrally stratified atmosphere in which the potential temperature has the constant value θ. The pressure gradient terms of the momentum equations are approximated by neglecting higher order terms in the perturbed quantities θ' and π' defined as

$$\theta = \theta + \theta' \quad , \qquad \pi = \pi_0 + \pi' \quad .$$

The momentum equations then become

$$\frac{du}{dt} + \theta\frac{\partial \pi}{\partial x} = 0 = \frac{du}{dt} + \theta\frac{\partial \pi'}{\partial x} \approx \frac{du}{dt} + \theta\frac{\partial \pi'}{\partial x} \quad ,$$

$$\frac{dw}{dt} + \theta\frac{\partial \pi}{\partial z} + g = \frac{dw}{dt} + \theta\frac{\partial \pi'}{\partial z} + g\frac{\theta'}{\theta} \approx \frac{dw}{dt} + \theta\frac{\partial \pi'}{\partial z} + g\frac{\theta'}{\theta} \quad , \tag{5.28}$$

where π_0 is defined from

$$\frac{\partial \pi_0}{\partial z} + g = 0 \quad .$$

The energy equation is solved exactly, while the mass conservation equation is approximated:

$$\frac{d\theta}{dt} = 0 \quad ,$$

$$\frac{\partial \rho_0 u}{\partial x} + \frac{\partial \rho_0 w}{\partial z} = 0 \quad . \tag{5.29}$$

According to Ogura and Phillips, the density is that associated with the neutrally stratified atmosphere. This system of equations can also be applied to an atmosphere which is not initially neutrally stratified. In this case there will be a static solution in which θ' and π' have non-zero values, $\bar{\pi}$ and $\bar{\theta}$, which depend on z alone satisfying the relation

$$\theta \frac{\partial \bar{\pi}}{\partial z} = - \frac{g}{\bar{\theta}} \quad . \tag{5.30}$$

We now consider the small amplitude behavior of Eqs. (5.28) and (5.29) by linearizing the solution about a steady state in which the atmosphere is arbitrarily stratified in parallel flow. The dependent variables are written

$$u = U + \hat{u} f \quad ,$$

$$w = \hat{w} f \quad ,$$

$$\theta = \bar{\theta} + \hat{\theta} f \quad ,$$

$$\pi = \bar{\pi} + \hat{\pi} f \quad .$$

Using Eq. (5.30) for the static solution we obtain

$$\begin{aligned} ik(U - c)\hat{u} + U'\hat{w} + ik\theta\hat{\pi} &= 0 \quad , \\ ik(U - c)\hat{w} + \theta\hat{\pi}' - \frac{g\hat{\theta}}{\theta} &= 0 \quad , \\ ik(U - c)\hat{\theta} + \overline{\theta}'\hat{w} &= 0 \quad , \\ ik\hat{u} + \hat{w}' + \frac{\hat{w}}{\rho_o}\rho_o' &= 0 \quad , \end{aligned} \tag{5.31}$$

in which differentiation with respect to z is denoted by a prime. Eliminating $\hat{u}$ and $\hat{\theta}$ we obtain

$$\begin{aligned} -\hat{w}' + \left[s_o + \frac{U'}{U - c}\right]\hat{w} + \frac{ik\theta\hat{\pi}}{U - c} &= 0 \quad , \\ \left[\frac{gS_o}{(U - c)^2} - k^2\right]\hat{w} + \frac{ik\theta\hat{\pi}'}{U - c} &= 0 \quad , \end{aligned} \tag{5.32}$$

where the parameters appearing are defined by

$$S_o = \frac{\overline{\theta}'}{\theta} \quad , \quad s_o = -\frac{\rho_o'}{\rho_o} \quad . \tag{5.33}$$

The equation for $\hat{w}$ is

$$\hat{w}'' - s_o\hat{w}' + \left[-k^2 + \frac{gS_o}{(U - c)^2} - \frac{s_oU'}{U - c} - \frac{U''}{U - c} - s_o'\right]\hat{w} = 0 \quad . \tag{5.34}$$

Comparing Eq. (5.34) with the correct Eq. (5.9) we find that (aside from small terms) the coefficients of $\hat{w}$ and $\hat{w}'$ are substantially in the same form. The corresponding terms differ, however; S_o is defined in terms of θ instead of $\theta + \bar{\theta}$ and s_o is formed from ρ_o, the neutrally stable density, which differs from $\bar{\rho}$ the density of the actual atmosphere.

Fortunately, the anelastic static stability S_o does not differ by a large amount from the actual value of S. Moreover, the atmospheric density gradient term s_o can be chosen to have the correct value s rather than that associated with the neutrally stratified atmosphere as specified by Ogura and Phillips. The density ρ_o enters only in the mass conservation equation where it occurs as a parameter; consequently there is no difficulty in assigning the actual static value to it.

In contrast to the "compressible" approximation, the anelastic approximation thus can be adjusted to give the correct value of the $\hat{w}'$ coefficient. Inspection of the derivation through Eqs. (5.31) and (5.32) shows that this takes place through the compensation of two approximations of the anelastic equations. First, a term proportional to S is omitted when, on differentiation of the horizontal momentum equation, the coefficient of $\hat{\pi}$ is approximated by the constant θ. The missing term just compensates for the difference between s_o, resulting from the appearance of ρ_o in the continuity equation, and the correct term, g/C_s^2, arising from the density perturbation, which according to Eq. (5.5), incorporates an S term.

5.6 CONCLUSIONS

Several approximations to the inviscid fluid dynamic equations for treating buoyant low-speed flow have been examined. In each case the equation governing the small amplitude vertical velocity perturbation has been derived and compared with that for the Euler equation. When waves are propagated through vertical distances comparable to the density scale height of the atmosphere the familiar Boussinesq approximation gives rise to amplitude errors. The "compressible" approximation introduces a correcting term, but the coefficient is too large, permitting waves to propagate upward too strongly. A readily accomplished modification of the "anelastic" approximation gives rise to the correct coefficient, while retaining a substantially correct vertical wavelength as well.

The modified approximation appears to be an attractive candidate for treatment of problems of deep convection or propagation of gravity waves through appreciable fractions of the atmospheric scale height. The behavior of the anelastic approximation under conditions in which large amplitude disturbances are produced is not currently known.

6. RADIATION IN THE EARTH'S ATMOSPHERE

The radiative transfer problem in the Earth's atmosphere reduces to the solution of the seemingly simple equation

$$\frac{dI_\nu}{ds} = J_\nu - \kappa_\nu I_\nu$$

which states that the radiant intensity, in traversing the element of length ds, will be augmented by sources in the amount $J_\nu\, ds$ and diminished by extinction in the amount $\kappa_\nu I_\nu\, ds$. In general, I_ν, the radiant intensity, and J_ν, the source function, depend on both a spatial coordinate $\vec{r}$ and an angular coordinate (direction) $\vec{\Omega}$ at the point $\vec{r}$, as well as upon the frequency ν. The time dependence of these quantities is ignored because the radiative state of the atmosphere is established, for all practical purposes, instantaneously. κ_ν is the extinction coefficient, which describes the relative depletion in the intensity of the beam, dI_ν/I_ν, upon traversing the element of distance ds. κ_ν is in general the sum of an absorption part and a scattering part. J_ν describes the additions made to the beam intensity along ds by thermal (Planckian) emission and by scattering.

6.1 INTRODUCTION

A substantial revision in our fundamental numerical technique for solving the radiation transport equation has taken place since the previous semiannual report of this contract.[1] This revision has led to some new numerical problems and has delayed the intended completion date of the radiation code, but we consider the new method sufficiently superior in both accuracy and computational economy to more than justify the delay.

The first part of the new method involves fitting the transmission function by a sum of exponentials and is discussed in Section 6.2. The second part involves the solution of the monochromatic equation of radiative transfer, which is the subject of Section 6.3. In Section 6.4 the treatment of Mie scattering, in particular the treatment of the forward scattering peak, is described. Finally, a block diagram of the code is given in Section 6.5, along with brief descriptions of the various blocks.

Minor modifications have been made in the equations presented in the previous report. First, the origin of coordinates is now taken at the top of the atmosphere; this facilitates the method of Section 6.3. Secondly, a new diffuse intensity i_ν has been defined as

$$i_\nu = \begin{cases} T_\nu & -1 \leq \mu < 0 \\ T_\nu - T_\nu^{\text{solar}} & 0 < \mu \leq 1 \end{cases} \tag{6.1}$$

where

$$\bar{I}_\nu^{\text{solar}} = \frac{S_\nu}{2\pi} e^{-\tau(z)/\mu_{\text{sun}}} \delta(\mu-\mu_{\text{sun}})$$

$$\tau(z) = \int_0^z \kappa_\nu(z')\, dz' \quad . \tag{6.2}$$

With this transformation, the monochromatic equation of transfer derived in the previous report assumes the form

$$\mu\frac{\partial i_\nu}{\partial z} + \kappa_\nu i_\nu = \alpha'_\nu B_\nu + \frac{\beta_\nu}{2}\int_{-1}^{1} \bar{P}_\nu(z,\mu,\mu')i_\nu(z,\mu')d\mu' + Q_\nu(z,\mu) \tag{6.3}$$

where

$$Q_\nu(z,\mu) = \frac{\beta_\nu S_\nu}{4\pi} \bar{P}_\nu(z,\mu,\mu_{\text{sun}})\, e^{-\tau(z)/\mu_{\text{sun}}} \quad .$$

The integral form of Eq. (6.3) is

$$i_\nu(z,\mu) = J_\nu^{(0)} + \frac{1}{\mu}\int_{z_o}^{z} [J_\nu^{(1)} + J_\nu^{(2)} + J_\nu^{(3)}]dz'' \tag{6.4}$$

where

$$J_\nu^{(0)} = i_\nu(z_o,\mu)\, \exp\left[-\frac{1}{\mu}\left|\tau(z) - \tau(z_o)\right|\right] \tag{6.5a}$$

$$J_\nu^{(1)} = \alpha'_\nu(z'')\, B_\nu[T(z'')]\, \exp\left[-\frac{1}{\mu}\left|\tau(z) - \tau(z'')\right|\right] \tag{6.5b}$$

$$J_\nu^{(2)} = \frac{\beta_\nu(z'')}{2} \int_{-1}^{1} \bar{\Gamma}_\nu(z'',\mu,\mu')\, i_\nu(z'',\mu')d\mu' \cdot \exp\left[-\frac{1}{\mu}\left\{\tau(z) - \tau(z'')\right\}\right] \tag{6.5c}$$

$$J_\nu^{(3)} = \frac{S_\nu \beta_\nu(z'')}{4\pi} \bar{\Gamma}_\nu(z'',\mu,\mu_{sun}) \cdot \exp\left[-\frac{1}{\mu_{sun}}\tau(z'') - \frac{1}{\mu}\left\{\tau(z) - \tau(z'')\right\}\right] . \tag{6.5d}$$

The z_o of Eq. (6.4) need not lie on a boundary of the system; it need only be less than z if $\mu > 0$ and greater than z if $\mu < 0$.

6.2 EXPONENTIAL-SUM FIT OF THE TRANSMISSION FUNCTION AND REDUCTION TO MONOCHROMATIC PROBLEMS

Let us consider the frequency-averaging of Eq. (6.4) over a frequency interval $\Delta\nu$ which may contain many (typically 20-100) absorption lines of H_2O, CO_2, etc., but which is narrow enough that B_ν, $\bar{\Gamma}_\nu$, β_ν, $\alpha_\nu'^{(cont)}$, and S_ν do not change appreciably across $\Delta\nu$. ($\alpha_\nu'^{(cont)}$ is the smoothly varying part of the absorption coefficient, due to Mie absorption, the H_2O continuum, the N_2 continuum, etc.) Let the subscript $\Delta\nu$ denote the frequency average of a quantity. For example,

$$i_{\Delta\nu} = \frac{1}{\Delta\nu}\int_{\Delta\nu} i_\nu \, d\nu \quad . \tag{6.6}$$

In frequency-averaging Eq. (6.4), the frequency integration is commuted with any factors containing only the smoothly varying

quantities $\bar{F}_\nu$, etc. by evaluating these quantities at the mid-point $\bar{\nu}$ of $\Delta\nu$. The two exceptions to this rule are the Planck function B_ν and solar flux S_ν, for which $B_{\Delta\nu}$ and $S_{\Delta\nu}$ are used instead of $B_{\bar{\nu}}$ and $S_{\bar{\nu}}$. The reasons for these exceptions are (1) if the Earth radiated as a blackbody the total radiation output to space would be given correctly by the scheme using $B_{\Delta\nu}$ and not by the scheme using $B_{\bar{\nu}}$, and (2) the total incident solar flux is given correctly by the scheme using $S_{\Delta\nu}$ and not by the scheme using $S_{\bar{\nu}}$. $B_{\Delta\nu}$ is computed correctly to about 5 decimal places by a combination table look-up and asymptotic formula subroutine called PLKAVG which has been developed especially for this code. $S_{\Delta\nu}$ is computed from the data of Thekaekara.[1]

According to Kirchhoff's Law,[19] which says that media which absorb strongly at a certain frequency emit strongly at that frequency, the intensity i_ν will tend to follow the rapid variations in the absorption coefficient $\alpha'^{(line)}_\nu$. If sufficiently many (> 1-2) mean free paths of line absorption intervene between the point z and the surface, the variation of $i_\nu(z,\mu)$ with ν will follow the variation of $\alpha'^{(line)}_\nu$ with ν fairly faithfully; that is, lines in $\alpha'^{(line)}_\nu$ will produce bright lines in the spectrum of intensities. Nearer the surface, lines in $\alpha'^{(line)}_\nu$ may produce dark lines in the upward directed intensities rather than bright lines, but the statement that i_ν varies as rapidly as $\alpha'^{(line)}_\nu$ still applies. Because of this rapid variation, i_ν cannot be commuted with the frequency integration in the terms $J^{(0)}_\nu$ and $J^{(2)}_\nu$. In the previous report, it was proposed to make the approximation that this commutation is valid, in order to facilitate the proposed method of solution. The argument was made that the errors so produced would have little impact on total fluxes because:

(1) in the case of $J_\nu^{(0)}$, only errors near the boundary z_o would be produced and these would damp out rapidly as we proceeded away from the boundary;

(2) in the case of the scattering source $J_\nu^{(2)}$, only a negligible fraction of the frequency groups which experience line absorption will have comparable amounts of scattering ($J_\nu^{(2)} \approx J_\nu^{(1)}$), so that even a large error in $J_\nu^{(2)}$ will not be felt.

These hypotheses are qualitatively correct, but a quantitative verification would demand a prohibitively expensive line-by-line calculation through the entire IR spectrum, which we were not prepared to do.

Therefore, it was fortunate that a literature search following the publication of the previous report uncovered a method for performing frequency-averaging which eliminates the need for the above hypotheses and instead requires certain others which are both more intuitively appealing and more easily verifiable. The technique is, simply stated, the fitting of the transmission function with an M-term exponential sum followed by the solution of M monochromatic problems, the sum of whose solutions gives the frequency-averaged intensity $i_{\Delta\nu}$. We give the details below.

After performing the commutation of the frequency integration with the slowly-varying functions of ν in $J_\nu^{(0)}$ through $J_\nu^{(3)}$, the following kinds of integrals remain;

$$T_{\Delta\nu} = \frac{1}{\Delta\nu} \int_{\Delta\nu} e^{-\tau_a(z_1,z_2)/\mu} \, d\nu \qquad (6.7)$$

$$K_{\Delta\nu} \equiv \frac{1}{\Delta\nu}\int_{\Delta\nu} i_\nu \, e^{-\tau_a(z_1,z_2)/\mu} \, d\nu \qquad (6.8)$$

$$L_{\Delta\nu} \equiv \frac{1}{\Delta\nu}\int_{\Delta\nu} \exp\left[-\frac{\tau_a(0,z_1)}{\mu_{sun}} - \frac{\tau_a(z_1,z_2)}{\mu}\right] d\nu \qquad (6.9)$$

where the line absorption optical depth τ_a is defined as

$$\tau_a(z_1,z_2) = \int_{z_1}^{z_2} \alpha_\nu'(\text{line})\,(z)\,dz$$

$T_{\Delta\nu}$ (Eq. (6.7)) is called a <u>transmission function</u>. A computationally fast and reliable computation of $T_{\Delta\nu}$ has been made available to us in the form of the subroutine LOTRAN developed at AFCRL.[20] LOTRAN was described in the semi-annual report, and prior to that date had been put on our computer but not adapted to the particular needs of the radiation code. Since then a substantial amount of coding having to do with Rayleigh scattering and Mie scattering and with atmospheric curvature (which is being neglected) has been removed from LOTRAN and the numerous associated data cards have been converted to FORTRAN DATA statements to avoid having to read data cards every time the code is executed. Further modifications of LOTRAN will be necessary in connection with the exponential fitting scheme discussed below. Consequently, it can be assumed that accurate values of $T_{\Delta\nu}$ for arbitrary z_1, z_2 are available.

6.2.1 The Scaling Approximation

LOTRAN assumes that optical depths are calculated in the scaling approximation, according to which $\alpha_\nu'^{(line)}$ is separable as follows:

$$\alpha_\nu'^{(line)} = \left(1 - e^{-h\nu/kT}\right) \alpha_1(\nu)\ \alpha_2(p,T)$$

(from here on the stimulated emission correction factor $1 - \exp(-h\nu/kT)$ will be evaluated at $\nu = \bar{\nu}$ since it is a slowly varying function of ν). This approximation gives less accuracy in optical depth computations than the familiar Curtis-Godson approximation,[21,22] but Zdunkowski[23] has recently shown, using exact line-by-line transmission function computations, that the scaling approximation is accurate to at least two decimal places for a wide range of vertical atmospheric paths. Also, it proves much easier in practice to carry through the analysis of Sections 6.2 and 6.3 with the scaling approximation than with the Curtis-Godson approximation. In the latter, the coefficients a_i and exponents k_i in an exponential sum fit to $T_{\Delta\nu}$ become functions of the Curtis-Godson mean pressure $\bar{p}$, which in turn is a function of the levels z_1 and z_2 between which $T_{\Delta\nu}$ is desired; in the former, the a_i and k_i depend only on the frequency group $\Delta\nu$, simplifying the analysis and subsequent programming considerably.

The optical depth in the scaling approximation is, following Goody,[24]

$$\tau_a(z_1,z_2) = \alpha_1(\nu) \int_{z_1}^{z_2} (1 - e^{-h\bar{\nu}/kT}) \, \alpha_2(p,T)\,dz$$

$$= \alpha_{\nu}^{(line)}(p_o,T_o) \int_{z_1}^{z_2} (1 - e^{-h\bar{\nu}/kT}) \, \frac{\alpha_2(p,T)}{\alpha_2(p_o,T_o)}\,dz$$

$$= \alpha_{\nu}^{(line)}(p_o,T_o) \; u_{\bar{\nu}}(z_1,z_2) \qquad (6.10)$$

where

$$u_{\bar{\nu}}(z_1,z_2) = \int_{z_1}^{z_2} (1 - e^{-h\bar{\nu}/kT}) \, \frac{\alpha_2(p,T)}{\alpha_2(p_o,T_o)}\,dz \qquad (6.11)$$

$u_{\bar{\nu}}$ is called the "equivalent absorber amount." p_o and T_o are a reference pressure and temperature (e.g., STP). Most authors, including McClatchey,[20] make the further assumption that α_2 is a power-law function of pressure and temperature:

$$\alpha_2(p,T) = Ap^{\gamma} T^{\delta}$$

McClatchey, et.al. pick values of γ and δ which lead to an optimal fit of the exact transmission function. Different values of γ and δ are used for water vapor, for ozone, for the uniformly mixed absorbers (CO_2, N_2O, CO, CH_4, etc.), for the nitrogen collision-induced continuum around 4μ, and for the water vapor continuum between 8μ and 13μ. (The last two properly fall into the province of $\alpha_{\nu}^{(cont)}$, but are mentioned here for completeness.)

McClatchey, et.al. do not include the stimulated emission correction factor in their definition of $u_{\bar{\nu}}$, so that their $u_{\bar{\nu}}$ does not in fact depend on frequency at all. The reason for this may be that LOTRAN was not conceived as a tool for radiative transfer calculations per se, but rather as a means of obtaining transmission functions for laser applications, IR photography, etc.

6.2.2 Exponential-Sum Fitting as a Lebesgue Quadrature Rule

The transmission function (6.7) can be written in the scaling approximation as

$$T_{\Delta\nu} = \frac{1}{\Delta\nu} \int_{\Delta\nu} e^{-k_\nu u_{\bar{\nu}}/\mu} \, d\nu$$

where

$$k_\nu \equiv \alpha_\nu^{(line)} (p_o, T_o) \quad .$$

Presume now that, at a sequence of values $u_i (i=1, \ldots, N_u)$ of $u_{\bar{\nu}}$, we fit $T_{\Delta\nu}$ by a sum of exponentials:

$$T_{\Delta\nu}(u) \cong \sum_{i=1}^{M} a_i \, e^{-k_i u/\mu} \qquad (6.12)$$

The fit could be, say, in the least squares sense. M is envisioned as being fairly small, on the order of 5-10. Such fits have been discussed in the literature[25,26,27,28] for at least two decades, although the application is usually to a whole absorption band rather than a fairly narrow group such as

is being considered here. Methods for computing the a_i and k_i, knowing $T_{\Delta\nu}$, will be discussed in Section 6.2.4.

Rewriting Eq. (6.12) as

$$\frac{1}{\Delta\nu}\int_{\Delta\nu} e^{-k_\nu u/\mu}\, d\nu \cong \sum_{i=1}^{M} a_i\, e^{-k_i u/\mu} \tag{6.13}$$

it becomes clear that the sum on the right-hand side of Eq. (6.13) may be interpreted as a quadrature rule. Since M is to be roughly 5-10, the quadrature cannot be of the familiar Gaussian or Newton-Cotes type, because such quadrature rules would require literally thousands of terms to accurately integrate the line structure in $e^{-k_\nu u/\mu}$ (this is why line-by-line integration of transmission functions is so expensive). The rule is rather of the Lebesgue type, in which the ordinate in the graph of the integrand is partitioned rather than the abscissa (for a fuller discussion of Lebesgue quadrature, refer to Appendix A). The a_i are interpreted as the fraction of the interval $\Delta\nu$ over which k_ν is near k_i. From this interpretation, it is clear that we shall wish to restrict the a_i to be positive in any numerical fitting scheme.

As pointed out in Appendix A, the weights (here the a_i) in a Lebesgue quadrature rule depend on the function being integrated. However, large classes of functions may be quite accurately integrated by the same set of a_i. Based on our earlier arguments that i_ν and k_ν tend to vary together, we make the conjecture that $i_\nu\, e^{-k_\nu u/\mu}$ belongs to the same class as $e^{-k_\nu u/\mu}$ in the above sense and, therefore, may be integrated by the same quadrature rule:

$$\frac{1}{\Delta\nu}\int_{\Delta\nu} i_\nu\, e^{-k_\nu u/\mu}\, d\nu \cong \sum_{i=1}^{M} a_i\, i_j\, e^{-k_i u/\mu} \qquad (6.14)$$

We further conjecture that the intensity i_ν alone, and the integrand in Eq. (6.9), may be similarly quadratured:

$$i_{\Delta\nu} = \frac{1}{\Delta\nu}\int i_\nu\, d\nu \cong \sum_{i=1}^{M} a_i\, i_i \qquad (6.15)$$

$$\frac{1}{\Delta\nu}\int_{\Delta\nu} \exp\left[-\frac{\tau_a(0,z_1)}{\mu_{sun}} - \frac{\tau_a(z_1,z_2)}{\mu}\right]d\nu$$

$$= \frac{1}{\Delta\nu}\int_{\Delta\nu} \exp\left[-k_\nu\left\{\frac{u_\nu(0,z_1)}{\mu_{sun}} + \frac{u_\nu(z_1,z_2)}{\mu}\right\}\right]d\nu \qquad (6.16)$$

$$= \sum_{i=1}^{M} a_i \exp\left[-k_i\left\{\frac{u_\nu(0,z_1)}{\mu_{sun}} + \frac{u_\nu(z_1,z_2)}{\mu}\right\}\right]$$

The intensities i_i are as yet unspecified. However, since each i_i is associated with an "absorption coefficient" k_i, it is a reasonable conjecture that i_i is the solution of a monochromatic transfer problem with absorption coefficient k_i. This conjecture is verified in Section 6.2.3.

6.2.3 Splitting into Monochromatic Problems

Using the quadrature formulas of Eqs. (6.13) through (6.16), the frequency integrals of $J_\nu^{(0)}$ through $J_\nu^{(3)}$ (see Eqs. (6.4) and (6.5)) may be approximated as

$$J_{\Delta\nu}^{(0)} \cong \exp\left[-\frac{1}{\mu}\int_{z_o}^{z} k_{\bar{\nu}}^{(c)}(z')dz\right]$$

$$\cdot \sum_{i=1}^{M} a_i \; i_i(z_o,\mu) \; e^{-k_i u_{\bar{\nu}}(z_o,z)/\mu} \qquad (6.17)$$

$$J_{\Delta\nu}^{(1)} \cong \mu B_{\Delta\nu}(T(z'')) \exp\left[-\frac{1}{\mu}\int_{z''}^{z} \beta_{\bar{\nu}}(z')dz'\right]$$

$$\cdot \frac{\partial}{\partial z''}\left\{\exp\left[-\frac{1}{\mu}\int_{z''}^{z} \alpha_{\bar{\nu}}^{(cont)}(z')dz'\right]\right. \qquad (6.18)$$

$$\left. \cdot \sum_{i=1}^{M} a_i \; e^{-k_i u_{\bar{\nu}}(z'',z)/\mu}\right\}$$

$$J_{\Delta\nu}^{(2)} \cong \frac{\beta_{\bar{\nu}}(z'')}{2}\int_{-1}^{+1} d\mu' \; \bar{P}_{\bar{\nu}}(z'',\mu,\mu')$$

$$\cdot \exp\left[-\frac{1}{\mu}\int_{z''}^{z} k_{\bar{\nu}}^{(c)}(z')dz\right] \qquad (6.19)$$

$$\cdot \sum_{i=1}^{M} a_i \; i_i(z'',\mu') \; e^{-k_i u_{\bar{\nu}}(z'',z)/\mu}$$

$$J_{\Delta\nu}^{(3)} \cong \frac{S_{\Delta\nu}\beta_{\bar{\nu}}(z'')}{4\pi}\, \bar{P}_{\bar{\nu}}(z'',\mu,\mu_{sun})$$

$$\cdot \exp\left| - \frac{1}{\mu_{sun}} \int_0^{z''} k_{\bar{\nu}}^{(c)} dz' - \frac{1}{\mu} \int_{z''}^{z} k_{\bar{\nu}}^{(c)} dz \right|$$

$$\cdot \sum_{i=1}^{M} a_i \exp\left\{ - k_i \left| \frac{u_{\bar{\nu}}(0,z'')}{\mu_{sun}} + \frac{u_{\bar{\nu}}(z'',z)}{\mu} \right| \right\} \qquad (6.20)$$

where the continuum part of the opacity is

$$k_{\nu}^{(c)} \equiv \alpha_{\nu}'^{(cont)} + \beta_{\nu} .$$

Now suppose that the approximations of Eqs. (6.17) through (6.20) are put into the frequency-average of the transfer equation (6.4):

$$\sum_{i=1}^{M} a_i\, i_i(z,\mu) \cong i_{\Delta\nu}(z,\mu) = J_{\Delta\nu}^{(0)}$$

$$+ \frac{1}{\mu} \int_{z_0}^{z} \left| J_{\Delta\nu}^{(1)} + J_{\Delta\nu}^{(2)} + J_{\Delta\nu}^{(3)} \right| dz'' .$$

The summations, and the coefficients a_i (which are altitude-independent in the scaling approximation), may be commuted with the altitude integration on the right-hand side. Then if we regard the i_i (i=1, ..., M) as unknowns, the simplest (but by no means the only) way to determine them from the last equation is to equate the sums on each side term-by-term:

$$
\begin{aligned}
i_i(z,\mu) = {} & i_i(z_o,\mu)\ \exp\left|-\ \tau_i(z_o,z)/\mu\right| + \int_{z_o}^{z} dz''\ B_{\Delta\nu}(T(z'')) \\
& \cdot \exp\left|-\ \tau^{(s)}(z'',z)/\mu\right|\ \frac{\partial}{\partial z''}\exp\left|-\ \tau_i^{(a)}(z'',z)/\mu\right| \\
& + \frac{1}{\mu}\int_{z_o}^{z} dz''\ \frac{\beta_{\bar{\nu}}(z'')}{2}\int_{-1}^{+1}\bar{P}_{\bar{\nu}}(z'',\mu,\mu') \\
& \cdot i_i(z'',\mu')d\mu'\ \exp\left|-\ \tau_i(z'',z)/\mu\right| \\
& + \frac{1}{\mu}\int_{z_o}^{z} dz''\ \frac{S_{\Delta\nu}\beta_{\bar{\nu}}(z'')}{4\pi}\ \bar{P}_{\bar{\nu}}(z'',\mu,\mu_{sun}) \\
& \cdot \exp\left|-\ \frac{\tau_i(0,z'')}{\mu_{sun}} - \frac{\tau_i(z'',z)}{\mu}\right| \qquad (i=1,\ \ldots,\ M)
\end{aligned}
\tag{6.21}
$$

in which we have defined the scattering optical depth $\tau^{(s)}$, absorption optical depth $\tau_i^{(a)}$, and total optical depth τ_i as

$$
\begin{aligned}
\tau^{(s)}(z_1,z_2) &= \int_{z_1}^{z_2}\beta_{\bar{\nu}}(z)dz \\
\tau_i^{(a)}(z_1,z_2) &= \int_{z_1}^{z_2}\alpha_{\bar{\nu}}^{(cont)}(z)dz + k_i\ u_{\bar{\nu}}(z_1,z_2) \qquad (6.22) \\
\tau_i(z_1,z_2) &= \tau^{(s)}(z_1,z_2) + \tau_i^{(a)}(z_1,z_2)
\end{aligned}
$$

If we further define

$$\begin{aligned} \alpha_i(z'') &\equiv -\frac{\partial}{\partial z''}\tau_i^{(a)}(z'',z) \\ &= \alpha_{\bar{\nu}}'^{(\mathrm{cont})}(z'') - k_i\frac{\partial}{\partial z''}u_{\bar{\nu}}(z'',z) \\ &= \alpha_{\bar{\nu}}'^{(\mathrm{cont})}(z'') + k_i\left(1 - e^{-h\bar{\nu}/kT(z'')}\right) \\ &\quad \cdot \frac{\alpha_2(p(z''),T(z''))}{\alpha_2(p_o,T_o)} \end{aligned} \tag{6.23}$$

then the second (thermal emission) term on the right-hand side of Eq. (6.21) can be rewritten as

$$\frac{1}{\mu}\int_{z_o}^{z} dz''\ \alpha_i(z'')\ B_{\Delta\nu}(T(z''))\ \exp\left[-\tau_i(z'',z)/\mu\right]$$

which completes the formal identification of Eq. (6.21) with the monochromatic transfer equation (6.4). The changes from Eq. (6.4) are simply that $\bar{\nu}$, $\alpha_\nu'^{(\mathrm{cont})}$, and β_ν are evaluated at $\bar{\nu}$, B_ν and S_ν are averaged over $\Delta\nu$, $\alpha_\nu'^{(\mathrm{line})}$ becomes

$$k_i\left(1 - e^{-h\bar{\nu}/kT}\right)\frac{\alpha_2(p,T)}{\alpha_2(p_o,T_o)}$$

and i_ν becomes i_i. The solutions of the M monochromatic Eqs. (6.21) are combined according to Eq. (6.15) to yield the frequency-averaged intensity $i_{\Delta\nu}$.

The basic idea of this approach is due to Yamamoto, et.al.[27] and to Grant and Hunt.[28] However, these authors do not explicitly make the Lebesgue quadrature identification embodied in Eqs. (6.14) and (6.16), nor do they present any evidence for the correctness of those quadratures. An important task remaining to be performed is to investigate the accuracy of the frequency quadrature scheme by comparison with simple line-by-line solutions of the transfer equation.

6.2.4 Exponential-Sum Fitting

Obtaining the exponential-sum fit to the transmission function (see Eq. (6.12)) in an automatic fashion, with guaranteed convergence from initial guesses for the a_i and k_i, and for an arbitrary $T_{\Delta\nu}$, has proved to be a major stumbling block in the code development. What follows is a brief chronicle of our experience with several fitting schemes.

The approach taken was to minimize

$$F(a_1, \ldots, a_M, k_1, \ldots, k_M) =$$

$$\sum_{j=1}^{N_u} w_j \left\{ \sum_{i=1}^{M} a_i \, e^{-k_i u_j} - T_{\Delta\nu}(u_j) \right\}^2 \qquad (6.24)$$

subject to the constraints

$$a_i > 0 \quad \text{and} \quad k_i > 0 \qquad (i=1, \ldots, M) \qquad (6.25)$$

A further constraint,

$$\sum_{i=1}^{M} a_i = 1$$

was added in the beginning to ensure $T_{\Delta\nu}(0) = 1$ exactly, but it proved difficult to handle and was eventually rejected in favor of using $u = 0$ as one of the u_j. The weights w_j were originally taken to be unity, but the various algorithms tried seemed to converge more rapidly when

$$w_j = \frac{1}{[T_{\Delta\nu}(u_j)]^2}$$

which amounts to summing relative rather than absolute residuals.

The first types of methods surveyed were those of unconstrained minimization of a general scalar function $F(\vec{x})$. Of various standard methods[29,30,31,32,33] the one used by most authors is the Fletcher-Powell-Davidon (FPD) method.[34] It is guaranteed to be "stable," in the sense that the function value F decreases with each iteration step, and it is computationally economical.

As pointed out by Bard,[35] the method will fail if the H-matrix involved becomes singular, causing the search to be restricted to a sub-space of the full parameter space. To avoid this contingency, our version of FPD re-initialized H to the identity matrix I whenever $\det(H) < K$, where K was a pre-selected constant (H=I gives the method of steepest descents). Nevertheless, the suspicion remains that the failure of FPD for some of our test problems is due to the near-singularity of H.

Since the FPD method must be unconstrained, the constraints of Eq. (6.25) were incorporated into a transformation (suggested by Box[36])

$$a_i = \sin^2 y_i \qquad k_i = s_i^2$$

in which y_i and s_i are new unconstrained parameters. (An alternative would be to use the constrained version of FPD developed by Goldfarb,[37] but the complexity of Goldfarb's method hardly seemed warranted by the simple constraints $a_i, k_i > 0$.)

Two versions of FPD were tested; one used cubic interpolation for the one-dimensional minimization (as suggested by Fletcher and Powell[34]), and the other employed parabolic interpolation. The two versions performed similarly on several test problems in which a 4-term exponential fit was required for the functions

$$\text{(I)} \quad T_{\Delta\nu}(u) = 0.4e^{-6u} + 0.3e^{-4u} + 0.2e^{-u} + 0.1e^{-0.25u}$$

$$\text{(II)} \quad T_{\Delta\nu}(u) = e^{-\sqrt{u}}$$

$$\text{(III)} \quad T_{\Delta\nu}(u) = 0.7e^{-3\sqrt{u}} + 0.3e^{-\frac{1}{2}u^{3/2}}$$

Problem II represents the strong-line limit of the Goody band model transmission function.[24]

The FPD method (and the non-linear least squares methods discussed later) requires initial guesses for the a_i and k_i . Our experience shows that, unless these initial guesses are fairly good (that is, F is small initially) FPD does not converge, or converges to an unsatisfactory local minimum. Therefore, some effort was made to devise a satisfactory initialization procedure. The best one, as judged by its ability to approximate the coefficients and exponents of the $T_{\Delta\nu}(u)$ of problem I, involved "peeling off" a's and k's starting from the largest u_j's and working downward. If $0 = u_1 < u_2 < \ldots u_{N_u}$, then presume u_{N_u-1} is large

enough that one term $a_1 e^{-k_1 u}$ dominates the sum for $u \geq u_{N_u - 1}$. Knowing $T_{\Delta\nu}(u_{N_u})$ and $T_{\Delta\nu}(u_{N_u - 1})$ then enables us to solve for a_1 and k_1. Subtracting $a_1 e^{-k_1 u}$ from $T_{\Delta\nu}(u)$, we may now peel off a_2 and k_2; and so forth. Checks must be made that

$$T_{\Delta\nu}(u) - \sum_{i=1}^{I} a_i e^{-k_i u} > 0$$

and

$$\sum_{i=1}^{I} a_i < 1$$

at every step I; when either criterion first fails to be satisfied, the procedure must be terminated. The remaining unevaluated a's may be distributed uniformly in order to satisfy

$$\sum_{1}^{M} a_i = 1 \qquad \text{and} \qquad a_i > 0 \quad .$$

The remaining k's may be distributed uniformly between the last evaluated k and $k_{max} = k_M$. To estimate k_{max}, assume u_2 is small enough that we may approximate every exponential by its two-term series expansion:

$$T(u_2) = \sum_1^M a_i \, e^{-k_i u_2} \cong \sum_1^M a_i \, (1 - k_i u_2)$$

$$= 1 - u_2 \sum_1^M a_i k_i \cong 1 - u_2 \, a_M k_M$$

whereupon

$$k_M = \frac{1 - T(u_2)}{u_2 a_M}$$

Using the above initialization, the FPD method converges for test problems I and II, and diverges for test problem III. The divergence indicated that FPD would be unsatisfactory for fitting general transmission functions.

To find an alternative to FPD, a further literature search was undertaken into methods which capitalized on the particular form of F in Eq. (6.24), the so-called <u>non-linear least squares</u> (LS) methods. The simplest of these, usually called the Gauss-Newton method[38] was programmed. A calculation of problem I, resulted in rapid divergence. The failure was due to a gross overshoot in estimating the position of the one-dimensional minimum on one of the iterations. Further literature search indicated overshooting is a rather common problem in LS fitting, and that Levenberg[39] and later Marquardt[40] have devised remedies. The subroutine CNLLS, which is a highly sophisticated LS fitter using a modified Levenberg method, was therefore adapted from the Oak Ridge numerical analysis library[41] and applied to the

test problems. The results were the same as with FPD, except that convergence was much faster on problems I and II. Divergence was again experienced on problem III.

There remain three possibilities for a successful LS exponential-sum fitting routine:

(1) a subroutine of Lang and Müller[42] which has been requested from a program library in Ireland and which has still not arrived; it purports to be able to do exponential-sum fits;

(2) the Marquardt subroutine from Ref. (41), which is currently being implemented; and

(3) CNLLS run in its more sophisiticated mode, in which pre-specified sub-sets of the parameters are held invariant for a pre-specified number of iterations or until convergence for the active sub-set is attained.

Particular interest attaches to possibility (1) because the authors claim that their subroutine suppresses divergences of the type we encountered in problem III.

However, we felt that we could not rely exclusively on an LS method. Therefore, a literature search for non-LS methods of exponential-sum fitting was undertaken, and a substantial number of algorithms were found[43,44,45,46,47,48] Lanczos[47] discusses the fundamental problem in exponential approximation, which is that the exponentials are highly non-orthogonal functions. This implies that algorithms such

as Hudson's,[43] Rice's,[45] and Prony's[46] are extremely ill-conditioned numerically. The values of the a_i and k_i turn out to be extremely sensitive to the data $T_{\Delta\nu}(u_j)$; small changes in the $T_{\Delta\nu}$'s , even in the fifth or sixth decimal place, can produce large changes in the a_i and k_i . This is a consequence of the fact that there are many fits, with widely varying a_i's, k_i's, and M's , which can approximate a given $T_{\Delta\nu}$ to the accuracy to which it is known. Lanczos and Hildebrand[46] give examples of this phenomenon.

This non-uniqueness raises the question of whether any physical interpretation can be attached to the k_i or whether the whole procedure of Sections 6.2.2 and 6.2.3 can only be judged by the correctness of $i_{\Delta\nu}$, the intervening steps being regarded purely as a mathematical device. The comments of Lanczos together with our own experience cause us to lean to the latter interpretation. It then also becomes incumbent that any two equally good fits of $T_{\Delta\nu}$ should lead to the same $i_{\Delta\nu}$, a requirement that remains to be checked.

The available algorithms divide rather naturally into those with pre-specified M[43,45,46,47] and those in which the algorithm determines M.[44,48] Since there is no a priori basis on which to choose M, having it determined by the algorithm seems to be a desirable property. Gardner's method,[44] which requires a numerical Fourier transform $g_{\Delta\nu}(k)$ of $T_{\Delta\nu}$, would be extremely difficult to program, since it involves a good deal of adjusting of the limits of integration of two infinite integrals in order to distinguish spurious peaks in $g_{\Delta\nu}(k)$ from real peaks (representing the k_i). As for the fixed-M methods, they suffer a further disadvantage in that they all solve for the k_i as roots of a polynomial whose coefficients are determined by a generally

ill-conditioned linear least squares procedure. The instability of polynomial roots to coefficient variations is well-known, and hence there is a substantial possibility of grossly mis-estimating the k_i in all the fixed-M methods. Furthermore, there is nothing to prevent negative or complex k_i. Thus, these methods are poor choices.

The remaining candidate is the Cantor and Evans method[48] which has several advantageous properties in addition to determining its own M. Of these the most important is unconditional convergence (to arbitrary accuracy). In addition, the size of M is controlled by the desired accuracy and $a_i > 0$ and $k_i > 0$. A disadvantage is that the u_j must be equally spaced. But, all things considered, the method of Cantor and Evans seems eminently suited to our problem.

Professor Evans, who is at the University of California at San Diego, has agreed to consult with us on his method. We anticipate a working version shortly.

6.3 THE MONOCHROMATIC EQUATION OF TRANSFER

The method of solution of the radiative transfer equation due to Grant and Hunt[49,50,51,52,53,54] has been chosen to solve the monochromatic problems arising in Section 6.2. Grant and Hunt's procedure requires no iteration in the presence of scattering, allows zones of arbitrary size, and is computationally economical. It brings together several lines of research in radiative transfer. On the one hand, it represents, for 1-D plane parallel problems, the culmination of the discrete space formulation of transfer theory associated with Preisendorfer[55] and van de Hulst.[56] On the other hand, it reduces in the limit of small zone size to the differential formulation of Rybicki and Usher,[57] which

represented an elegant formulation of the method of invariant imbedding. Lastly, it improves upon the S_n method[58] (by eliminating the need for zone-centered intensities) to the point where previous S_n methods for plane parallel geometry are now virtually obsolete.

The elimination of scattering iteration is a very significant feature of the Grant and Hunt method. To iterate in the previously proposed fashion[1] when optically thick clouds are present would have been prohibitively expensive. Other attractive features of the method are:

(1) a single inequality imposed on the "primary layer thickness" $\Delta\tau_p$ (cf. Section 6.3.1) assures both positivity of intensities and computational stability;

(2) flux is conserved provided only that the phase function F_ν is correctly normalized (cf. Section 6.4); and

(3) error estimates are available.

More generally the Grant and Hunt method possesses a certain elegance, simplicity, and freedom from *ad hoc* assumptions which alternative methods lack.

The basis of the Grant and Hunt method is the *interaction principle*,[50]

$$u^+(\tau_2) = t(\tau_2,\tau_1)\, u^+(\tau_1) + r(\tau_1,\tau_2)\, u^-(\tau_2) + \Sigma^+(\tau_1,\tau_2)$$

$$u^-(\tau_1) = r(\tau_2,\tau_1)\, u^+(\tau_1) + t(\tau_1,\tau_2)\, u^-(\tau_2) + \Sigma^-(\tau_1,\tau_2) \qquad (6.26)$$

Figure 6.1 illustrates the various quantities involved in describing the interactions in the slab between τ_1 and τ_2. The total optical depth coordinate is τ and $\mu = \cos\theta$ is the cosine of the angle between the ray and the vertical. The u^+'s are positively directed ($\mu > 0$) intensities, the u^-'s negatively directed ($\mu < 0$) intensities (the μ-dependence is implicit). The r's and t's are integral operators representing reflection from and transmission through the slab $[\tau_1,\tau_2]$, and the Σ's represent effective internal sources in $[\tau_1,\tau_2]$. We now approximate the angular integrals in the interaction principle by half-range Gaussian or Radau quadratures with weights c_i and angles $0 < \mu_1 < \ldots < \mu_m \leq 1$ ($\mu_m = 1$ for Radau quadrature). (By using half-range quadrature, an idea originally due to Krook,[59] in which separate but symmetric quadrature formulas are used for $0 \leq \mu \leq 1$ and $-1 \leq \mu \leq 0$, discontinuities in the intensity across $\mu = 0$ ($\theta = 90°$) which may occur physically are allowed for.) The r's and t's become matrix operators, and the u's and Σ's become vectors:

$$u^{\pm}(\tau) = \begin{bmatrix} i_\nu(\tau,\pm\mu_1) \\ \vdots \\ i_\nu(\tau,\pm\mu_m) \end{bmatrix} \qquad \Sigma^{\pm}(\tau_1,\tau_2) = \begin{bmatrix} \Sigma(\tau_1,\tau_2,\pm\mu_1) \\ \vdots \\ \Sigma(\tau_1,\tau_2,\pm\mu_m) \end{bmatrix} \qquad (6.27)$$

where i_ν has been written as a function of τ rather than z. Eq. (6.26) will now be taken to be in this matrix-vector form.

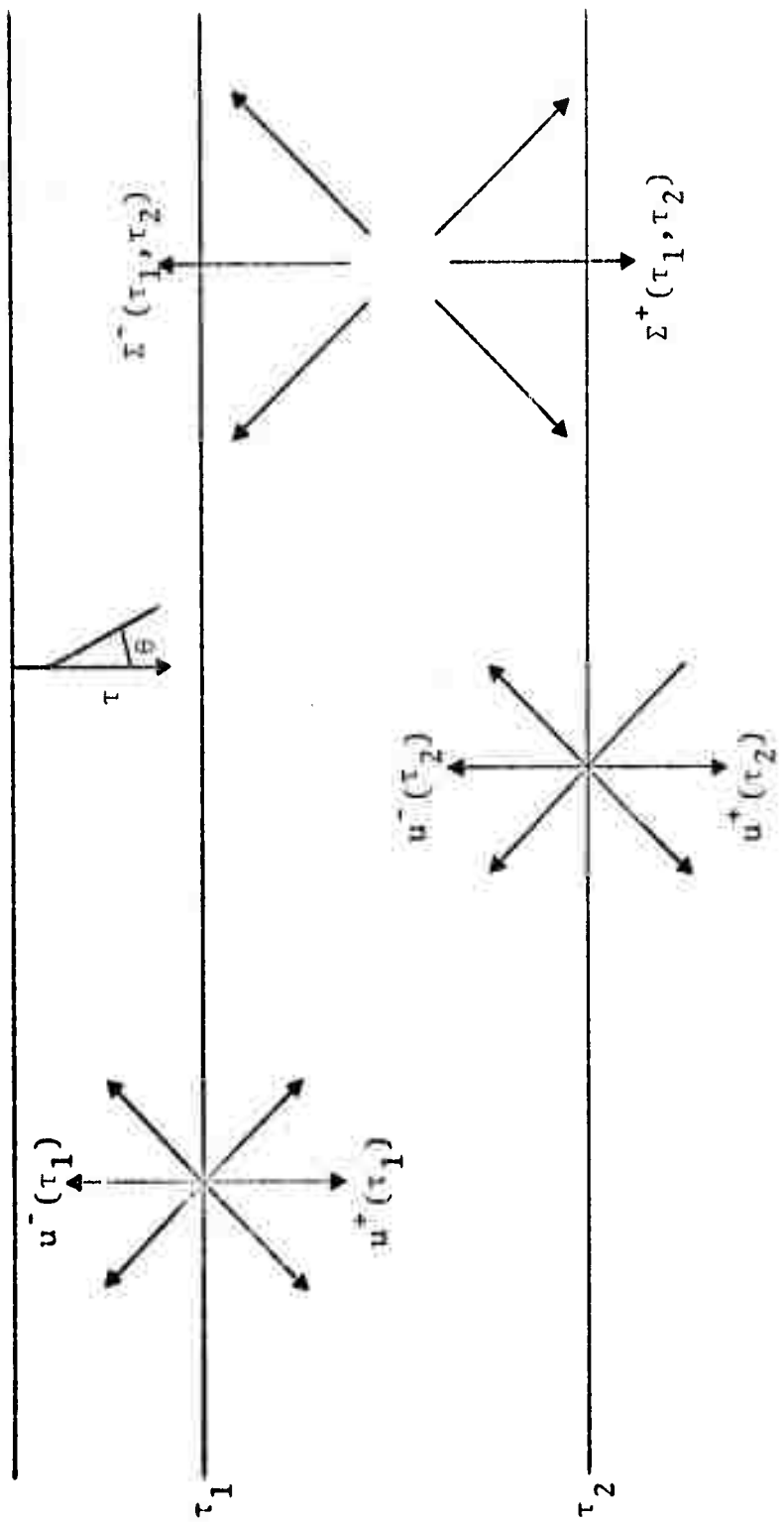

Figure 6.1. Diagram of interaction principle.

For the sake of computational economy, we intend to use only a relatively few ($m \leq 7$) angles. Therefore, the desirability of solving for the diffuse intensity i_ν rather the full intensity $\bar{I}_\nu$, which includes the solar flux, is apparent; if we used $\bar{I}_\nu$, many more angles μ_i would be needed to resolve the solar peak, and these could no longer be distributed in the optimal (Gaussian) way. We are, of course, ignoring a possible specular reflection peak in i_ν, which has not been subtracted out. (This would be of concern only over fairly smooth water surfaces.) Tests will be performed for a variety of situations to ensure that the angular discretization is adequate to determine fluxes accurately.

6.3.1 Layer Composition

We now consider how r, t, Σ for each zone are to be obtained. Each zone is divided into sub-layers called primary layers, which are optically thin enough that r, t, Σ for each primary layer can be obtained from the physical quantities B_ν, $\bar{P}_\nu$, etc. of the differential formulation, Eq. (6.3). Then the primary-layer r's, t's, Σ's are "added up," by a process we shall call layer composition, to obtain r's, t's, and Σ's for the entire zone.

The appropriate primary-layer quantities, derived by comparing the limits as $\Delta\tau = \tau_2 - \tau_1 \to 0$ of Eqs. (6.26) with Eq. (6.3), are[50]

$$t(\tau_2,\tau_1) = t(\tau_1,\tau_2) = I - M^{-1}\left[I - \frac{\omega(\xi)}{2} P^{++}(\xi)c\right]\Delta\tau + O(\Delta\tau^2)$$

$$r(\tau_2,\tau_1) = r(\tau_1,\tau_2) = \frac{\omega(\xi)}{2} M^{-1} P^{+-}(\xi)c\Delta\tau + O(\Delta\tau^2) \quad (6.28)$$

$$\Sigma^{\pm}(\tau_1,\tau_2) = M^{-1} B^{\pm}(\xi)\Delta\tau + O(\Delta\tau^2)$$

To $O(\Delta\tau)$, $t(\tau_2,\tau_1)$ and $t(\tau_1,\tau_2)$ are identical; however, they may differ in $O(\Delta\tau^2)$ terms. A similar remark applies to r. The various scalars, matrices, and vectors occurring in Eqs. (6.28) are defined as

$$\Delta\tau = \tau_2 - \tau_1 \quad , \quad \tau_1 \leq \xi \leq \tau_2 \quad ,$$

$$M = [\mu_i \delta_{ij}] \quad , \quad c = [c_i \delta_{ij}] \quad ,$$

$$P^{++}(\tau) = [\bar{P}_\nu(\tau,\mu_i,\mu_j)] = [\bar{P}_\nu(\tau,-\mu_i,-\mu_j)] \quad ,$$

$$P^{+-}(\tau) = [\bar{P}_\nu(\tau,\mu_i,-\mu_j)] = [\bar{P}_\nu(\tau,-\mu_i,\mu_j)] \quad ,$$

$$\omega(\tau) = \frac{\beta_\nu(\tau)}{\kappa_\nu(\tau)} \tag{6.29}$$

$$\hat{B}(\tau,\mu) = [1 - \omega(\tau)]\, B_\nu(T(\tau)) + \frac{S_\nu\, \omega(\tau)}{4\pi}\, \bar{P}_\nu(\tau,\mu,\mu_{sun}) e^{-\tau/\mu_{sun}}$$

$$B^{\pm}(\tau) = \begin{bmatrix} \hat{B}(\tau,\pm\mu_1) \\ \vdots \\ \hat{B}(\tau,\pm\mu_m) \end{bmatrix}$$

It is worthwhile to note that the error terms in Eqs. (6.28) will, in fact, be $O(\Delta\tau^3)$ if ξ is chosen as the mid-point of $[\tau_1,\tau_2]$. This follows from Taylor's theorem.

In order to guarantee positive intensities, all elements of the primary-layer r- and t-matrices in Eq. (6.28) must be positive. Ignoring $O(\Delta\tau^2)$ terms, this reduces to

the requirement that the diagonal elements of t be positive, which gives us the following restriction on $\Delta\tau$:

$$\Delta\tau < \Delta\tau_{max} = \min_{1\le i\le m}\left[\frac{\mu_i}{1 - \frac{\omega(\xi)}{2} c_i \overline{P}_\nu(\xi,\mu_i,\mu_i)}\right] \qquad (6.30)$$

It is also true that this property of positive elements in r and t is preserved by layer composition,[51] so that no restrictions beyond Eq. (6.30) are necessary.

The question of truncation error, that is, the error incurred by neglecting $O(\Delta\tau^2)$ terms in Eqs. (6.28), is also of concern. Grant and Hunt have used as a practical criterion[51]

$$\Delta\tau = \frac{1}{2}\Delta\tau_{max}$$

Grant* has also made some estimates of the growth of truncation error during the process of layer composition. He finds that if T_n and R_n are the correct transmission and reflection matrices for a layer of thickness $n\Delta\tau$, and if this is built up by composing primary layers of thickness $\Delta\tau$, then the effect of <u>small</u> truncation errors η in T_1 and ρ in R_1 is to give approximate matrices t_n, r_n such that

$$\begin{aligned} ||T_n - t_n|| &< Cn\lambda^n(||\rho|| + ||\eta||) \\ ||R_n - r_n|| &< 2n(||\rho|| + ||\eta||) \end{aligned} \qquad (6.31)$$

*Private communication.

where C and λ are defined such that

$$||t_n|| < C\lambda^n \qquad (0 < \lambda \leq 1)$$

and $||\ ||$ is the norm of Ref. (51). Thus, for fixed $\Delta\tau$, the absolute error in R_n and the relative error in T_n grow about linearly with n. If we use an approximation in which

$$||\rho|| + ||\eta|| = O(\Delta\tau^{\alpha+1})$$

and write $n = H/\Delta\tau$ for fixed H, then

$$\begin{aligned} ||T(H) - t(H)|| &< KCH\ \lambda^n\ \Delta\tau^{\alpha} \\ ||R(H) - r(H)|| &< 2KH\ \Delta\tau^{\alpha} \end{aligned} \qquad (6.32)$$

so that the errors tend to zero as $\Delta\tau \to 0$. Currently, we intend to ignore $O(\Delta\tau^2)$ terms in Eqs. (6.28), so that $\alpha = 1$ (or $\alpha = 2$ if ξ is taken as the mid-point). If time permits, however, we may investigate the advantages of carrying more terms in the expansion.

The layer composition formulas are derived as follows. Suppose $\tau_1 < \tau_2 < \tau_3$. Write down the interaction principle (6.26) for the layer $[\tau_1,\tau_2]$, and again for the layer $[\tau_2,\tau_3]$. Eliminate $u^+(\tau_2)$ and $u^-(\tau_2)$ from two of these equations using the remaining two. Put the first two equations in the form of an interaction principle for the layer $[\tau_1,\tau_3]$. Then identify $r_{13} \equiv r(\tau_1,\tau_3)$, etc. from this principle. The results are

$$
\begin{aligned}
r_{13} &= r_{23} + t_{32}\Gamma\, r_{12}\, t_{23} \\
r_{31} &= r_{21} + t_{12}\hat{\Gamma}\, r_{32}\, t_{21} \\
t_{31} &= t_{32}\Gamma\, t_{21} \\
t_{13} &= t_{12}\hat{\Gamma}\, t_{23} \\
\Sigma^{+}_{13} &= t_{32}\Gamma\,(r_{12}\,\Sigma^{-}_{23} + \Sigma^{+}_{12}) + \Sigma^{+}_{23} \\
\Sigma^{-}_{13} &= t_{12}\hat{\Gamma}\,(r_{32}\,\Sigma^{+}_{12} + \Sigma^{-}_{23}) + \Sigma^{-}_{12}
\end{aligned}
\tag{6.33}
$$

where

$$
\begin{aligned}
\Gamma &= (I - r_{12}\, r_{32})^{-1} \\
\hat{\Gamma} &= (I - r_{32}\, r_{12})^{-1} = 1 + r_{32}\Gamma\, r_{12}
\end{aligned}
\tag{6.34}
$$

In the special case when the layer $[\tau_1,\tau_3]$ is <u>homogeneous</u>, (i.e., when $\omega(\tau)$, $P^{++}(\tau)$, and $P^{+-}(\tau)$ do not vary significantly across $[\tau_1,\tau_3]$) and if the two layers $[\tau_1,\tau_2]$ and $[\tau_2,\tau_3]$ are of equal thickness $\Delta\tau$, then formulas (6.33) simplify somewhat:

$$
\begin{aligned}
r_1 \equiv r_{13} = r_{31} &= r_o + t_o\,\Gamma_o\, r_o\, t_o \\
t_1 \equiv t_{13} = t_{31} &= t_o\,\Gamma_o\, t_o \\
\Sigma^{+}_1 \equiv \Sigma^{+}_{13} &= t_o\,\Gamma_o(r_o\,\Sigma^{-}_o + \Sigma^{+}_o) + \Sigma^{+}_o \\
\Sigma^{-}_1 \equiv \Sigma^{-}_{13} &= t_o\,\Gamma_o(r_o\,\Sigma^{+}_o + \Sigma^{-}_o) + \Sigma^{-}_o
\end{aligned}
\tag{6.35}
$$

where

$$\Gamma_o = (I - r_o\, r_o)^{-1}$$

and

$$\begin{aligned} r_o &\equiv r_{12} = r_{21} = r_{23} = r_{32} \\ t_o &\equiv t_{12} = t_{21} = t_{23} = t_{32} \\ \Sigma_o^{\pm} &\equiv \Sigma_{12}^{\pm} = \Sigma_{23}^{\pm} \end{aligned} \tag{6.36}$$

Relations (6.36) follow from Eqs. (6.28) by the assumptions of homogeneity and equal $\Delta\tau$'s . The single-subscript notation indicates that r, t, Σ depend on only one argument instead of two, that argument being the corresponding layer thickness. Defining

$$r_n = r(2^n\, \Delta\tau) \quad , \quad \text{etc.}$$

it is possible to continue the above process, called <u>doubling</u>, through any homogeneous region,

$$\begin{aligned} t_{n+1} &= t_n\, \Gamma_n\, t_n \\ r_{n+1} &= r_n + t_n\, \Gamma_n\, r_n\, t_n \\ \Sigma_{n+1}^{+} &= t_n\, \Gamma_n (r_n\, \Sigma_n^{-} + \Sigma_n^{+}) + \Sigma_n^{+} \\ \Sigma_{n+1}^{-} &= t_n\, \Gamma_n (r_n\, \Sigma_n^{+} + \Sigma_n^{-}) + \Sigma_n^{-} \end{aligned} \tag{6.37}$$

Doubling is much faster than simple layer addition as embodied in Eqs. (6.33). To add 2^N primary layers comprising a homogeneous layer requires $2^N - 1$ layer additions versus only N doublings.

In the future the code will allow for arbitrarily larger zones, which may or may not be homogeneous. If a zone is homogeneous, doubling will be used; if it is not, the code will partition it into sub-zones which <u>are</u> homogeneous, double within each of the sub-zones, and add the sub-zones using Eqs. (6.33). For now, however, the code will be constructed on the assumption that each zone is homogeneous. This is fairly restrictive, since it implies that neither the scattering nor the absorption coefficient vary substantially across a zone. No more than 40 zones should be necessary, however, and this does not seem overly burdensome (Grant and Hunt run with about 40 zones*).

6.3.2 <u>Source Doubling</u>

The problem of an inhomogeneous source $\Sigma^{\pm}$ in a zone which is otherwise homogeneous requires special attention. An inhomogeneous source region will occur frequently on account of the factor $e^{-\tau/\mu_{sun}}$ in $\hat{B}(\tau,\mu)$ and on account of the rapid variation of $B_\nu(T)$ with T in many spectral regions. It turns out, however, that the most frequently occurring types of source inhomogeneity still admit a modified form of doubling. Inhomogeneous sources can be doubled right along with r and t with the resulting saving of computing time.

Let us begin by developing a general formula for source composition when the source variation across an otherwise homogeneous zone is described by $f(\tau)$. Referring to

---

*Private communication.

Figure 6.2 and Eqs. (6.28), let the source vector for any one of the primary layers be

$$\Sigma_i^{\pm} = \Sigma_p^{\pm} f(\xi_i) \qquad i = 1, \ldots, 2^N \tag{6.38}$$

where $\Sigma_p^{\pm}$ are independent of τ, and ξ_i is the mid-point of primary layer i,

$$\xi_i = \tau_o + i\Delta\tau - \frac{\Delta\tau}{2} \tag{6.39}$$

Adding the sources in layers 1 and 2 according to Eqs. (6.33), it is clear that the source $\Sigma_{1+2}^{\pm}$ for the combined layer will be a linear combination of $f(\xi_1)$ and $f(\xi_2)$:

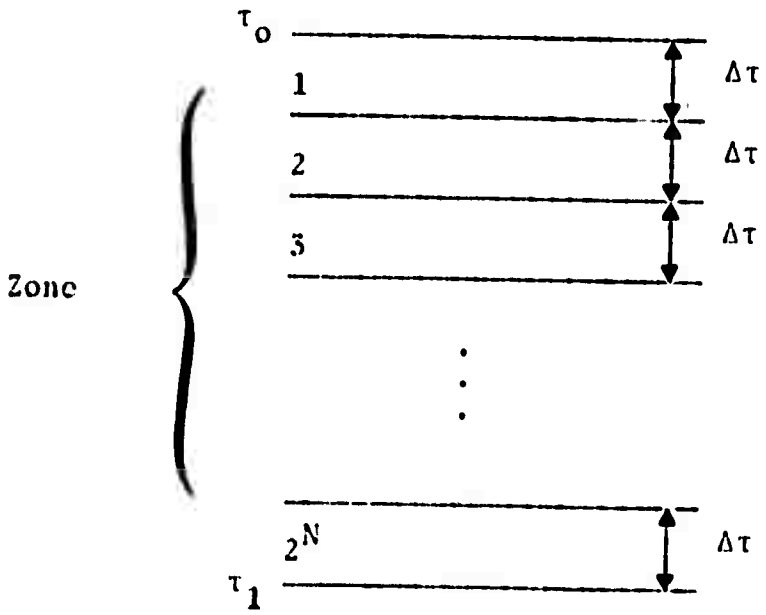

Figure 6.2. Homogeneous zone composed of 2^N primary layers.

$$\Sigma^{\pm}_{1+2} = V^{\pm}_{1}(1)\ f(\xi_1) + V^{\pm}_{2}(1)\ f(\xi_2)$$

(The expressions for the V's are not of interest here.) Similarly, the source for the combined layer 3+4 involves only a change in the ξ's:

$$\Sigma^{\pm}_{3+4} = V^{\pm}_{1}(1)\ f(\xi_3) + V^{\pm}_{2}(1)\ f(\xi_4)$$

Then, upon combining layers 1+2 and 3+4, a linear combination of $f(\xi_1)$ through $f(\xi_4)$ results:

$$\Sigma^{\pm}_{1+2+3+4} = \sum_{\ell=1}^{4} V^{\pm}_{\ell}(2)\ f(\xi_\ell)$$

Suppose that any 2^n adjacent primary layers have been superposed in the above manner. Using the notation

$$\Sigma^{\pm}_{(i,n)} = \Sigma^{\pm}_{i+(i+1)+\ \ldots\ +(i+2^n-1)}$$

where i denotes the first primary layer in the grouping, it is possible to prove by induction that

$$\Sigma^{\pm}_{(i,n)} = \sum_{\ell=1}^{2^n} V^{\pm}_{\ell}(n)\ f(\xi_{i+\ell-1}) \qquad (6.40)$$

We now specialize our considerations to the solar source $(f(\tau) = e^{-\tau/\mu_{sun}})$ and the Planck source $\{f(\tau) = B_\nu(T(\tau))\}$. By the linearity of the source composition formulas (6.33) it is possible to compose the solar

source and Planck source separately and then simply add the results at the end to obtain the full source.

For the case of the solar source, the quantities $\Sigma_P^{\pm}$ of Eq. (6.38) are, from Eqs. (6.28) and (6.29),

$$\Sigma^{\pm}_{P,sol} = \frac{S_\nu\ \omega(\bar{\tau})}{4\pi}\ \Delta\tau\ M^{-1} \begin{bmatrix} \bar{P}_\nu(\bar{\tau}, \pm\mu_1, \mu_{sun}) \\ \\ \bar{P}_\nu(\bar{\tau}, \pm\mu_m, \mu_{sun}) \end{bmatrix} \tag{6.41}$$

Since ω and $\bar{P}_\nu$ are assumed not to vary across the zone, the argument $\bar{\tau}$ refers to the mid-point of the entire zone in Figure 6.2. Now assume that, beginning with the $\Sigma^{\pm}_{P,sol}$ and Eq. (6.38), the first 2^n primary layers have been composed, so that the $\Sigma^{\pm}_{(1,n)}$ are known. The adjacent 2^n primary layers will then, by Eq. (6.40), have source vectors

$$\begin{aligned} \Sigma^{\pm}_{(1+2^n,n)} &= \sum_{\ell=1}^{2^n} V_\ell^{\pm}(n)\ f(\xi_{\ell+2^n}) \\ &= \sum_{\ell=1}^{2^n} V_\ell^{\pm}(n)\ e^{-(\tau_o + (\ell+2^n)\Delta\tau - \frac{\Delta\tau}{2})/\mu_{sun}} \\ &= e^{-2^n\Delta\tau/\mu_{sun}}\ \Sigma^{\pm}_{(1,n)} \\ &= h_n\ \Sigma^{\pm}_{(1,n)} \end{aligned} \tag{6.42}$$

where

$$h_n = e^{-2^n \Delta\tau/\mu_{sun}} \tag{6.43}$$

Remembering the definitions $r_n = r(2^n \Delta\tau)$, etc., the sources $\Sigma^{\pm}_{(1,n+1)}$ for the combined layer, containing 2^{n+1} primary layers, are

$$\begin{aligned}
\Sigma^{+}_{(1,n+1)} &= t_n \Gamma_n \left(r_n \Sigma^{-}_{(1+2^n,n)} + \Sigma^{+}_{(1,n)} \right) + \Sigma^{+}_{(1+2^n,n)} \\
&= t_n \Gamma_n \left(r_n h_n \Sigma^{-}_{(1,n)} + \Sigma^{+}_{(1,n)} \right) + h_n \Sigma^{+}_{(1,n)} \\
\Sigma^{-}_{(1,n+1)} &= t_n \Gamma_n \left(r_n \Sigma^{+}_{(1,n)} + \Sigma^{-}_{(1+2^n,n)} \right) + \Sigma^{-}_{(1,n)} \\
&= t_n \Gamma_n \left(r_n \Sigma^{+}_{(1,n)} + h_n \Sigma^{-}_{(1,n)} \right) + \Sigma^{-}_{(1,n)}
\end{aligned} \tag{6.44}$$

These are adaptations of the source composition formulas in Eqs. (6.33). From the definition of h_n, it is obvious that

$$h_{n+1} = h_n^2 \tag{6.45}$$

Together, Eqs. (6.44) and (6.45) form a doubling scheme for the solar (or any exponential) source. The scheme is initialized by

$$\begin{aligned}
\Sigma^{\pm}_{(1,0)} &= \Sigma^{\pm}_{P,sol} \, e^{-(\tau_o + \frac{\Delta\tau}{2})/\mu_{sun}} \\
h_o &= e^{-\Delta\tau/\mu_{sun}}
\end{aligned} \tag{6.46}$$

and iterated from $n = 0$ to $n = N - 1$.

In order to derive doubling formulas for the Planck source, it is necessary to have a more tractable functional form for $f(\tau)$ than $B_\nu(T(\tau))$. In Appendix B it is shown that it is reasonable to assume B_ν is piecewise linear in τ, so that

$$f(\tau) = B_\nu(T(\tau)) = B_o + B'(\tau - \tau_o) \tag{6.47}$$

across the zone of Figure 6.2, where

$$B_o \equiv B_\nu(T(\tau_o))$$

$$B' \equiv \frac{B_\nu(T(\tau_1)) - B_\nu(T(\tau_o))}{\tau_1 - \tau_o}$$

Expressing this in terms of ξ_i (see Eq. (6.39)),

$$\begin{aligned} f(\xi_i) &= B_o + B'(\tau_o + i\Delta\tau - \frac{\Delta\tau}{2} - \tau_o) \\ &= B'_o + B'\, i\Delta\tau \end{aligned} \tag{6.48}$$

where

$$B'_o = B_o - B'\,\frac{\Delta\tau}{2}$$

The sources $\Sigma^{\pm}_{(1,n)}$ for the first 2^n primary layers then become

$$\Sigma^{\pm}_{(1,n)} = \sum_{\ell=1}^{2^n} V^{\pm}_{\ell}(n)\ (B'_o + B'\ell\,\Delta\tau)$$

while for the adjacent 2^N primary layers

$$\Sigma^{\pm}_{(1+2^n,n)} = \sum_{\ell=1}^{2^n} V_\ell^{(n)} \left[B'_0 + B'(\ell+2^n)\Delta\tau\right]$$
$$= \Sigma^{\pm}_{(1,n)} + 2^n B' \Delta\tau \, Y^{\pm}_n \qquad (6.49)$$

where

$$Y^{\pm}_n \equiv \sum_{\ell=1}^{2^n} V^{\pm}_\ell(n)$$

The $Y^{\pm}_n$ refer to a constant source $f(\tau) = 1$, and so may be calculated by doubling as in Eqs. (6.37). A further simplification is that symmetry prevails,

$$Y_n \equiv Y^+_n = Y^-_n$$

This is intuitively obvious, since a constant source would be expected to emit the same at $-\mu$ as at $+\mu$. It can be proven inductively by first noting that the $\Sigma^{\pm}_p$ of Eq. (6.38), which for the Planck source are,

$$\Sigma^{\pm}_{P,p1k} = \left[1 - \omega(\bar{\tau})\right]\Delta\tau \, M^{-1} \begin{bmatrix} 1 \\ 1 \\ \vdots \\ 1 \end{bmatrix}$$
$$= \left[1 - \omega(\bar{\tau})\right]\Delta\tau \begin{bmatrix} 1/\mu_1 \\ \vdots \\ 1/\mu_m \end{bmatrix} \qquad (6.50)$$

are equal,

$$\Sigma_{p,p1k} \equiv \Sigma^{+}_{p,p1k} = \Sigma^{-}_{p,p1k} \quad .$$

Because $f(\tau) \equiv 1$,

$$Y^{\pm}_{o} = \Sigma_{p,p1k} \tag{6.51}$$

by Eq. (6.38), so that symmetry is proved for $n = 0$. If symmetry has been proved for a general n , then from the doubling formulas (6.37)

$$Y^{+}_{n+1} = t_n \Gamma_n (r_n Y_n + Y_n) + Y_n$$

$$Y^{-}_{n+1} = t_n \Gamma_n (r_n Y_n + Y_n) + Y_n = Y^{+}_{n+1}$$

which completes the induction proof, and gives us the simplified doubling formula

$$Y_{n+1} = [I + t_n \Gamma_n (I + r_n)] Y_n \tag{6.52}$$

for Y_n .

The two layers, each containing 2^n primary layers, are now composed just as for the exponential source (see Eqs. (6.44)):

$$\Sigma^{+}_{(1,n+1)} = t_n \Gamma_n\left[r_n(\Sigma^{-}_{(1,n)} + 2^n B' \Delta\tau Y_n) + \Sigma^{+}_{(1,n)}\right] + \Sigma^{+}_{(1,n)} + 2^n B' \Delta\tau Y_n$$

$$\Sigma^{-}_{(1,n+1)} = t_n \Gamma_n\left[r_n \Sigma^{+}_{(1,n)} + \Sigma^{-}_{(1,n)} + 2^n B' \Delta\tau Y_n\right] + \Sigma^{-}_{(1,n)} \qquad (6.53)$$

Together, Eqs. (6.52) and (6.53) form a doubling scheme for the Planck (and any linear-in-τ) source. The scheme is initialized by Eq. (6.51) and by

$$\Sigma^{\pm}_{(1,0)} = (B'_0 + B' \Delta\tau)Y_0 \qquad (6.54)$$

and iterated from $n = 0$ to $n = N - 1$.

More accurate piecewise polynomial approximations to $B_\nu(T(\tau))$ are possible, at the expense of more complicated source doubling formulas. In particular, economical piecewise quadratic and piecewise cubic schemes have been derived and will be programmed at a future date to ascertain if the increased accuracy of the heating-rate calculations so obtained warrants the additional computational expense.

6.3.3 Forward and Backward Passes

By the procedures of sections 6.3.1 and 6.3.2, we obtain reflection and transmission matrices and source vectors for every zone of the atmosphere. If the zone structure is

$$0 = \tau_1 < \tau_2 < \ldots < \tau_{N+1}$$

and the notation is

$$u_n^{\pm} = u^{\pm}(\tau_n)$$

$$r_{n,n\pm1} \equiv r(\tau_n,\tau_{n\pm1}) \qquad (6.55)$$

$$t_{n,n\pm1} \equiv t(\tau_n,\tau_{n\pm1})$$

$$\Sigma^{\pm}_{n,n+1} = \Sigma^{\pm}(\tau_n,\tau_{n+1})$$

then according to the Grant and Hunt algorithm (whose derivation is lengthy and will not be repeated here) the solution for the intensity vectors $u_n^{\pm}$ splits into two parts.

The first part is the <u>forward pass</u>. In the forward pass, the m×m matrices E_n, G_n, and H_n and the m-vectors $V_n^{(1)}$, $V_n^{(2)}$, and $V_n^{(3)}$ are calculated recursively as follows:

$$E_1 = 0 \qquad V_1^{(1)} = V_1^{(2)} = V_1^{(3)} = 0 \qquad (6.56a)$$

$$\tilde{\Gamma}_{n+1} = (I - r_{n+1,n}\, E_n)^{-1} \qquad (6.56b)$$

$$H_{n+1} = \tilde{\Gamma}_{n+1}\, t_{n,n+1} \qquad (6.56c)$$

$$G_{n+1} = E_n\, H_{n+1} \qquad (6.56d)$$

$$E_{n+1} = r_{n,n+1} + t_{n+1,n}\, G_{n+1} \qquad (6.56e)$$

$$V_{n+1}^{(1)} = \tilde{\Gamma}_{n+1}\,(r_{n+1,n}\, V_n^{(3)} + \Sigma^{-}_{n,n+1}) \qquad (6.56f)$$

$$V_{n+1}^{(2)} = V_n^{(3)} + E_n \, V_{n+1}^{(1)} \qquad (6.56g)$$

$$V_{n+1}^{(3)} = t_{n+1,n} \, V_{n+1}^{(2)} + \Sigma_{n,n+1}^{+} \qquad (6.56h)$$

$$(n = 1,2, \ldots, N)$$

The initialization of $V_1^{(3)}$ at zero reflects the fact that there is no incident diffuse radiation at the top of the atmosphere, $\tau = 0$ (the incident solar radiation is already accounted for by the transformation from T_ν to i_ν). Economy of storage is achieved by performing the sub-layer superpositions, which yield the r's, t's, and Σ's, simultaneously with the forward pass; in this way the r's, t's, and Σ's need not be saved as a function of zone.

In order to identify certain quantities in the backward pass formulas, it is necessary to look at the surface boundary condition as derived in the previous report:[1]

$$i_\nu(\tau_{N+1},\mu) = f_b(|\mu|) + 2 \int_0^1 \mu' \, \bar{\rho}_\nu(\mu',|\mu|) \cdot i_\nu(\tau_{N+1},\mu') \, d\mu' \qquad (-1 \le \mu < 0) \qquad (6.57)$$

where

$$f_b(\mu) = \varepsilon_\nu(\mu) \, B_\nu(T_g) + \frac{S_\nu}{\pi} \mu_{sun} \, \bar{\rho}_\nu \, (\mu_{sun},\mu) \, e^{-\tau_{N+1}/\mu_{sun}}$$

Applying our half-range Gaussian quadrature to the integral in Eq. (6.57),

$$i_\nu(\tau_{N+1}, -\mu_i) = f_b(\mu_i) + 2 \sum_{j=1}^{m} c_j \mu_j \bar{\rho}_\nu(\mu_j, \mu_i) i_\nu(\tau_{N+1}, \mu_j)$$

$$(i = 1, \ldots, m)$$

This can be written in matrix-vector form, using the notation of Eq. (6.55), as

$$u_{N+1}^- = w + r_G u_{N+1}^+$$

where

$$w = \begin{bmatrix} f_b(\mu_1) \\ \vdots \\ f_b(\mu_m) \end{bmatrix} \tag{6.58}$$

$$(r_G)_{ij} = 2c_j \mu_j \bar{\rho}_\nu(\mu_j, \mu_i) \quad .$$

The backward pass may now be written

$$\begin{aligned} u_{N+1}^+ &= (I - E_{N+1} r_G)^{-1} (E_{N+1} w + V_{N+1}^{(3)}) \\ u_{N+1}^- &= w + r_G u_{N+1}^+ \end{aligned} \tag{6.59}$$

and

$$u_n^+ = G_{n+1}\, u_{n+1}^- + V_{n+1}^{(2)}$$

$$u_n^- = H_{n+1}\, u_{n+1}^- + V_{n+1}^{(1)} \qquad (6.60)$$

$$n = N, N-1, \ldots, 1$$

From the components $i_\nu(\tau_n, \pm\mu_i)$ of the $u_n^\pm$, the fluxes are obtained:

$$F_\nu(\tau_n) = 2\pi \int_{-1}^{1} \mu i_\nu(\tau_n, \mu)\, d\mu + \mu_{sun}\, S_\nu e^{-\tau_n/\mu_{sun}}$$

$$= 2\pi \int_0^1 [\mu i_\nu(\tau_n, \mu) - \mu i_\nu(\tau_n, -\mu)]\, d\mu$$

$$+ \mu_{sun}\, S_\nu\, e^{-\tau_n/\mu_{sun}} \qquad (6.61)$$

$$= 2\pi \sum_{i=1}^{m} c_i\, \mu_i [i_\nu(\tau_n, \mu_i) - i_\nu(\tau_n, -\mu_i)]$$

$$+ \mu_{sun}\, S_\nu\, e^{-\tau_n/\mu_{sun}} \quad .$$

This completes the algorithm.

6.4 MIE SCATTERING TREATMENT

Additional effort has been expended since the semi-annual report[1] to make the Mie scattering calculation as

fully automatic and independent of ad hoc assumptions as possible. This work is summarized in Section 6.4.1. Secondly, when the phase function has a strong forward peak, it can introduce serious errors into the numerical formulation of Section 6.3.3[53] unless a considerably larger number of angles μ_i is used than we intend. Therefore, Section 6.4.2 describes a method for eliminating this peak. In Section 6.4.3, the azimuthal integration of the phase function is treated. And finally, a method for re-normalization of the phase function is suggested in Section 6.4.4.

6.4.1 Mie Scattering Computation

Our subroutine (MIESCT) for calculating the Mie scattering coefficient $\beta_{\nu,M}$, Mie absorption coefficient $\alpha_{\nu,M}$, and Mie phase function $P_{\nu,M}$ for a particle of radius a follows standard techniques,[60,61,62,63,65,66] with minor modifications to achieve computational efficiency. The subroutine was tested against two sets of tables[64,65] as well as against certain graphs in Kerker[63] and agreed in all cases with the published results.

Techniques for the integration of the Mie quantities over a size distribution $n(a)$ are considerably less standard. The most comprehensive study of this problem is due to Deirmendjian,[66] who used a trial-and-error method to discover just how small the integration increments $\Delta\alpha$, where

$$\alpha = \frac{2\pi a}{\lambda} \qquad (\lambda = \text{wavelength}) ,$$

needed to be in many different cases. Deirmendjian offered no universally applicable method for picking $\Delta\alpha$'s small enough

to ensure accuracy but large enough to avoid wasting computer time. Studies by Dave[67,68] are of limited applicability since they were restricted to the visible spectrum. However, the work of Dave and especially that of Deirmendjian established certain ground rules for the integration: (1) it is best to use trapezoidal integration since the Mie functions oscillate so rapidly with α that higher-order Newton-Cotes quadrature schemes lead to no increase (and may actually lead to a decrease) in accuracy; (2) the necessary $\Delta\alpha$ is inversely proportional to λ ; (3) the larger α_{max} (the upper limit of integration), the finer the angular mesh needed to properly resolve $P_{\nu,M}$; and (4) the larger the interval of integration, $\alpha_{max} - \alpha_{min}$, the larger the allowable $\Delta\alpha$.

To these observations, we added several of our own. First, the computational expense increases enormously with increasing α_{max} , due to the fact that the number of terms in the Mie series (summed by MIESCT) is roughly equal to α . Therefore, it was decided to split the size integration into two integrations, the first of which is for the purpose of reducing α_{max} as far as possible. To reduce the cost of this preliminary trapezoidal integration, a coarse integration mesh ($\Delta\alpha = (\alpha_{max} - \alpha_{min})/30$) is chosen. The initial value of α_{max} comes from a conservative estimate of a_{max} which accompanies $n(a)$. The integration proceeds step-by-step from α_{min} until the relative changes in all quantities ($\beta_{\nu,M}$, $\alpha_{\nu,M}$, $P_{\nu,M}(\theta_i)$) become smaller than a pre-specified number δ_o (currently 0.001), at which value of α the integration is stopped and α taken as the new α_{max} . This procedure proved entirely satisfactory in the cases in which it was compared with Deirmendjian[66], although the scheme tended to choose α_{max}'s somewhat larger than his. When this was the case, the need for the larger α_{max}'s was indicated by the

differences between our results and his tables; when we used his α_{max}'s instead the differences were no longer found.

We also observed that the angular interval needed to resolve the forward peak in $P_{\nu,M}(0)$ is inversely proportional to α_{max}, but that progressively larger angular steps could be taken away from the peak. The sharpest forward peak will result from particles with $\alpha = \alpha_{max}$. The forward diffraction peak is proportional to

$$F(z) = \left(\frac{2\,J_1(z)}{z}\right)^2$$

where $z = \alpha\sin\theta$, and J_1 is the spherical Bessel function of order one. The quantity is shown in Figure 6.3. Since the function changes rapidly over an interval $\Delta z \cong \alpha\Delta\theta$ of unity, we choose as a measure of the angular width of the sharpest forward peak,

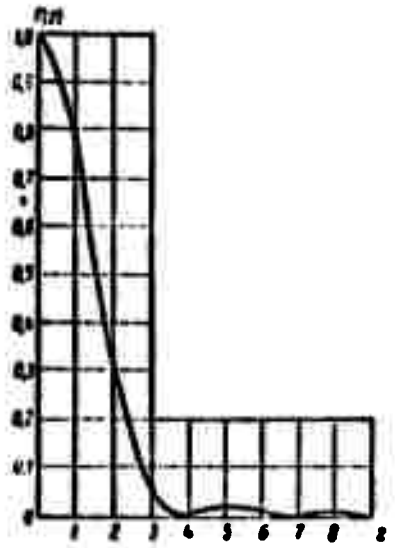

Figure 6.3. Graph of F(z).

$$(\Delta\theta)_o = \frac{30^\circ}{\alpha_{max}} \quad \text{(degrees)} \quad .$$

In addition, we apply the restriction that

$$0.125^\circ \leq (\Delta\theta)_o \leq 1^\circ \quad .$$

The tabulation takes place for enough intervals of $(\Delta\theta)_o$ to cover the forward peak. The remaining angular mesh has intervals of a pre-set number of $2(\Delta\theta)_o$, then $4(\Delta\theta)_o$, then $8(\Delta\theta)_o$ to complete the set, with the restriction that $\Delta\theta \leq 5^\circ$.

With α_{max} and the angular mesh determined, the final Mie calculation is performed using Romberg integration.[69] Trapezoidal sums for the integration over α are calculated for step sizes of $\Delta\alpha$, $\Delta\alpha/2$, $\Delta\alpha/4$ and $\Delta\alpha/8$. The value of $\Delta\alpha$ is determined from N_α, the number of intervals, which is defined as:

$$N_\alpha = \begin{cases} 25 & \text{for } \alpha_{max} < 25 \\ 25 + 0.55\,(\alpha_{max} - 25) & \text{for } \alpha_{max} > 25 \end{cases}$$

with the constraint that

$$N_\alpha \leq 80 \quad .$$

$\Delta\alpha$ is then taken as

$$\Delta\alpha = \frac{\alpha_{max} - \alpha_{min}}{N_\alpha}$$

The four trapezoidal sums are then used in the Romberg deferred-approach-to-the-limit scheme.

The above scheme has proven highly satisfactory in duplicating Deirmendjian's tables[66] without the need for trial-and-error determinations of the $\Delta\alpha$'s . The adjustment of a few simple parameters would enable the scheme to work for any class of size distributions.

6.4.2 Truncation of the Phase Function in the Forward Peak

Hansen[70] has shown that the forward peak of the phase function can be truncated without significantly changing the results of the transport calculation. Thus, for

$$0 \leq \theta \leq \theta^t \quad ,$$

where θ^t is the truncation angle, the real phase function $P_\nu(z,\theta)$ is replaced by a truncated phase function $P_\nu^t(z,\theta)$ in the manner of Figure 6.4. The logarithm of P_ν^t is taken to be a linear function of θ on $[0,\theta^t]$, and the values of P_ν^t and its derivative are matched to those of P_ν at $\theta = \theta^t$.

The truncation scattering angle θ^t is selected according to the following rules. If P_ν for $\theta = 0$ is less than a prescribed P_{max} , P_ν is not truncated at all. The currently used value for P_{max} is 5 . We also require that $\theta^t \leq 20°$ and $P_\nu^t(z,\theta) < P_\nu(z,\theta)$. Within these constraints, θ^t is chosen to give the maximum value of $P_\nu^t(z,0)$ bounded above by P_{max} .

Truncating the phase function modifies the scattering terms in the transport equations. Let F be the fraction of

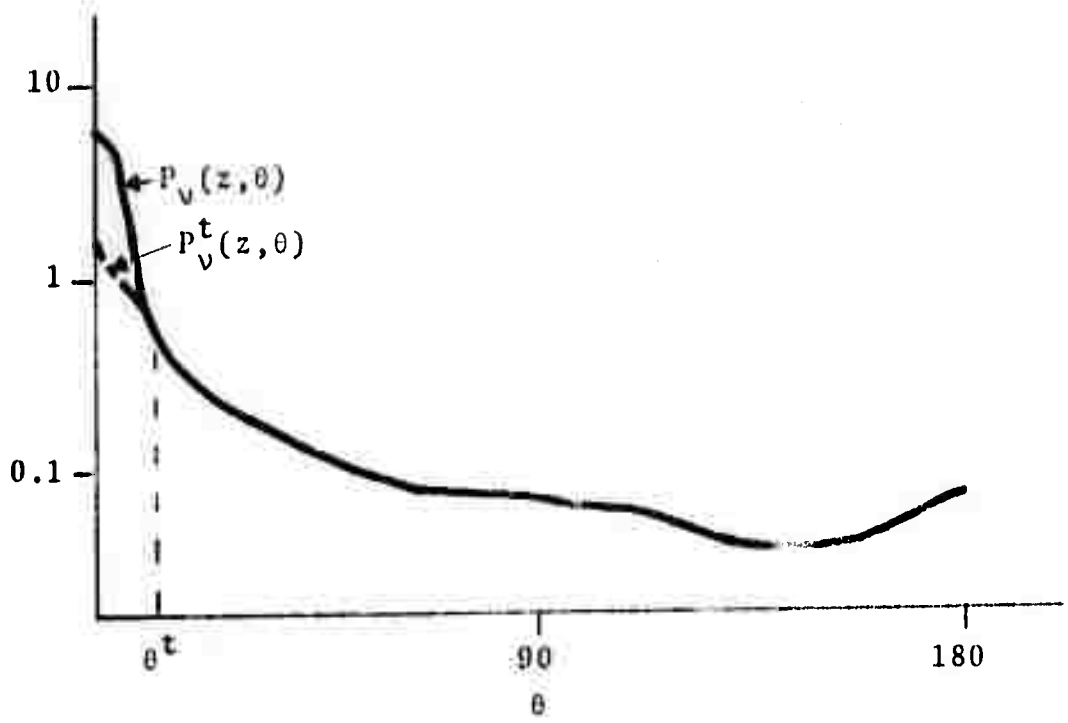

Figure 6.4. Example of truncated phase function.

the scattering which the truncated phase function fails to take into account:

$$F = \frac{1}{4\pi}\int (P - P^t)d\Omega' \quad .$$

The neglected scattering can be approximated by a delta function in the forward direction,

$$P = P - P^t + P^t \quad ,$$

$$\underset{\sim}{} f\,\delta(\vec{\Omega}' - \vec{\Omega}) + P^t \quad .$$

The approximate phase function must be correctly normalized, imposing the requirement

$$\frac{1}{4\pi}\int f\,\delta(\vec{\Omega}' - \vec{\Omega})d\Omega' + \frac{1}{4\pi}\int P^t d\Omega' = 1 \quad ,$$

$$\frac{f}{4\pi} + 1 - F = 1 \quad ,$$

$$f = 4\pi F \quad .$$

The second step comes from the definition of F and the assumption that P is correctly normalized (to unity). In this approximation the scattering terms of the radiative transfer equation become

$$\text{scat. terms} = \frac{\beta}{4\pi}\int P(\vec{\Omega},\vec{\Omega}')I(\Omega')d\Omega' - \beta\, I(\vec{\Omega})$$

$$\underset{\sim}{} \frac{\beta}{4\pi}\int\left[4\pi F\,\delta(\vec{\Omega}'-\vec{\Omega}) + P^t\right]I(\Omega')d\Omega' - \beta\, I(\vec{\Omega})$$

$$= \frac{\beta}{4\pi}\int P^t(\vec{\Omega},\vec{\Omega}')I(\Omega')d\Omega' - \beta(1-F)I(\vec{\Omega})$$

$$= \frac{\beta(1-F)}{4\pi}\int \frac{P^t(\vec{\Omega},\vec{\Omega}')}{1-F}\, I(\vec{\Omega}')d\Omega' - \beta(1-F)I(\vec{\Omega})$$

$$= \frac{\beta'}{4\pi}\int P'(\vec{\Omega},\vec{\Omega}')I(\vec{\Omega}')d\Omega' - \beta' I(\vec{\Omega}) \quad ,$$

where

$$\beta' = (1 - F)\beta \quad ,$$

$$P' \equiv \frac{P^t}{1 - F} \quad .$$

Therefore, the scattering terms have their original form, but P and β are replaced by P' and β' defined above. The quantity F can be calculated as follows:

$$F = \frac{1}{4\pi}\int(P - P^t)d\Omega' = \frac{1}{2}\int_o^{\pi} [P(\theta) - P^t(\theta)]d\theta$$

$$= \frac{1}{2}\int_o^{\theta^t} [P(\theta) - P^t(\theta)]d\theta \quad ,$$

since $P^t = P$ for $\theta > \theta^t$. Using the analytical form of P^t ,

$$\log_{10} P^t = a + b\theta_s \quad ,$$

we obtain

$$P^t = a' e^{b'\theta_s} \quad , \quad a' = 10^a \quad , \quad b' = b \ln 10 \quad .$$

Then

$$\int_o^{\theta^t} P^t(\theta)d\theta = \frac{a'}{b'}\left(e^{b'\theta^t} - 1\right) \quad .$$

The integration of P over the forward peak must be performed numerically, since P is only tabulated for a discrete set of θ. It is not possible to use a high-order integration scheme such as Romberg or Gaussian due to the unequal spacings of the θ points. We have chosen to make a piecewise quadratic fit to P, and integrate the quadratic. If P_0, P_1, and P_2 are three phase function values corresponding to θ_0, θ_1, and θ_2, then the quadratic satisfying

$$Q(\theta_i) = P_i \qquad (i=0,1,2)$$

is given by

$$Q(\theta) = \sum_{i=0}^{2} P_i \, L_i(\theta) \quad ,$$

$$L_i = a_i \prod_{j=0}^{2}{}' (\theta - \theta_j) \quad ,$$

$$a_i = \frac{1}{\prod_{j=0}^{2}{}' (\theta_i - \theta_j)} \quad ,$$

where $\prod'$ indicates a product of terms with the i^{th} term deleted. The integral is, then

$$\int_{\theta_o}^{\theta_2} Q(\theta)d\theta = (\theta_2 - \theta_o) \sum_{i=0}^{2} P_i \, a_i \left[c - d(c - \theta_i) + \prod_{k=0}^{2}{}' \theta_k \right]$$

$$c = (\theta_2^2 + \theta_2 \, \theta_o + \theta_o^2)/3 \quad ,$$

$$d = (\theta_o + \theta_2)/2 \quad ,$$

$$e = \sum_{i=0}^{2} \theta_i \quad .$$

6.4.3 Azimuthal Integration of Phase Function

The phase function, $P_\nu(z,\vec{\Omega},\vec{\Omega}')$, determines the fraction of the photons within a volume element around z traveling in the direction $\vec{\Omega}'$ that will be scattered into the cone $d\Omega$ of directions around $\vec{\Omega}$. P_ν depends only on the angle between $\vec{\Omega}$ and $\vec{\Omega}'$, where cosine is μ_s. If P_ν is integrated over the azimuth angle ϕ, an average phase function, $\overline{P}_\nu(z,\mu,\mu')$ results which does not depend on ϕ or ϕ', as discussed in Ref. 1. It is this azimuth-averaged quantity which is relevant to the problem of radiative energy transfer in a plane parallel atmosphere:

$$\overline{P}_\nu(z,\mu,\mu') = \frac{1}{2\pi} \int_0^{2\pi} P_\nu(z,\mu_s)d\phi$$

$$= \frac{1}{2\pi} \int_0^{2\pi} P_\nu\left(z,\mu\mu' + \sqrt{(1-\mu^2)(1-\mu'^2)}\,\cos\phi\right)d\phi \quad .$$

μ and μ' are cosines of the angles θ and θ' between the positive z-axis and $\vec{\Omega}$ and $\vec{\Omega}'$, respectively.

If $P_\nu(z,\mu_s)$ is a sum of Legendre polynomials in μ_s, the integral can be done analytically. In the present case, however, P_ν and μ_s are given only for a finite set of points. Hence, we must numerically integrate the tabular data.

The problem is to generate a set of (P_{ν_i},ϕ_i) from the given set of (P_{ν_j},μ_{s_j}) for $0 \leq \phi_i \leq 2\pi$. The transformation is

$$\mu_s = \mu\mu' + \sqrt{(1-\mu^2)(1-\mu'^2)}\cos\phi \quad ,$$

$$= C_1 + C_2 \cos\phi \quad ,$$

or

$$\phi = \cos^{-1}\left(\frac{\mu_s - C_1}{C_2}\right) \quad . \tag{6.62}$$

The relationship of μ_s and ϕ is shown in Figure 6.5. Note that $\mu_s(\phi)$ is symmetrical about π. This means we may limit the numerical quadrature to $0 \leq \phi \leq \pi$. The set of (P_{ν_i},ϕ_i) is generated from the (P_{ν_j},μ_{s_j}) by selecting all those μ_{s_j} which give

$$-1 \leq \frac{\mu_{s_j} - C_1}{C_2} \leq 1$$

and computing the ϕ_i from Eq. (6.62). There may be no μ_{s_j} which yields 0 or π for ϕ, yet these values are needed

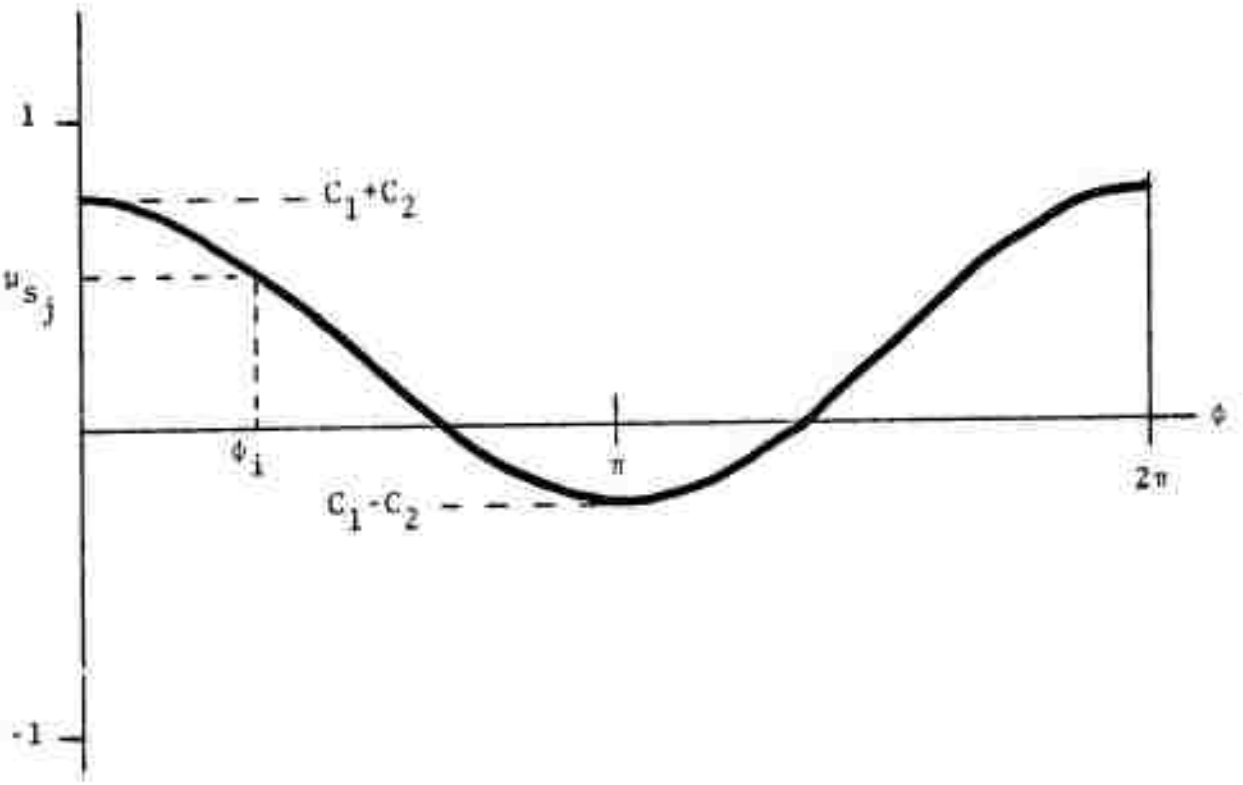

Figure 6.5. The scattering angle μ_s vs the azimuth angle ϕ.

to complete the integration at the end points. In this case, an interpolation is done for P_ν as a function of μ_s to yield a $P_\nu(z,\mu_s^*)$, where μ_s^* is the value required to give $\phi = 0$ or $\phi = \pi$.

Given the complete set of (P_{ν_i},ϕ_i), a quadrature method may be applied. Trapezoidal integration is being used currently. Since the set of scattering angles has been chosen carefully to define the phase function well, and since the rapid change in the phase function near the peak is eliminated by truncation, it is likely that the trapezoidal integration scheme will be adequate.

The calculation of $\bar{P}_\nu$ described above must be carried out for each non-redundant pair (μ,μ') from the set of μ_i . Symmetry relations resulting from the definition of $\bar{P}_\nu$ are used to reduce the amount of computing,

$$\bar{P}_\nu(z,\mu_i,\mu_j) = \bar{P}_\nu(z,\mu_j,\mu_i) \tag{6.63}$$

$$\bar{P}_\nu(z,-\mu_i,-\mu_j) = \bar{P}_\nu(z,\mu_i,\mu_j) \quad . \tag{6.64}$$

By combining Eqs. (6.63) and (6.64), one can also show

$$\bar{P}_\nu(z,-\mu_i,-\mu_j) = \bar{P}_\nu(z,\mu_j,\mu_i) \quad . \tag{6.65}$$

From Eq. (6.63), and referring to Figure 6.6, all points above the positive sloping diagonal may be derived from points below the diagonal. From Eq. (6.65), points in octant 6 map to points in octant 1 and points in octant 7 map to points in octant 8. Hence, $P_\nu(z,\mu,\mu')$ need be calculated only for combinations of (μ,μ') which lie in octants 1 or 8. In addition, if either μ or μ' is ± 1 , then $P_\nu(z,\mu_s)$ has no ϕ dependence. The integral becomes

$$\bar{P}_\nu(z,\mu,\mu') = \frac{1}{2\pi}\int_0^{2\pi} P_\nu(z,\mu\mu')d\phi = P_\nu(z,\mu\mu')$$

$P_\nu(z,\mu\mu')$ is found by setting

$$\mu_s = \mu\mu'$$

and interpolating in the set of $P(z,\mu_{s_j})$.

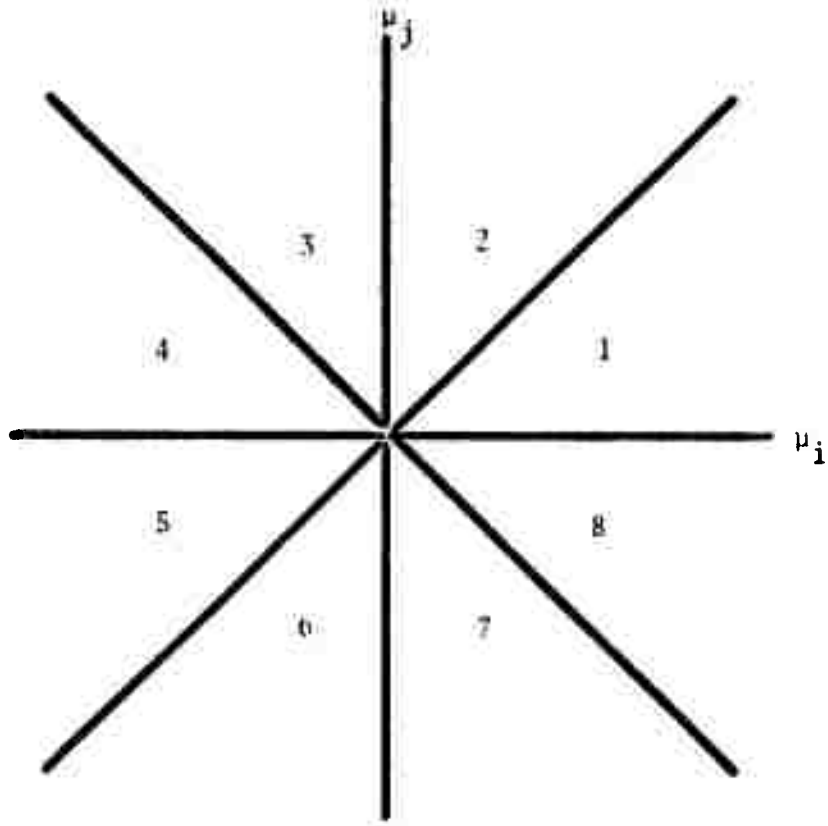

Figure 6.6. Octants for μ_i, μ_j space.

6.4.4 Renormalization of the Phase Function

Grant and Hunt[51] stress the importance of using numerically properly normalized phase functions. In terms of the angular quadrature scheme, this implies

$$\frac{1}{2} \sum_{j=1}^{m} c_j \, \rho_{jk} = 1 \qquad (k=1, \ldots, m) \qquad (6.66)$$

where

$$\rho_{jk} = P^{++}_{jk} + P^{+-}_{jk}$$

$$P^{++}_{jk} = \bar{P}_{\nu}(z,\mu_j,\mu_k)$$

$$P^{+-}_{jk} = \bar{P}_{\nu}(z,\mu_j,-\mu_k)$$

The importance of Eq. (6.66) lies in the fact that it ensures flux conservation.

Eq. (6.66) would be satisfied exactly if $\bar{P}_{\nu}$ were free of error. Errors are introduced, however, from the following sources:

(1) the truncation of the Mie series summation in MIESCT (this is a relatively inconsequential source of error);

(2) the integration over sizes (Section 6.4.1);

(3) the approximate integration to obtain the area under the forward peak of P_{ν}, when truncating (Section 6.4.2); and

(4) the azimuthal integration (Section 6.4.3).

Basically, there are two ways in which a correction can be applied to the calculated matrix ρ^{calc}_{jk}. An additive correction can be made:

$$\rho_{jk} = \rho_{jk}^{calc} + \epsilon_{jk}$$

or, a multiplicative correction can be applied

$$\rho_{jk} = (1 + \epsilon_{jk})\, \rho_{jk}^{calc}$$

In either case, there are $\frac{m(m-1)}{2}$ unknowns ϵ_{jk} (the number is reduced from m^2 by the symmetry requirement $\epsilon_{kj} = \epsilon_{jk}$) and there are only m equations (Eqs. (6.66)) to determine them. This underspecification can be handled in many ways, no one of which seems much preferable on physical grounds over any other. Grant* corrects only the diagonal elements, $\epsilon_{jk} = \epsilon_j \delta_{jk}$, and so has a determinate set of equations for the ϵ_j. He points out that the phase matrices ρ_{jk} are usually strongly diagonally dominant and that his procedure thus incorporates the entire correction where it makes the smallest relative change.

An alternative procedure is proposed. First, assume

$$\epsilon_{jk} = \epsilon_j^{(1)}$$

and solve

$$\frac{1}{2} \sum_{j=1}^{m} c_j\, \rho_{jk}^{calc} \left(1 + \epsilon_j^{(1)}\right) = 1 \qquad (k=1, \ldots, m)$$

for the $\epsilon_j^{(1)}$; then assume

---

*Private communication.

$$e_{jk} = e_k^{(2)}$$

and solve

$$\frac{1}{2} \sum_{j=1}^{m} c_j \rho_{jk}^{calc} \left(1 + e_k^{(2)}\right) = 1 \qquad (k=1, \ldots, m)$$

for the $e_k^{(2)}$. Finally, to ensure symmetry of e_{jk} form

$$e_{jk} = \frac{e_j^{(1)} + e_k^{(2)}}{2} ,$$

which is to be applied as the multiplicative correction to ρ_{jk}^{calc} . No decision has as yet been made between the latter procedure and that of Grant.

6.5 CODE ORGANIZATION

In Figure 6.7 a block diagram of the code is given. Those sections for which computer coding and testing are complete are enclosed in solid boxes; those parts which are not yet programmed or only partially programmed are enclosed in dashed boxes. A brief description of each of the component parts is given below.

INPUT	Provides for read-in of zoning flags, atmospheric specifications (pressure, temperature, mixing ratios, aerosol content, etc.), code parameters, option flags, and editing flags.
SETUP	From user input, generates zone structure, angular groups, and frequency groups.

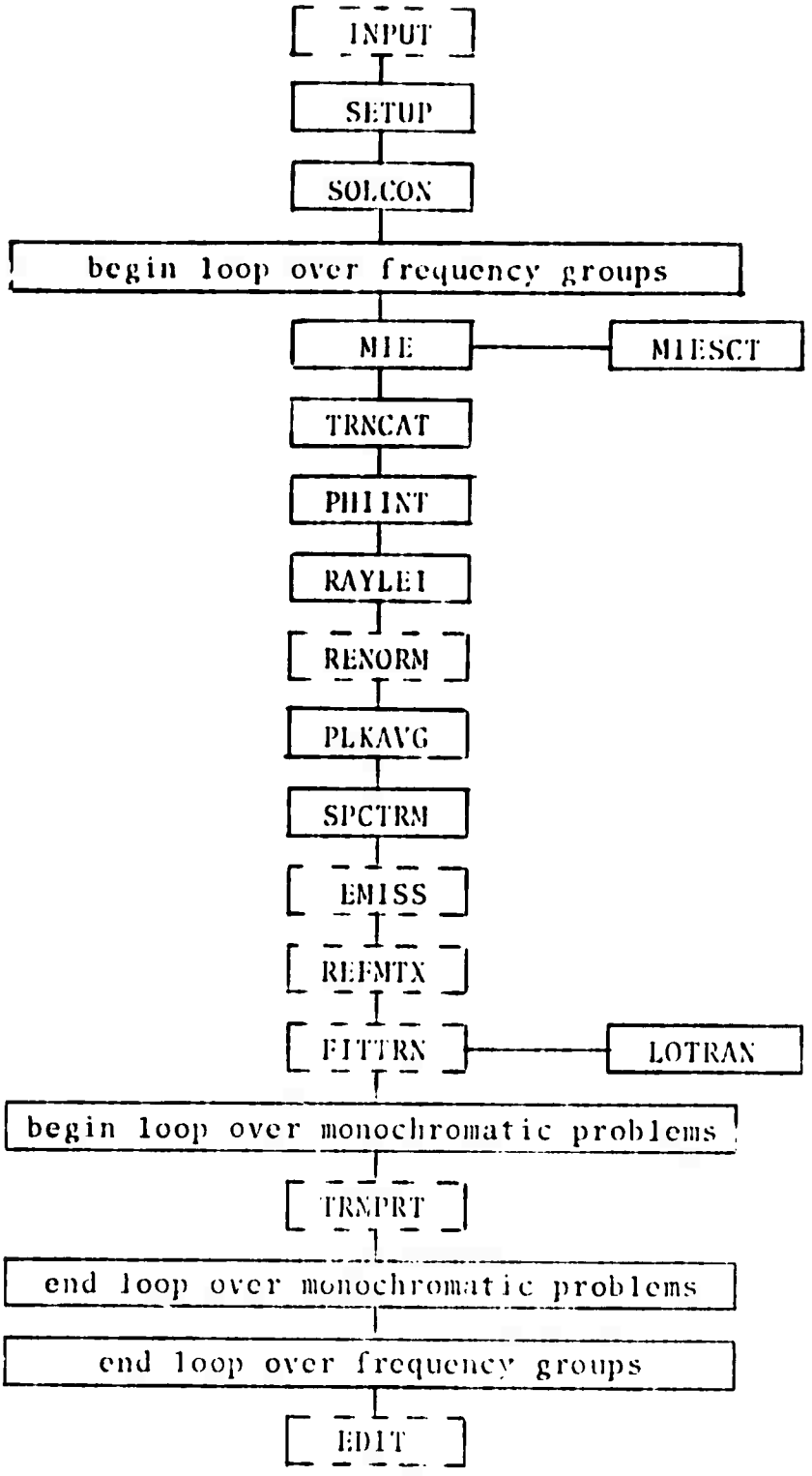

Figure 6.7. Block diagram of atmospheric radiation code.

SOLCON	From date, time, longitude, and latitude generates solar zenith angle and Earth-sun distance.
MIESCT	Computes Mie scattering and extinction coefficients and phase function for a single spherical particle.
MIE	Integrates the Mie quantities from MIESCT over a size distribution of spherical particles.
TRNCAT	Truncates the forward peak from the Mie phase function, if necessary, and re-re-adjusts the Mie quantities appropriately.
PHIINT	Integrates the Mie phase function over azimuth.
RAYLEI	Computes the Rayleigh scattering coefficient and phase function.
RENORM	Re-normalizes the total phase function numerically.
PLKAVG	Computes $B_{\Delta\nu}$, the average of the Planck function B_ν over the frequency group $\Delta\nu$.
SPCTRM	Computes $S_{\Delta\nu}$, the average of the solar constant S_ν over the frequency group $\Delta\nu$, correcting for the actual Earth-sun distance.
EMISS	Returns a surface emissivity $\epsilon_\nu(\mu)$ for the frequency group $\Delta\nu$ according to user specification of the surface composition.
REFMTX	Returns a surface reflection matrix r_G appropriate to the frequency group $\Delta\nu$ and the user specified surface composition for use in Eq. (6.59) of the Grant and Hunt algorithm.
LOTRAN	Computes transmission functions $T_{\Delta\nu}$.

FITTRN	Fits the transmission function $T_{\Delta\nu}$ by a sum of exponentials.
TRNPRT	Solves a monochromatic radiative transfer problem by the Grant and Hunt method (Section 6.5).
EDIT	Prints or writes to tape, at the user's option, fluxes, intensities, and heating rates.

7. PARAMETERIZATION CONSIDERATIONS – FUTURE PLANS

The next contract period should see the completion of the family of meso-scale codes which can be used to form a detailed parameterization of the wave drag caused by flow over mountain ranges.

The test problems completed to date have given some indication of the effects of atmospheric stability, compressibility, and moisture on momentum transfer. In particular, the results detailed in the last semiannual report[1] indicated differences in wave drag edits of factors of greater than two due to atmospheric stability and horizontal wind profiles alone. When compressible effects were included in the formulation of the equations and the results of a test problem compared with those from the Boussinesq code, differences of the order of 25 percent are indicated. Moisture effects studies, which have just been initiated, indicate small differences in momentum transfer when compared with the Boussinesq results.

S^3 intends to complete two additional meso-scale codes which will be used to study the effects of turbulence and Corilis forces on momentum transfer. With the family of HAIFA codes, a matrix of problems will then be completed. The results will allow a designed and detailed parameterization to be formed of momentum flux caused by orographically induced

induced flow. Hopefully, this parameterization will then be tested using one of the global circulation models presently available.

The next several months of work on the atmospheric radiation portion of the contract will have as its primary thrust the completion of the radiation code, its testing, and comparisons with the Mintz-Arakawa radiation package. To this end, several further tasks must be completed. Foremost among these is the exponential-sum approximating subroutine to be developed in collaboration with Prof. Evans. Next is the completion of the coding of the Grant and Hunt algorithm. In this connection, a basic set of data and analytic representations for surface emissivities and reflectivities must be programmed. The assembled code must then be debugged and tested against any known solutions (for example, the ones for pure Rayleigh scattering). Comparisons with the Mintz-Arakawa radiation package will then be done and used as the basis of a paper to be delivered at the AMS Conference on Atmospheric Radiation at Fort Collins, Colorado, August 7-9, 1972. Further studies to validate the primary approximations in the code are also planned, but may be squeezed out by lack of time between now and the conference.

REFERENCES

1. "The Effects of Meso-Scale and Small-Scale Interactions on Global Climate," Report No. 3SR-795 (30 September 1971), Systems, Science and Software, La Jolla, Calif.

2. E. Palm and A. Foldvik, "Contribution to the Theory of Two-Dimensional Mountain Waves," Geofysiske Publikaszoner Geophysica Norvegrca (1959), Vol. 6.

3. D.K. Lilly, private communication with M.G. Wurtele (1971).

4. I. Vergeiner, "An Operational Linear Lee Wave Model for Arbitrary Basic Flow and Two-Dimensional Topography," Qtrly. J. R. Met. Soc. (1971), Vol. 97.

5. "Investigations of Mountain Lee Waves and the Air Flow Over the Sierra Nevada," (March 1957), Dept. of Meteorology, University of California at Los Angeles.

6. W.P. Crowley, "Numerical Advection Experiments," Monthly Weather Review (January 1968), Vol. 1.

7. W.G. England, B.L. Freeman, and M.G. Wurtele, "Effects of Compressibility on Orographically Induced Gravity Waves," Fall Annual Meeting of the American Geophysical Union, San Francisco, Calif., 9 December 1971.

8. J.Y. Liu and H.D. Orville, "Numerical Modeling of Precipitation and Cloud Shadow Effects on Mountain Induced Cumuli," J. Atmos. Sci. (November 1969), Vol. 6.

9. R.J. List, "Smithsonian Meteorological Tables," (1958), Smithsonian Institute.

10. R.C. Srivastava, "A Study of the Effects of Precipitation on Cumulus Dynamics," J. Atmos. Sci. (1967), Vol. 24.

11. H.D. Orville, "Ambient Wind Effects on the Initiation and Development of Cumulus Clouds Over Mountains," J. Atmos. Sci. (May 1968).

12. Y. Ogura, "The Evolution of a Moist Convection Element in A Shallow, Conditionally Unstable Atmosphere: A Numerical Calculation," J. Atmos. Sci. (1963), Vol. 20.

REFERENCES, contd.

13. Y. Agnra and N.A. Phillips, "Scale Analysis of Deep and Shallow Convection in the Atmosphere," J. Atmos. Sci. (1962), Vol. 19.

14. E. Kessler, "On the Distribution and Continuity of Water Substance in Atmospheric Circulation," Meteor. Monographs (November 1969), No. 32.

15. K.C. Brundidge, et.al. "Project Themis Prediction of Environmental Parameters," Technical Report ECOM-0073-5 (March 1971), United States Army Electronics Command, Fort Monmouth, New Jersey.

16. Queney, "The Problem of Air Flow Over Mountains: A Summary of Theoretical Studies," Bull. Am. Soc. (January 1948), Vol. 29.

17. P.D. Thompson, "Numerical Weather Analysis and Prediction," The MacMillan Co., New York (1961).

18. M.G. Kurtele, unpublished notes on Mountain Lee Waves, University of California at Los Angeles (1965).

19. E.A. Milne, "Thermodynamics of the Stars," in Selected Papers on the Transfer of Radiation, D. Menzel ed., Dover, New York (1966).

20. R. McClatchey, et.al., "Optical Properties of the Atmosphere," Report No. AFCRL-70-0527 (1970), Air Force Cambridge Research Lab, Cambridge, Mass.

21. B. Armstrong, "Analysis of the Curtis-Godson Approximation and Radiation Transmission through Inhomogeneous Atmospheres," J. Atmos. Sci. (1968), Vol. 25 pp. 312.

22. C.D. Walshaw and C.D. Rodgers, "The Effects of the Curtis-Godson Approximation on the Accuracy of Radiative Heating Rate Calculations," Qtrly. J. Roy. Met. Soc. (1963), Vol. 89, pp. 122.

23. W. Zdunkowski and B. Raymond, "Exact and Approximate Transmission Calculations for Homogeneous and Non Homogeneous Atmospheres," Beitrage zur Physik der Atmosphäre (1970), Vol. 43, pp. 186.

REFERENCES, contd.

24. R. Goody, Atmospheric Radiation, Oxford University Press (1964).

25. K. Ya. Kondratyev, Radiation in the Atmosphere, Academic Press, New York (1969).

26. G. Yamamoto, M. Tanaka, and S. Asano, "Radiative Transfer in Water Clouds in the Infrared Region," J. Atmos. Sci. (1970), Vol 27, pp. 282.

27. G. Yamamoto, M. Tanaka, and S. Asano, "Radiative Heat Transfer in Water Clouds by Infrared Radiation," JQSRT (1971), Vol. 11, pp. 697.

28. G. Hunt and I. Grant, "Discrete Space Theory of Radiative Transfer and Its Application to Problems in Planetary Atmospheres," J. Atmos. Sci. (1969), Vol. 26, pp. 963.

29. M.J.D. Powell, "A Survey of Numerical Methods for Unconstrained Optimization," SIAM Rev. (1970), Vol. 12, pp. 79.

30. J.D. Pearson, "Variable Metric Methods of Minimization," Comp. J. (1969), Vol. 12, pp. 171.

31. R. Fletcher, ed., Optimization, Academic Press, New York (1969).

32. R. Brent, "Algorithms for Finding Zeros and Extrema of Functions Without Calculating Derivatives," Report No. STAN-CS-71-198 (February 1971), Stanford Comp. Sci. Dept., Stanford University, California.

33. Y. Bard, "Comparison of Gradient Methods for the Solution of Non-Linear Parameter Estimation Problems," SIAM J. Numer. Anal. (1970), Vol. 7, pp. 157.

34. R. Fletcher and M.J.D. Powell, "A Rapidly Convergent Descent Method for Minimization," Comp. J. (1963), Vol. 6, pp. 163.

35. Y. Bard, "On A Numerical Instability of Davidon-Like Methods," Math. Comp. (1968), Vol. 22, pp. 665.

36. M.J. Box, "A Comparison of Several Current Optimization Methods, and the Use of Transformations in Constrained Problems," Comp. J. (1966), Vol. 9, pp. 67.

REFERENCES, contd.

37. D. Goldfarb, "Extension of Davidon's Variable Metric Method to Maximization Under Linear Equality and Inequality Constraints," SIAM J. Appl. Math. (1969), Vol. 17, pp. 739.

38. M.J.D. Powell, "A Method for Minimizing a Sum of Squares of Non-Linear Functions Without Calculating Derivatives," Comp. J. (1965), Vol. 7, pp. 303.

39. K. Levenberg, "A Method for the Solution of Certain Non-Linear Problems in Least Squares," Qtrly. Appl. Math. (1944), Vol. 2, pp. 164.

40. D. Marquardt, "An Algorithm for Least Squares Estimation of Non-Linear Parameters," J. SIAM (1963), Vol. 11, pp. 431.

41. G.W. Westley and J. Watts, "The Computing Technology Center Numerical Analysis Library," Report No. CTC-39, Oak Ridge Computing Technology Center (available through NTIS Clearinghouse).

42. J. Lang and R. Müller, "A Procedure for Non-Linear Least Squares Refinement in Adverse Practical Conditions," Comp. Phys. Comm. (1971), Vol. 2, pp. 79.

43. G.E. Hudson, "Trend Analysis of Physical Data," Am. J. Phys. (1953), Vol. 21, pp. 362.

44. D. Gardner, et.al., "Method for the Analysis of Multi-component Exponential Decay Curves," J. Chem. Phys. (1959), Vol. 31, pp. 978.

45. J.R. Rice, "Chebyshev Approximation by Exponentials," J. SIAM (1962), Vol. 10, pp. 149.

46. F. Hildebrand, Introduction to Numerical Analysis, McGraw-Hill, New York (1956), pp. 378.

47. Lanczos, Applied Analysis, Prentice-Hall, New York (1956), pp. 272.

48. D. Cantor and J. Evans, "On Approximation by Positive Sums of Powers," SIAM J. Appl. Math. (1970), Vol. 18, pp. 380

REFERENCES, contd.

49. I. Grant and G. Hunt, "Solution of Radiative Transfer Problems Using the Invariant S_n Method," Mon. Not. Roy. Astron. Soc. (1968), Vol. 141, pp. 27.

50. I. Grant and G. Hunt, "Discrete Space Theory of Radiative Transfer I. Fundamentals," Proc. Roy. Soc. Lond. A. (1969), Vol. 313, pp. 183.

51. I. Grant and G. Hunt, "Discrete Space Theory of Radiative Transfer II. Stability and Non-Negativity," Proc. Roy. Soc. Lond. A. (1969), Vol. 313, pp. 199.

52. I. Grant and G. Hunt, "Solution of Radiative Transfer Problems in Planetary Atmospheres," Icarus (1968), Vol. 9, pp. 526.

53. G. Hunt, "The Effect of Coarse Angular Discretization on Calculations of Radiation Emerging from A Model Cloudy Atmosphere," JQSRT (197.), Vol. 11, pp. 309.

54. D. McCleese, J. Margolis, and G. Hunt, "Laboratory Simulation of Absorption Spectra in Cloudy Atmospheres," Nature (Phys. Sci.) (1971), Vol. 233, pp. 102.

55. R.W. Preisendorfer, Radiative Transfer on Discrete Spaces, Pergamon Press, Oxford (1965).

56. H.C. van de Hulst, "A New Look at Multiple Scattering," unpublished report (1963), NASA Inst. for Space Studies, New York.

57. G. Rybicki and P. Usher, "The Generalized Ricatti Transformation as a Simple Alternative to Invariant Imbedding," Astrophys. J. (1966), Vol. 146, pp. 871.

58. K. Lathrop and B. Carlson, "Numerical Solution of the Boltzmann Transport Equation," J. Comp. Phys. (1967), Vol. 2, pp. 173.

59. M. Krook, "On the Solution of Equations of Transfer I," Astrophys. J. (1955), Vol. 122, pp. 488.

REFERENCES, contd.

60. J. Dave, "Subroutines for Computing the Parameters of the Electromagnetic Radiation Scattered by a Sphere," IBM Program 360D-17.4.002 (December 1968).

61. G. Kattawar and G. Plass, "Electromagnetic Scattering from Absorbing Spheres," Appl. Opt. (1967), Vol. 6, pp. 1377.

62. H.C. van de Hulst, Light Scattering by Small Particles, John Wiley and Sons, New York (1957).

63. M. Kerker, The Scattering of Light and Other Electro-Magnetic Radiation, Academic Press, New York (1969).

64. D. Deirmendjian, "Tables of Mie Scattering Cross Sections and Amplitudes," RAND Report No. R-407-PR (January 1963), RAND Corp., Santa Monica, Calif.

65. H. Denman, W. Heller and W. Pangonis, Angular Scattering Functions for Spheres, Wayne State University Press, Detroit, Michigan (1966).

66. D. Deirmendjian, Electromagnetic Scattering on Spherical Polydispersions, Elsevier, New York (1969).

67. J. Dave, "Effect of Coarseness of the Integration Increment on the Calculation of the Radiation Scattered by Polydispersed Aerosols," Appl. Opt. (1969), Vol. 8, pp. 1161.

68. J. Dave, "Effect of Varying Integration Increment on the Computed Polarization Characteristics of the Radiation Scattered by Polydispersed Aerosols," Appl. Opt. (1969), Vol. 8, pp. 2155.

69. A. Ralston and H. Wilf, Mathematical Methods for Digital Computers II., Wiley, New York (1967).

70. J. Hansen, J. Atm. Sci. (1969), Vol. 26, pp. 478.

APPENDIX A
THE LEBESGUE INTEGRAL

The Lebesgue integral was originally devised as an extension of integration to functions which are so discontinuous as not to be Riemann integrable. However, the Lebesgue integral concept is also useful in the integration of continuous functions (such as line spectra) which vary so wildly and erratically as to have the aspect of discontinuous functions.

Viewing integration as an approximation process, the fundamental partitioning in Riemann integration is of the abscissa, as in Figure A-1. Figures such as trapezoids are then constructed using the partitioning intervals as bases, and the sum of the areas of all these figures is taken as an approximation to the integral.

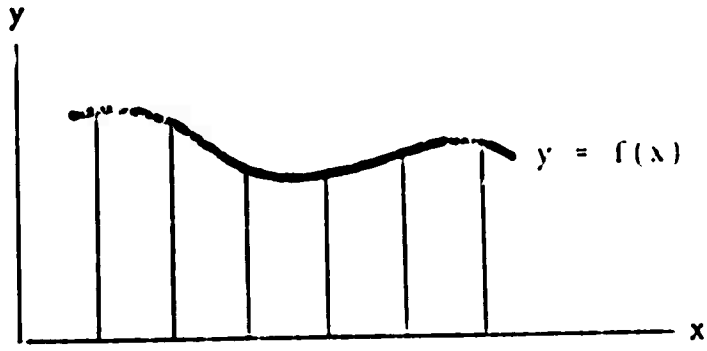

Figure A-1. Riemann integration.

In Lebesgue integration, it is the ordinate rather than the abscissa which is partitioned. Consider the shaded strip between y_i and y_{i+1} in Figure A-2. The x-intervals in $[a,b]$ for which $f(x) \in [y_i, y_{i+1}]$ are of lengths Δ_1, Δ_2, Δ_3, Δ_4 respectively. The sum

$$a_i = \Delta_1 + \Delta_2 + \Delta_3 + \Delta_4$$

is called the measure of the set $\{x \in [a,b] : f(x) \in [y_i, y_{i+1}]\}$. Multiplying a typical value $f_i \in (y_i, y_{i+1})$ by the measure a_i, and summing over all i, gives an approximation

$$\int_a^b f(x)dx \approx \sum a_i f_i \qquad (A.1)$$

to the Lebesgue integral.

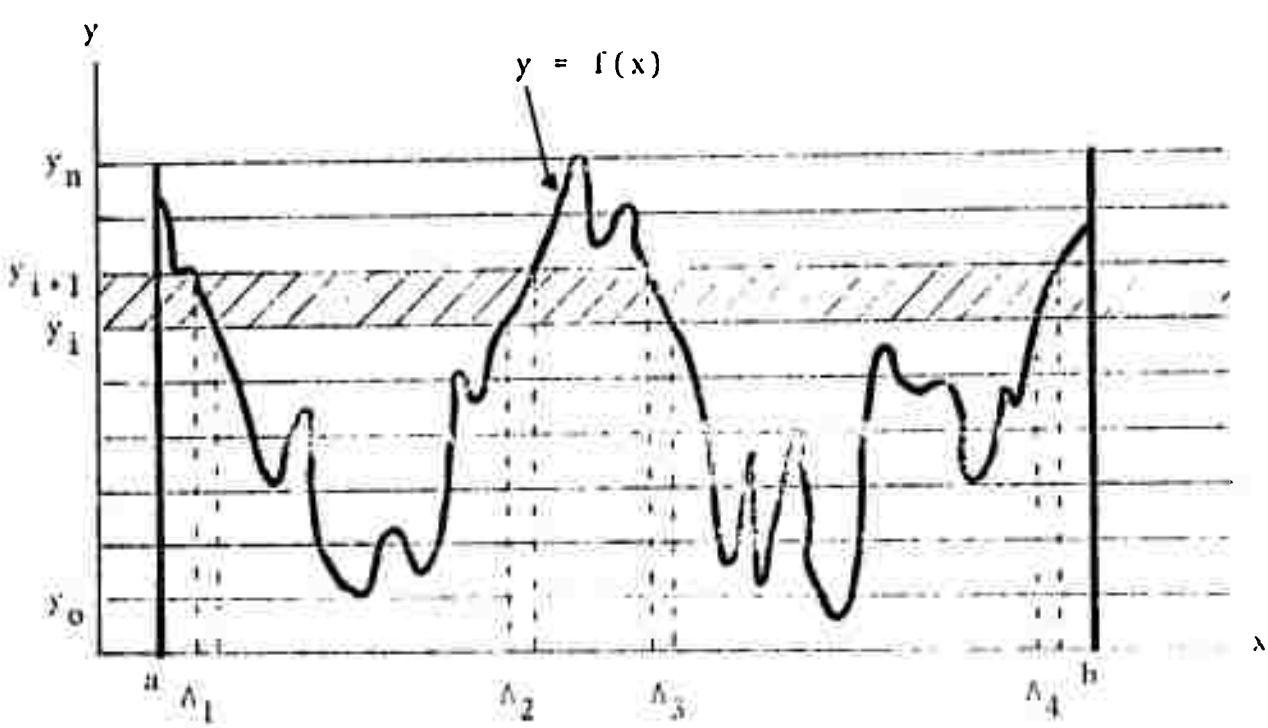

Figure A-2. Lebesgue integration.

The formula (A.1) has the appearance of a Riemann quadrature rule like Simpson's rule or Gaussian quadrature. The analogy is valid, of course, but the resemblance is only superficial. All Riemann quadrature rules of the form (A.1) are based on polynomial approximation of the integrand $f(x)$; no such approximation is made, or even seems possible, in the case of Lebesgue integration. Also, the a_i in Riemann quadrature rules are proportional to the length of a single x-partition, whereas the measures a_i represent the sum of the lengths of an indefinite number of disjoint x-partitions. Furthermore, the a_i in Riemann quadrature rules are independent of the function being integrated; in Lebesgue quadrature rules, they depend on the function.

The advantages of Lebesgue quadrature are obvious in the case of functions which vary rapidly over $[a,b]$. Riemann quadrature would demand an extremely fine x-partition, involving perhaps hundreds or thousands of points, whereas Lebesgue quadrature could furnish equivalent accuracy with a much smaller number of y-partitions. The a_i's are, of course, function-dependent for Lebesgue quadrature, but within certain large classes of functions, e.g., randomly-varying ones, the a_i's would be essentially function-independent.

APPENDIX B
THE VARIATION OF $B_\upsilon(T)$ WITH τ

Consider an arbitrary zone. The total opacity κ in this zone is made up of three parts: (1) a Rayleigh scattering part, (2) a Mie scattering and absorption part, and (3) a line absorption part. The Rayleigh part varies as p/T, or substantially as p, which is exponential with altitude. The Mie scattering part is found experimentally* to decrease exponentially with height or be constant with height (a degenerate exponential). And the line absorption part, according to the approximations employed in Sections 6.2.2 and 6.2.3, varies as p^γ, which is again exponential. Hence, a plausible interpolation of κ across the zone is

$$\kappa = \kappa_o e^{-z'/H} \tag{B.1}$$

where z' is measured from the zone boundary z_o ($z=z_o+z'$). The different components of κ have different scale heights, so that the H of Eq. (B.1) represents some sort of mean value.

Computing the optical depth τ' (again measured from the zone boundary $\tau_o = \tau(z_o)$), and solving for z',

---

* R. Penndorf, Geophysics Research Paper No. 25 (1954), Geophysics Research Directorate, AFCRL.

$$\tau' = \int_0^{z'} \kappa(z)\,dz = \kappa_0 H\left(1 - e^{-z'/H}\right)$$

$$z' = -H \ln\left(1 - \frac{\tau'}{\kappa_0 H}\right) \tag{B.2}$$

It is assumed in the current version of the code that κ does not vary substantially across a zone. Therefore, z'/H must be small compared to unity. Expanding Eq. (B.2),

$$\frac{\tau'}{\kappa_0} = H\left[1 - \left(1 - \frac{z'}{H} + O\left(\left(\frac{z'}{H}\right)^2\right)\right)\right] \approx z' \tag{B.3}$$

To an excellent degree of approximation, the temperature varies linearly across a zone:

$$T = T_0 + T'z$$

T' is the lapse rate. Since $T' \leq 9°/\text{km}$, $T_0 \geq 200°$, and $z' \leq 1$ km, it is valid to expand

$$\exp\left(\frac{h\nu}{kT}\right) \approx \exp\left[\frac{h\nu}{kT_0}\left(1 - \frac{T'}{T_0}z\right)\right]$$

$$= e^{h\nu/kT_0} \exp\left[\frac{h\nu}{kT_0}\frac{T'}{T_0} H \ln\left(1 - \frac{\tau'}{\kappa_0 H}\right)\right]$$

$$= e^{h\nu/kT_0}\left(1 - \frac{\tau'}{\kappa_0 H}\right)^{\delta}$$

where

$$\delta = \frac{h\nu}{kT_o} \frac{T'}{T_o} \Pi$$

The question now is, is it valid to expand the binomial? That is, can we expand

$$\exp\left(\frac{h\upsilon}{kT}\right) \simeq e^{h\nu/kT_o}\left(1 - \epsilon\right) \qquad (B.4)$$

where

$$\epsilon = \delta\frac{\tau'}{\kappa_o\Pi} = \frac{h\nu}{kT_o} \frac{T'}{T_o} \frac{\tau'}{\kappa_o} \quad ?$$

The answer is, yes, if ϵ is small compared to unity. Taking the worst possible cases for the various quantities, $\lambda = 3\mu$, $T_o = 200°K$, $T'/T_o = 8/200 = 0.04\ km^{-1}$, leads to

$$\epsilon \simeq \frac{\tau'}{\kappa_o}$$

But from Eq. (B.3), with $z' \leq 1$ km, this means

$$\epsilon \leq 1$$

Hence, for most zones in most frequency groups the expansion (B.4) is valid. The cases for which it is not valid (small λ, small T) will generally be associated with negligible values of $B_\nu(T)$. Using the expansion (B.4) in the Planck function,

$$B_\nu = \frac{A}{\exp\left(\frac{h\nu}{kT}\right) - 1} \simeq \frac{A}{e^{h\nu/kT_o}(1-\epsilon) - 1}$$

$$\simeq \frac{A}{e^{h\nu/kT_o} - 1}\left[1 + \frac{e^{h\nu/kT_o}}{e^{h\nu/kT_o} - 1}\,\epsilon\right] \qquad (B.5)$$

which is linear in τ because

$$\epsilon \propto \tau' = \tau - \tau_o \quad .$$

Hence, it is reasonable to approximate B_ν as piecewise linear in τ through the mesh.

The final step in Eq. (B.5) assumes that

$$\frac{h\nu}{kT_o} = O(1) \quad .$$

If $h\nu/kT_o << 1$,

$$B_\nu \approx A\,\frac{kT}{h\nu}$$

which is linear in z' , and hence approximately linear in τ by Eq. (B.3).

APPENDIX C
COMPRESSIBLE CODE LISTING

```
COMPRESS*ISLE.MAIN
      1       C     HAFFA IS A TWO DIMENSION INCOMPRESSIBLE FLUID DYNAMICS CODE UTILIZING THE
      2       C     BOUSSINESQ APPROXIMATION.
      3       C
      4       C*************************************************************************
      5       C     ALL UNITS IN THIS CODE ARE MKS. TEMPERATURE IN DEGREES KELVIN
      6       C*************************************************************************
      7       C
      8       C     ************************************************************
      9       C          D E F I N I T I O N   O F   V A R I A B L E S
     10       C       NX.....NUMBER OF CELLS IN X DIRECTION
     11       C       NY.....NUMBER OF CELLS IN Y DIRECTION
     12       C       DX.....SIZE OF CELL IN X DIRECTION (METERS)
     13       C       DY.....SIZE OF CELL IN Y DIRECTION (METERS)
     14       C       TIME...CURRENT PROBLEM TIME
     15       C       TMAX...MAXIMUM TIME LIMIT FOR CALCULATION
     16       C       DT.....TIME STEP FOR CURRENT CYCLE
     17       C       ICYCL..CURRENT CYCLE NUMBER
     18       C       CYCMAX.MAXIMUM NUMBER OF CYCLES FOR CALCULATION
     19       C       P......PSI (STREAMFUNCTION)
     20       C       T......TEMPERATURE DIFFERENCE FROM INITIAL CONDITIONS
     21       C       TI.....CHANGE IN T ARRAY FOR ONE CYCLE
     22       C       W......VORTICITY
     23       C       WI.....CHANGE IN W ARRAY FOR ONE CYCLE
     24       C       U......VELOCITY IN X DIRECTION
     25       C       V......VELOCITY IN Y DIRECTION
     26       C       DV.....EDDY DIFFUSION CONSTANT FOR MOMENTUM
     27       C       DTP....EDDY DIFFUSION CONSTANT FOR TEMPERATURE
     28       C       TOI....DERIVATIVE OF ORIGINAL TEMPERATURE PROFILE W.R.T. Y
     29       C              PLUS GAMMA
     30       C       WTOI...GRAVITONAL CONSTANT/(2.0*DX*ORIGINAL TEMPERATURE)
     31       C       TEMP...ORIGINAL TEMPERATURE
     32       C                    OUTPUT FLAGS
     33       C       IPRINT.PRINTER EDIT ON CYCLES
     34       C       TPRINT.PRINTER EDIT ON TIME
     35       C       IPLOT..CONTOUR PLOTS ON CYCLES
     36       C       TPLOT..CONTOUR PLOTS ON TIME
     37       C       IDUMP..TAPE DUMP ON CYCLES
     38       C       TDUMP..TAPE DUMP ON TIME
     39       C                    CONTOUR PLOT FLAGS
     40       C       TITEMP..TOTAL TEMPERATURE
     41       C       VORT...VORTICITY
     42       C       PSIC...STREAMFUNCTION
     43       C       TEMPD..TEMPERATURE DIFFERENCE FROM ORIGINAL PROFILE
     44       C       VELCD..U AND V VELOCITY
     45       C                    OPTIONS
     46       C       DTFIX..FORCE CONSTANT TIME STEP
     47       C       RESTRT.RESTART A PROBLEM FROM TAPE
     48       C       ISTART.RESTART CYCLE
     49       C       NSPC...NUMBER OF IRREGULAR POINTS IN STREAMFUNCTION
     50       C     ************************************************************
     51
     52
     53             INCLUDE MYFUNC.LIST
```

```
C
C
C     ..READ PROBLEM DATA
C
      CALL INPUT
C
C     ..SET UP SPECIFICATIONS FOR THE POISSON EQTN SOLVER
C
      [illegible]
      [illegible]
      CALL [illegible]
C
      IF([illegible] .GT. 0.0) GO TO 23
C
C     ..IF THERE ARE IRREGULARITIES IN THE POISSON GRID, CALL OBSET
C
      IF([illegible] .EQ. 0) GO TO 10
      CALL [illegible]
      CALL LAPLAC
C     .. COMPUTE VELOCITIES AND PLOT
   10 CALL VELOC
      CALL OUTPUT
C
C     ..[illegible] VARIABLES
C
      CALL [illegible]
C     ..[illegible] TIME QUANTITIES
      [illegible]
   22 [illegible]
      [illegible] .GT. 0.0 .OR. [illegible] .GT. 0) SAVE=STRUE.
C*************************************************************************
C                 MAIN LOOP
C*************************************************************************
   23 [illegible]
C     ..IF THERE IS NOT ENOUGH TIME TO COMPLETE ANOTHER CYCLE, AND
C         A DUMP OF FINAL RESULTS WAS BEEN REQUESTED, DUMP NOW
      IF(SAVE) CALL [illegible]
      [illegible]
      [illegible]
C
C     ..COMPUTE THE NEW CONCENTRATION, VORTICITY, AND TEMPERATURE
C         FIELDS DUE TO ADVECTION, DIFFUSION, AND SOURCES
C
      CALL UPDATE
C
C     ..SOLVE POISSON EQUATION TO OBTAIN NEW STREAMFUNCTION PSI
C
      CALL LAPLAC
C
C     ..COMPUTE U AND V VELOCITIES
C
      CALL VELOC
C
C     ..ADVANCE THE TIME
```

```
C
      TIME=TIME+DT
C
C     **COMPUTE THE TIME STEP FOR THE NEXT CYCLE BASED ON WIND VELOCITY,
C           DIFFUSION VELOCITY, AND EQUIVANT RISE VELOCITY
C
      CALL TIMSTP
C
C     **DETERMINE IF THIS CYCLE'S RESULTS ARE TO BE PLOTTED, PRINTED,
C           OR DUMPED
C
      PLOT=.FALSE.
      PRINT=.FALSE.
      DUMP=.FALSE.
      CALL PRINT
C
C     **SELECT OUTPUT ROUTINES
      IF(PRINT) CALL EDIT
      IF(PLOT) CALL OUTPUT
      IF(DUMP) CALL MTAPE
C
C     **IS THIS RUN COMPLETE?
C
      IF(TIME .GE. TMAX  .AND.  TMAX .GT. 0.0) GO TO 200
      IF(CYCLE .GE. CYCMAX  .AND.  CYCMAX .GT. 0) GO TO 200
C
C     **RETURN TO MAIN LOOP FOR ANOTHER CYCLE
C
      GO TO 99
C
C     **NORMAL EXIT
  200 IF(SAVE  .AND.  (.NOT. DUMP)) CALL MTAPE
      IF(.NOT. PLOT) CALL OUTPUT
      IF(.NOT. PRINT) CALL EDIT
      STOP NORMAL
      END

$EOF      CONVERGENCE.CENTUR
```

```
SUBROUTINE CONTOUR(X,Y,K,M,XINC,YINC,KK,TAB,KKK)
      INCLUDE 'FTNCOM'
      DIMENSION TAB(2),X(1),Y(1)
      DATA MSG/'MAXLOOPL/2*0.0/
C     ADJUST PRINTER SPACING
      CALL ORTN(1,'S',2,0.)
      CALL PRTS('L',2,'')
      WRITE(1,1000) ITAB(1),ITAB(2),ICYCLE,TIME
      CALL FLAG(X,IX,Y,IX,CMIN,CMAX,LOOPL)
C     RESET NORMAL PRINTER SPACING
      CALL PRTS('N',66,0,'')
C
      RETURN
C
C     FORMATS
C
 1000 FORMAT('1',3X,2A6,4X,'CYCLE = ',I5,6X,'TIME = ',
     1   E13.3)
      END

$EOF      COMPRESS-SBLE,DEFINE
```

```
COMPRESS•ISLE.DEFINE
      1            SUBROUTINE DEFINE
      2            INCLUDE 'IFINC'
      3            RDX=1.0/DX
      4            RDY=1.0/DY
      5            DUM(1)=RDY•RDY
      6            DUM(2)=RDX•RDX
      7            RDXSQ=DUM(2)
      8            RDYSQ=DUM(1)
      9            DUM(3)=DX•RDY
     10            DUM(4)=DY•RDX
     11            TIMX=0.0
     12            TIMN=0.0
     13            TIMO=0.0
     14      C     ••NOMINAL TIME STEP CRITERION
     15            IF(DT .LT. 1.0E-20) DT=0.01
     16      C     ••GRID LIMITS
     17            NXM1=NX-1
     18            NYM1=NY-1
     19            NXM2=NX-2
     20            NYM2=NY-2
     21            NYM3=NY-3
     22            NXM3=NX-3
     23      C     ••TIME STEP COEFFICIENTS
     24            DSMIN1(DX,DY)
     25            VT=AMAX1(DTP•DV)/DS
     26            IF(DTP•DV .LT. 1.0E-8) VT=1.0
     27      C          DTI IS THE MAXIMUM TIME STEP FOR DIFFUSION
     28            DTI=0.8•DS/VT
     29            IF(DTI .LT. 0.0) DTI=1.0E10
     30            DT=1.0E10
     31            DDT=1.2•DT
     32      C     ••COEFFICIENTS FOR VORTICITY
     33            DY2=0.5•DY
     34            DX2=0.5•DX
     35            TPDY=DTP•DUM(1)
     36            VDY=DV•DUM(1)
     37            TPDX=DTP•DUM(2)
     38            VDX=DV•DUM(2)
     39            NODIFF=0
     40            DUM(10)=TPDY•VDY•TPDX•VDX
     41            IF(DUM(10) .LT. 1.0E-20) NODIFF=10
     42            RETURN
     43            END


$PRT      COMPRESS•ISLE.EDIT
```

```
COMPRESS.TBLE.EDIT
      1             SUBROUTINE EDIT
      2             INCLUDE 'PIPING'
      3             WRITE(6,2000) ICYCL,TIME
      4             LINEC=0
      5             DO 100 J=1,NYP1
      6             DO 90  I=1,NXP1
      7             IF(MOD(LINE,50) .NE. 0.1) WRITE(6,1100)
      8             WRITE(6,1200) J,I,P(I,J),U(I,J),V(I,J),W(I,J),T(I,J),RHO(I,J),
      9            1   S1(I,J),S2(I,J)
     10             LINE=LINE+1
     11          90 CONTINUE
     12         100 CONTINUE
     13             RETURN
     14        1000 FORMAT(    /,1X,121(1H*)),/,20X,19HSUMMARY OF RESULTS,20X,
     15            1   8HCYCLE = ,I4,20X,7HTIME = ,1PE12.5,/,1X,121(1H*)) )
     16        1100 FORMAT(14H1,3X,1HJ,4X,1HI,2X,7X,3HPSI,13X,1HU,14X,1HV,11X,
     17            1   9HVORTICITY,8X,6HS TEMP,9X,3HRHO,12X,2HS1,13X,2HS2 )
     18        1200 FORMAT(2X,I3,3X,I3,2X,7(2X,1PE13.6),1X,1PE10.3)
     19             END


$PRT      COMPRESS.TBLE.INPUT
```

```
COMPILE,S.PLS.INPUT
      SUBROUTINE INPUT
      INCLUDE WIRING
C     ******************************************************************
C        PARAMETERS TO DEFINE TEMPERATURE BELOW INVERSION LAYER
C     KT,AT1,AT2,AT3,AT4,ALPHA    T(Y)=AT1+AT2*Y+KT*AT3*Y**(KT+1)+AT4*
C                                          EXP(-ALPHA*Y)
C        PARAMETERS TO DEFINE TEMPERATURE ABOVE INVERSION LAYER
C     NT,BT1,BT2,BT3,BT4,BETA     T(Y)=BT1+BT2*Y+NT*BT3*Y**(NT+1)+BT4*
C                                          EXP(-BETA*Y)
C        PARAMETERS TO DEFINE INITIAL U VELOCITY PROFILE
C     MT,DT1,DT2,DT3,DT4,ZETA U(YP)=MT*DT2*YP**(MT-1)+(MT+1)*DT3*YP
C                                  **MT-(DT4*ZETA)*EXP(-ZETA*YP)
C     ******************************************************************
      EXTERNAL FIN
      COMMON /TP/ BT1,BT2,BT3,BT4,BETA,NT,AT1,AT2,AT3,AT4,ALPHA,KT,YINV
      DIMENSION PRESS(N?),VX(?)
      EQUIVALENCE (PRESS(1),DU(1)),(VX(1),RR(1))
      LOGICAL REL
      DATA MAXIT,EPS,REL  /20,1.0E-4,.TRUE. /
C     **INPUT NAMELIST *START*
      NAMELIST /START/ RESTRT,ISTART,TMAX,CYCMAX,CHANGE
C     **INPUT NAMELIST *SPECS*
      NAMELIST /SPECS/ IDUMP,IPRINT,IPLOT,IPLCT,TPRINT,TDUMP,DTFIX,
     1     PSET,VISC,ITEMP,VELOC
C     **INPUT NAMELIST *GEN*
      NAMELIST /GEN/ DX,DY,TIME,DT,GT,DY,DTP,DV,KT,AT1,AT2,AT3,AT4,NOBS,
     1   ALPHA,NT,BT1,BT2,BT3,BT4,BETA,YINV,MT,DT1,DT2,DT3,DT4,ZETA,
     2   PHRUST,MSML,MIXR,MINTOP,FLAG1,FLAG2,FLAG3,FLAG4,FLAG5,FLAG6
C
      READ(5,START)
      WRITE(6,START)
C
C     **IS THIS TO BE A TAPE RESTART?
C
      IF(RESTRT .LT. 1.0E-20) GO TO 5
C
C*********************************************************************
C                 TAPE RESTART
C*********************************************************************
      CALL START
C     **ARE CHANGES TO CONTROL VARIABLES REQUESTED?
      IF(CHANGE .LT. 1.0E-20) GO TO 100
      READ(5,SPECS)
      WRITE(6,SPECS)
      GO TO 100
C
C*********************************************************************
C                    GENERATE PROFILES FROM CARDS
C*********************************************************************
    5 READ(5,SPECS)
      WRITE(6,SPECS)
      READ(5,GEN)
      WRITE(6,GEN)
```

```
C
C        CONSTANTS USED
C        GRAV=ACCELERATION OF GRAVITY  (9.81 METERS/SEC**2)
C        GAMMA=ADIABATIC LAPSE RATE FOR AIR  (0.01 DEG K/METER)
C     R=RECIPROCAL OF UNIVERSAL GAS CONSTANT
      G=9.81
      GAMMA=0.01
      R=1.0/(29.3*9.81)
C
      DO 50 J=1,NY
      Y=(J-0.5)*DY
      YP=Y
      U(1,J)=UT*DT2*YP**(NT-1)*(NT+1)*DT3*YP**NT-(DT4*ZETA)*
     1     EXP(-BETA*YP)
      V(1,J)=0.0
      IF(YINV .LT. 1.0E-20) YINV=NYP1*DY
      IF (Y.LT.YINV)TEMP(J)=AT1*(AT2+AT3*Y)*Y**KT*AT4*EXP(-ALPHA*Y)
      IF(Y.GT.YINV)TEMP(J)=BT1*(BT2+BT3*Y)**NT*BT4*EXP(-BETA*Y)
      Y0=(J-1)*DY
      IF (Y.LE.YINV)  GO TO 20
      GO TO 30
   20 TDI(J)=AT2*KT*Y**(KT-1)*(KT+1)*AT3*Y**KT-ALPHA*AT4*EXP(-ALPHA*Y)
      IF(KT .EQ. 0) TDI(J)=AT3
      GO TO 40
   30 TDI(J)=BT2*NT*Y**(NT-1)*(NT+1)*BT3*Y**NT-BETA*BT4*EXP(-BETA*Y)
      IF(NT .EQ. 0) TDI(J)=BT3
   40 IF(ABS(TDI(J)).LT.1.0E-5) TDI(J)=0.0
   50 CONTINUE
      CALL DEFINT
C
C    **NUMERICAL INTEGRATION TO OBTAIN PRESSURE AND DENSITY PROFILES
C
      DO 99 J=1,NY
      YY(1)=0.0
      YY(2)=(J-0.5)*DY
C    **FORM INTEGRAL DZ-ZP OF DZ/TEMP(Z) AND COMPUTE PRESSURE
      SUM(1)=SIMINT(FTN,YY,ERR,REL,MAXIT,1.0E-5,1000)
      PRESS(J)=PNOUT*EXP(-G*R*SUM(1))
C    **CALCULATE INITIAL DENSITY PROFILE
      RHO1(J)=PRESS(J)*R/TEMP(J)
      RHO(1,J)=RHO1(J)
      SI(1,J)=RHO(1,J)*U(1,J)
   99 CONTINUE
C
C    **FORM STREAMFUNCTION-AND VORTICITY-LIKE QUANTITIES
C
      P(1,1)=0.0
      WI(1,1)=0.0
      DO 150 J=1,NY
      P(1,J+1)=P(1,J)+DY*RHO(1,J)*U(1,J)
      IF(J .EQ. NYP1) GO TO 150
      WI(1,J+1)=RDY*(SI(1,J+1)-SI(1,J))
  150 CONTINUE
C
```

```
      C     **FORM ZETA
      C
            DO 175 J=2,NYM1
            W(1,J)=0.5*(W(1,J+1)+W(1,J))
        175 CONTINUE
            W(1,NY)=2.0*W(1,NYM1)-W(1,NYM2)
            W(1,1)=2.0*W(1,2)-W(1,3)
      C
      C     **INITIALIZE ARRAYS WITH NO X-DIRECTION DEPENDENCE
      C
            DO 200 J=1,NYP1
            DO 200 I=1,NXP1
            P(I,J)=P(1,J)
            IF(J .EQ. NYP1) GO TO 190
            U(I,J)=U(1,J)
        190 IF(I .EQ. NXP1) GO TO 200
            V(I,J)=V(1,J)
            IF(J .EQ. NYP1) GO TO 200
            T(I,J)=0.0
            W(I,J)=W(1,J)
            RHO(I,J)=RHO(1,J)
        200 CONTINUE
      C
      C     **EDIT INITIAL DATA
      C
            WRITE(6,2000)
            DO 300 J=1,NY
            WRITE(6,2100) J,TEMP(J),U(1,J),V(1,J),TOT(J),RHO1(J),PRESS(J),
           1   W(1,J),P(1,J)
        300 CONTINUE
      C
        400 RETURN
      C
      C     **ERROR IN NUMERICAL INTEGRATION
        1000 STOP SIMPSN
      C     **FORMATS
        2000 FORMAT(1H1,//,20X,22H*INITIAL ARRAY VALUES*,//,1X,1HJ,5X,4HTEMP,
           1   6X,1HU,9X,1HV,9X,3HTOT,7X,4HRHO1,6X,5HPRESS,5X,1HW,9X,1HP,/)
        2100 FORMAT(3X,I3,1X,8(1PE9.3,1X))
            END

@RT           .LAPLAC
```

```
HAUSER-L•TPFS.LAPLAC
     1              SUBROUTINE LAPLAC
     2        C     ••THIS SUBROUTINE CONTROLS THE SOLUTION OF POISSON'S EQTN
     3        C                LAPLACIAN(PSI)=CONSTANT
     4        C
     5              INCLUDE 'FSINC
     6              DIMENSION Q(NX•NYP1)•QB(NX•NYP1)•DELPSI(NI)•DELQ(NI)
     7              EQUIVALENCE (Q•S1)•(QB•S2)•(DELPSI(1)•UU(1))•(DELQ(1)•VV(1))
     8        C•••••••••••••••••••••••••••••••••••••••••••••••••••••••••••••••••••••••••••••••
     9        C•••••••••••••••••••••••••••••••••••••••••••••••••••••••••••••••••••••••••••••••
    10        C
    11        C     ••FORM CONSTANT TERMS FOR POISSON EQTNS
    12              DO 125 I=1•NX
    13              DO 100 J=2•NY
    14              WBAR=0.25•(W(I-1•J-1)•W(I-1•J)•W(I•J)•W(I•J-1))
    15              IF(I .EQ. 1) WBAR=0.25•(W(1•J)•W(1•J-1)•W(NX•J)•W(NX•J-1))
    16              Q(I•J)=WBAR•DYSQ
    17            100 CONTINUE
    18              Q(I•1)=P(I•1)
    19              Q(I•NYP1)=P(I•NYP1)
    20            125 CONTINUE
    21              IF(NOBS .EQ. 0) GO TO 200
    22        C     ••SAVE THE INITIAL Q'S IF THIS IS AN OBSTACLE PROBLEM
    23              DO 175 I=1•NX
    24              DO 175 J=1•NYP1
    25              QB(I•J)=Q(I•J)
    26            175 CONTINUE
    27        C
    28        C     ••SOLVE THE UNPERTURBED GRID PROBLEM
    29        C          (THIS WILL RESULT IN ARRAY Q BEING TRANSFORMED
    30        C           TO STREAMFUNCTION VALUES)
    31        C
    32            200 CALL XYPOIS(0)
    33        C     ••ARE IRREGULAR STREAMFUNCTION POINTS IN THE GRID?
    34              IF(NOBS .EQ. 0) GO TO 900
    35        C     ••COMPUTE ERROR IN OBSTACLE STREAMFUNCTION VALUES
    36              DO 300 I=1•NOBS
    37              I1=INDEX(I•1)
    38              I2=INDEX(I•2)
    39              DELPSI(I)=PSIFIX(I)-Q(I1•I2)
    40            300 CONTINUE
    41        C     ••COMPUTE CORRECTION TO VORTICITIES
    42              CALL MXMLT(C•DELPSI•DELQ•NOBS•NOBS•1•NI•NI)
    43        C     ••MODIFY THE QB VALUES
    44              DO 400 I=1•NOBS
    45              I1=INDEX(I•1)
    46              I2=INDEX(I•2)
    47              QB(I1•I2)=QB(I1•I2)•DELQ(I)
    48            400 CONTINUE
    49        C     ••APPLY POISSON EQTN SOLVER
    50              CALL XYPOIS(QB)
    51        C
    52        C     ••PUT NEW STREAMFUNCTION VALUES IN THE P(•••) ARRAY
    53        C
```

```
      DO 700 I=1,NX
      DO 700 J=2,NY
      PI(I,J)=PI(I,J)
  700 CONTINUE
      GO TO 1500
C
C
C     **CASE WITH NO IRREGULAR GRID POINTS
C
  800 DO 900 I=1,NX
      DO 900 J=2,NY
      PI(I,J)=PI(I,J)
  900 CONTINUE
C
C     **SET PSI AT I=NX+1 FOR CYCLIC BOUNDARY CONDITION
 1500 DO 1750 J=2,NY
      PINXPI(J)=PI(1,J)
 1750 CONTINUE
C
      RETURN
      END

$PRT     COMPRESS=ISLE,OBJECT
```

```
COMPRESS.IBLE.OBSET
     1              SUBROUTINE OBSET
     2              INCLUDE 'FIPINC'
     3              DIMENSION B(NX*NYP1),RUM(NI),VX(2)
     4              EQUIVALENCE (Q,SI),(RUM(1),UU(1)),(VX(1),VV(1))
     5        C     **MAKE INDICES GLOBAL
     6              INTEGER K,NOBS
     7              I=0
     8              WRITE(6,2007)
     9        C     **READ OBSTACLE NODE INDICES AND SPECIFIED PSI VALUES
    10           10 I=I+1
    11              READ(5,1000) INDEX(I,1),INDEX(I,2),PSIFIX(I)
    12              WRITE(6,2010) I,INDEX(I,1),INDEX(I,2),PSIFIX(I)
    13              IF(I .EQ. NOBS) GO TO 50
    14              GO TO 10
    15        C
    16        C     **DEVELOP INFLUENCE MATRIX
    17        C
    18           50 DO 100 K=1,NOBS
    19              CALL APYZPO(0,NX*NYP1)
    20              I1=INDEX(K,1)
    21              I2=INDEX(K,2)
    22              B(I1,I2)=1.0
    23              CALL YYPOIS(B)
    24              CALL CLOAD
    25          100 CONTINUE
    26        C
    27        C     **FORM THE INVERSE OF INFLUENCE MATRIX (STORE IN SAME MATRIX)
    28        C
    29              VX(1)=1.0
    30              CALL SJR(F,NI,NI,NOBS,NOBS,$250,RUM,VX)
    31        C
    32              RETURN
    33        C
    34        C     **FORMATS
    35        C
    35         1000 FORMAT(2I5,1PE10.3)
    37         2000 FORMAT(1H1,///,1CX,18HOBSTACLE NODE DATA,//,1CX,1HN,9X,1HI,9X,1HJ,
    38             1    9X,13HPSI VALUE )
    39         2010 FORMAT(5X,I5,5X,I5,5X,I5,5X,1PE14.6)
    40        C     **ERROR TERMINATION FROM SJR
    41          250 STOP 'BADINV'
    42        C*****************************************************************
    43        C                    SUBROUTINE CLOAD
    44        C*****************************************************************
    45              SUBROUTINE CLOAD
    46              DO 100 J=1,NOBS
    47              J1=INDEX(J,1)
    48              J2=INDEX(J,2)
    49              C(K,J)=B(J1,J2)
    50          100 CONTINUE
    51              RETURN
    52              END

 SPPT      COMPRESS.IBLE.ORDER2
```

```
COMPRESS*IBLE.ORDER2
     1              SUBROUTINE ORDER2(XX)
     2              INCLUDE 'TFINC'
     3              DIMENSION XX(NX,NY)
     4        C
     5        C     **STEP ONE -- X DIRECTION
     6        C
     7              CO=0.5*DTDX
     8              DO 200 J=1,NY
     9        C     **I=1 AND I=NX   USE CYCLIC BOUNDARY CONDITIONS
    10              COV=CO*(P(1,J+1)-P(1,J))*RDY
    11              FOLD=COV*(XX(1,J)+XX(NX,J))-2.0*CO*(XX(1,J)-XX(NX,J))
    12              FSAVE=FOLD
    13              DO 75 I=1,NXM1
    14              COV=CO*(P(I+1,J+1)-P(I+1,J))*RDY
    15              FNEW=COV*(XX(I+1,J)+XX(I,J))-2.0*COV*(XX(I+1,J)-XX(I,J))
    16              XX(I,J)=XX(I,J)+(FOLD-FNEW)/RHO(I,J)
    17              FOLD=FNEW
    18           75 CONTINUE
    19        C     **CASE I=NX
    20              XX(NX,J)=XX(NX,J)+(FNEW-FSAVE)/RHO(NX,J)
    21          100 CONTINUE
    22        C
    23        C     **STEP TWO -- Y DIRECTION
    24        C
    25              CO=0.5*DTDY
    26              DO 300 I=1,NX
    27              FOLD=0.0
    28        C
    29              DO 175 J=1,NYM1
    30              COV=CO*(P(I,J+1)-P(I+1,J+1))*RDX
    31              FNEW=COV*(XX(I,J+1)+XX(I,J))-2.0*COV*(XX(I,J+1)-XX(I,J))
    32              XX(I,J)=RHO(I,J)*XX(I,J)+FOLD-FNEW
    33              FOLD=FNEW
    34          175 CONTINUE
    35        C     **CASE J=NY
    36              XX(I,NY)=RHO(I,NY)*XX(I,NY)+FOLD
    37          200 CONTINUE
    38              RETURN
    39              END


$EOT      COMPRESS*IBLE.OUTPUT
```

```
@ELT,L ...SLE.OUTPUT
      SUBROUTINE OUTPUT
      INCLUDE ...
      DIMENSION V1(2),V2(2),V3(2),V4(2),V5(2),V6(2)
      DATA (V1(I),I=1,2)  /12HU VELOCITY    /
      DATA (V2(I),I=1,2)  /12HV VELOCITY    /
      DATA (V3(I),I=1,2)  /12HA TEMP        /
      DATA (V4(I),I=1,2)  /12HPSI           /
      DATA (V5(I),I=1,2)  /12HVORTICITY     /
      DATA (V6(I),I=1,2)  /12HTEMPERATURE     /
      DATA JCYCL /-1/
C     ...  THE EDITS OF THE SAME CYCLE
      IF(NCYCL .EQ. JCYCL) RETURN
      JCYCL=NCYCL
C     ...  AND ...  EDIT
      CALL [illegible]
      IF(... .EQ. 2) CALL CONTUR(NX,NY,T,C,TIME,2,V3,1)
      IF(...) 8,9,7
    7 DO 8 I=1,NX
      DO 8 J=1,NY
    8 T(I,J) = T(I,J)* [illegible]
      CALL CONTUR(NX,NY,T,C,TIME,2,V6,1)
    9 IF(... .EQ. 2) CALL CONTUR(NX,NY,U,C,TIME,2,V5,1)
      IF(...) 10,10,15
   10 CALL CONTUR(NXP1,NY,U,C,TIME,2,V1,1)
      CALL CONTUR(NX,NYP1,V,C,TIME,2,V2,1)
   15 IF(... .EQ. 2) CALL CONTUR(NXP1,NYP1,P,C,TIME,2,V4,1)
      CALL CONTUR(NX,NY,RHO,C,TIME,2,...RHO...,1)
C
      RETURN
      END

@FIN     [illegible]
```

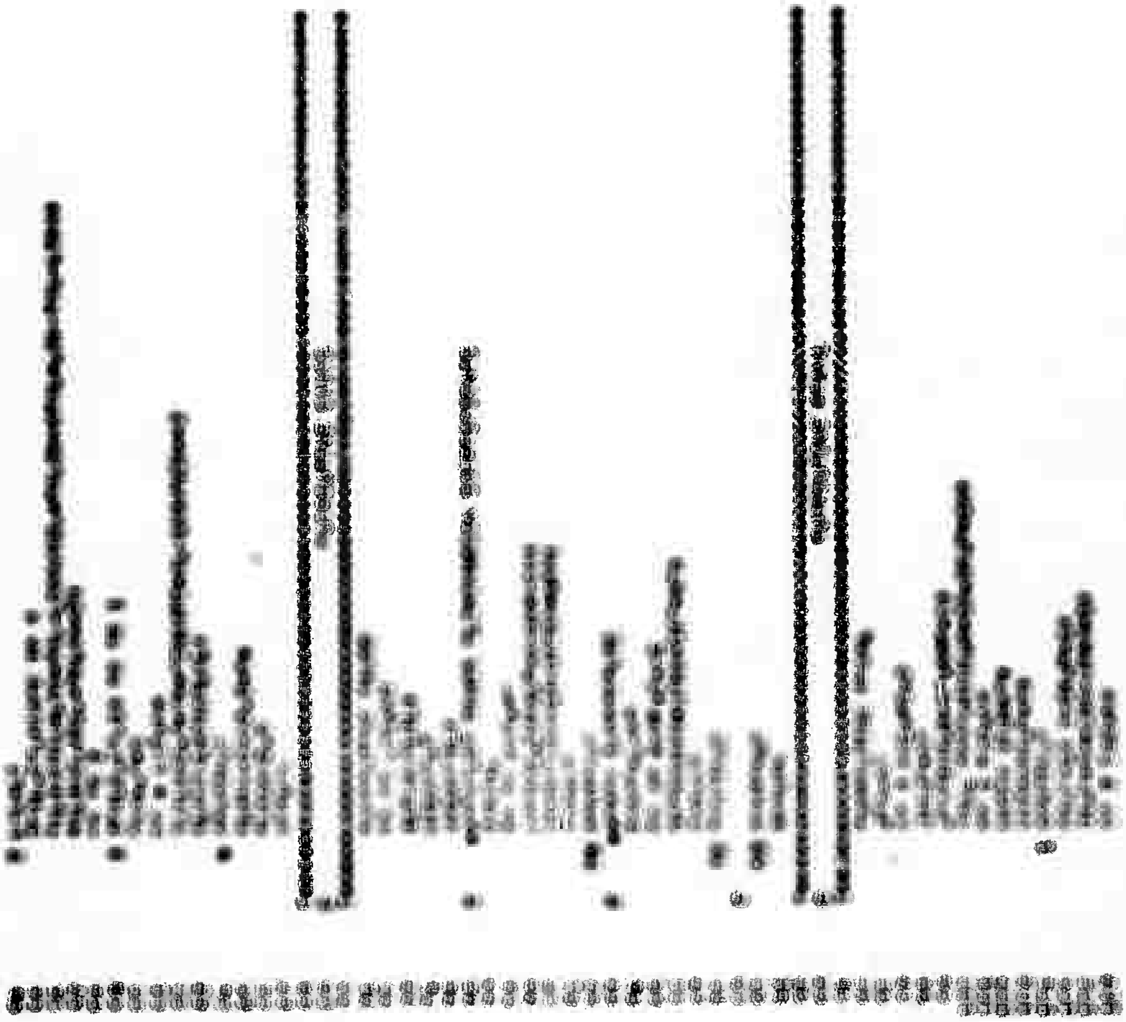

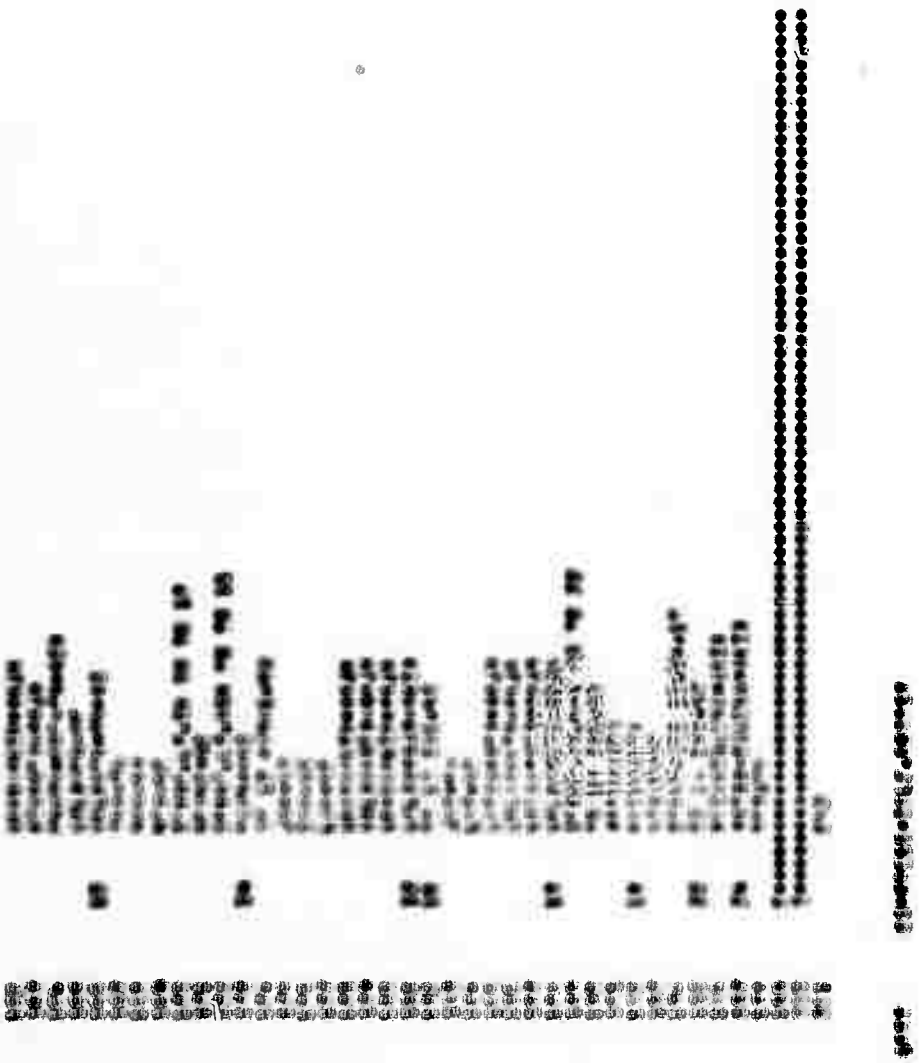

```
[illegible]
      SUBROUTINE OUTPUT
      INCLUDE [illegible]
C
C     ..OUTPUT SUBROUTINE CONTROLS PRINTED EDITS, PLOTS, AND TAPE DUMPS
C
C     .....PLOTS
      IF([illegible] .EQ. 0) GO TO 30
      IF([illegible] .GT. [illegible]) GO TO 30
      [illegible]
   30 IF([illegible] .LT. 1.0E-06) GO TO 50
      [illegible]
      IF([illegible] .LT. [illegible]) GO TO 50
      [illegible]
      [illegible]
C     .....PRINTED EDITS
   50 IF([illegible] .EQ. 0) GO TO 70
      IF([illegible] .GT. [illegible]) GO TO 70
      [illegible]
   70 IF([illegible] .LT. 1.0E-06) GO TO 80
      [illegible]
      IF([illegible] .LT. [illegible]) GO TO 80
      [illegible]
      [illegible]
C     .....TAPE DUMPS
   80 IF([illegible] .EQ. 0) GO TO 95
      IF([illegible] .GT. [illegible]) GO TO 95
      [illegible]
   95 IF([illegible] .LT. 1.0E-06) GO TO 100
      [illegible]
      IF([illegible] .LT. [illegible]) GO TO 100
      [illegible]
      [illegible]
C     ..ALWAYS PLOT CYCLE ONE, AND DUMP IF DUMPS HAVE BEEN REQUESTED
  100 IF([illegible] .NE. 1) GO TO 150
      [illegible]
      IF([illegible]) [illegible]
C
  150 RETURN
      END

[illegible]     [illegible]
```

[illegible]

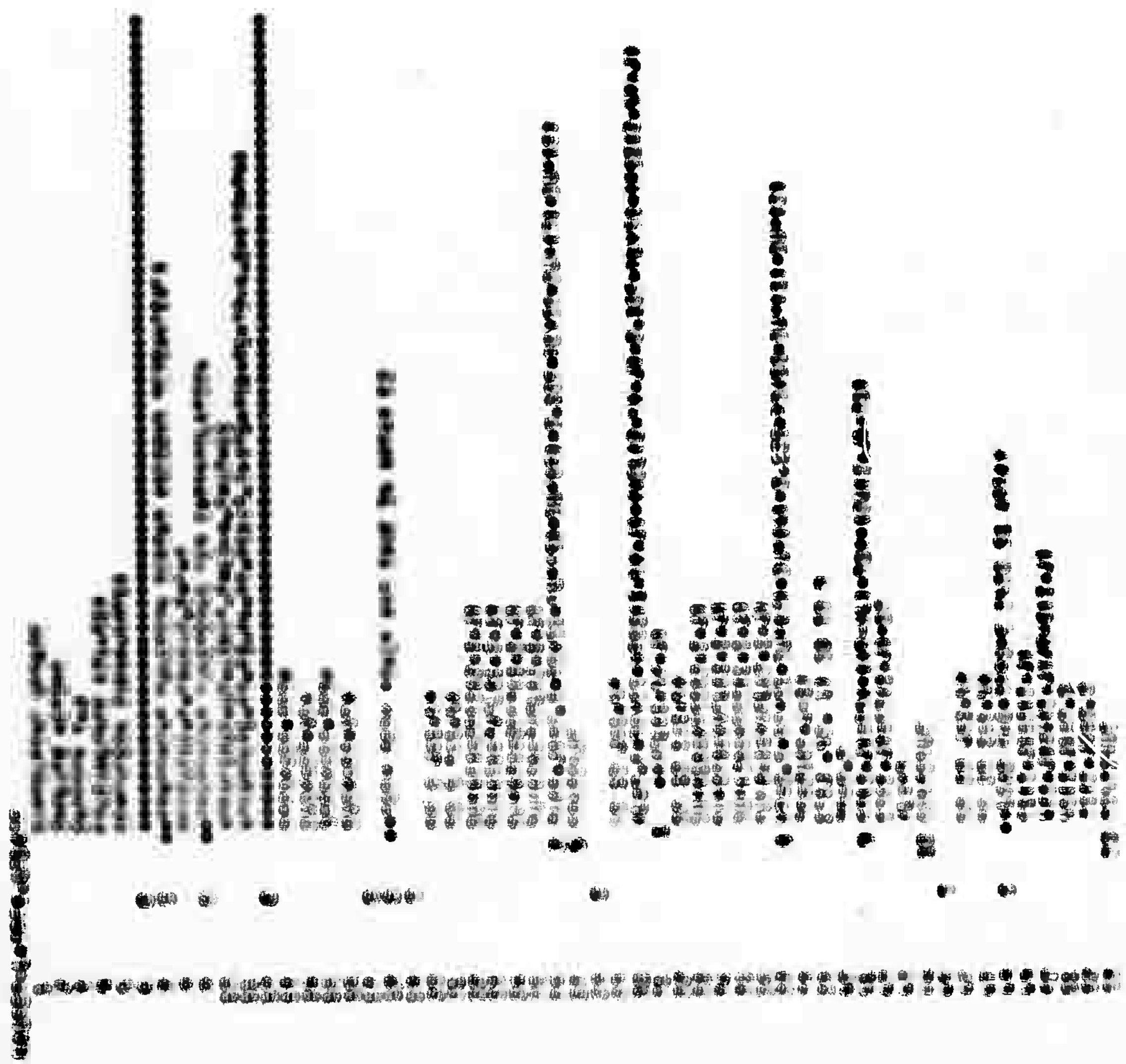

```
C     ****************************************************************
C
C     **[illegible]
C
      CALL [illegible]
      CALL [illegible]
C     ****************************************************************
C     **[illegible] CALCULATION?
      IF(N[illegible] .[illegible]. [illegible]) GO TO 75
C
C     **[illegible]
C
      DO [illegible]
      DO [illegible]
      [illegible]
      [illegible]
      [illegible]
      [illegible]
   [illegible]
      [illegible]
      [illegible]
      [illegible]
   [illegible]
      [illegible]
   [illegible]
      [illegible]
      [illegible]
      [illegible]
   [illegible]
      [illegible]
      [illegible]
      [illegible]
   [illegible]
      [illegible]
   [illegible] = [illegible] + [illegible] + [illegible] + [illegible] + [illegible]
      [illegible] = [illegible] + [illegible] + [illegible] + [illegible] + [illegible]
   [illegible] CONTINUE
   [illegible] CONTINUE
C     ****************************************************************
C     **[illegible] TEMPERATURE AND VORTICITY
   75 DO [illegible]
      DO [illegible]
      [illegible]
      IF([illegible]) [illegible]
      [illegible]
      IF([illegible]) [illegible]
      [illegible]
      IF(J .[illegible]. [illegible]) GO TO [illegible]
      [illegible]
      [illegible]/([illegible])*[illegible]
     1    [illegible]
      [illegible]*(RHO(I,J)*TOX(J)
     1    [illegible]
  150 CONTINUE
```

```
      C
      C     **COMPUTE RHO AND T PRIME
      C
            DO 200 J=1,NY
            DO 200 I=1,NX
            RHO(I,J)=RHO1(J)-P1(I,J)/TEMP(J)
            T(I,J)=S2(I,J)/RHO(I,J)
        200 CONTINUE
      C
            RETURN
      C*************************************************************************
            FUNCTION ZVEL(ID,I,J)
            INCLUDE HIFINC
            GO TO (10,50),ID
      C     **DV/DX
         10 IM1=I-1
            IF(I .EQ. 1) IM1=NX
            IP1=I+1
            IF(I .EQ. NX) IP1=1
            DUM(ID)=V(IP1,J+1)-V(IM1,J+1)
            GO TO 100
      C     **DV/DY
         50 DUM(ID)=V(I,J+2)-V(I,J)
            IF(J .NE. NY) GO TO 100
            DUM(ID)=V(I,NYP1)-V(I,NYM1)
      C     **GET ZVEL
        100 ZVEL=DUM(ID)
            RETURN
      C*************************************************************************
      C*************************************************************************
            FUNCTION TPSI(ID,I,J)
            GO TO (10,50),ID
      C     **D(PSI)/DY
         10 DUM(ID)=P(I,J+2)+P(I+1,J+2)-P(I,J)-P(I+1,J)
            IF(J .NE. NY) GO TO 100
            DUM(ID)=EXTRAP2(P(I,NYM1),P(I+1,NYM1),P(I,NY),P(I+1,NY),P(I,NYP1),
           1   P(I+1,NYP1))
            GO TO 100
      C     **D(PSI)/DX
         50 DUM(ID)=P(I+1,J+1)-P(I,J+1)
      C     **GET TPSI
        100 TPSI=DUM(ID)
            RETURN
      C*************************************************************************
      C*************************************************************************
            FUNCTION XVEL(ID,I,J)
            GO TO (10,50),ID
      C     **DU/DX
         10 IP2=I+2
            IF(I .EQ. NX) IP2=2
            DUM(ID)=U(IP2,J)-U(I,J)
            GO TO 100
      C     **DU/DY
         50 DUM(ID)=U(I+1,J+1)-U(I+1,J-1)
```

```
      IF(J .NE. 1  .AND.  J .NE. NY) GO TO 100
      IF(J .EQ. NY) GO TO 70
      DUM(IC)=-XTRAP1(U(I+1,3),U(I+1,2),U(I+1,1))
      GO TO 100
   70 DUM(IC)=XTRAP1(U(I+1,NYM2),U(I+1,NYM1),U(I+1,NY))
C     **TEST YVEL
  100 XVEL=DUM(IC)
      RETURN
C-----------------------------------------------------------------------
C-----------------------------------------------------------------------
      FUNCTION XPSI(IC,I,J)
      GO TO (10,50),IC
C     **D(PSI)/DZ
   10 DUM(IC)=P(I+1,J+1)-P(I+1,J)
      GO TO 100
C     **D(PSI)/DX
   50 IP2=I+2
      IF(I .EQ. NX) IP2=2
      DUM(IC)=P(IP2,J)+P(IP2,J+1)-P(I,J)-P(I,J+1)
C     **TEST XPSI
  100 XPSI=DUM(IC)
      RETURN
C-----------------------------------------------------------------------
C-----------------------------------------------------------------------
      END
```

```
$PRT      COMPRESS,IBLE,VELOC
```

```
      SUBROUTINE WTSLC
C     SUBROUTINE WTSLC
C
C     EXECUTION BEGINS
C
      DO 10 I=1,NVAR
      DO 10 J=1,NVAR
      IF(I.GT.J) GO TO 10
      IF(I.EQ.J) GO TO 5
      WTSLC(I,J)=WTSLC(I,J)/SQRT(WTSLC(I,I)*WTSLC(J,J))
      GO TO 10
    5 WTSLC(I,J)=1.0
   10 CONTINUE
      RETURN
      END
```

```
$ENT    COMPRESSSELF.WTSLC
```

```
[illegible]
      SUBROUTINE WTAPE
      INCLUDE [illegible]
      [illegible]
      WRITE (NTAPE) [illegible]
      WRITE (NTAPE) [illegible]
      WRITE(6,1000) [illegible]
C
      RETURN
C
C     [illegible]
 1000 FORMAT([illegible] CYCLE = [illegible], TIME = [illegible]
     1  [illegible] ON TAPE. [illegible] )
      END
```

[illegible]